

Kinetic Modeling-Guided Process Development for a Novel Epoxy Resin

Matthias Lukas Feigel

Vollständiger Abdruck der von der TUM School of Natural Sciences der Technischen
Universität München zur Erlangung eines

Doktors der Ingenieurwissenschaften (Dr.-Ing.)

genehmigten Dissertation.

Vorsitz: Prof. Dr. Thomas Brück

Prüfer der Dissertation:

1. Prof. Dr.-Ing. Kai-Olaf Martin Hinrichsen
2. Prof. Dr. Dr. h. c. Bernhard Rieger

Die Dissertation wurde am 23.07.2024 bei der Technischen Universität München eingereicht
und durch die TUM School of Natural Sciences am 17.09.2024 angenommen.

*All models are wrong,
but some are useful.*

-George Box, 1976

Danksagung

An allererster Stelle möchte ich mich bei meinem Doktorvater Prof. Dr.-Ing. Kai-Olaf Hinrichsen für die Aufnahme in die Arbeitsgruppe des Lehrstuhls I für Technische Chemie und die Möglichkeit, diese Arbeit dort zu schreiben, bedanken. Im Verlauf der vergangenen Jahre hatten Sie stets ein offenes Ohr für jeglichen wissenschaftlichen Diskurs und so ein Gelingen des Projekts stark gefördert. Dafür danke ich Ihnen sehr.

Ich möchte mich bei allen Projektpartnern des "Green Carbon" Verbundprojekts bedanken. Im Einzelnen danke ich Prof. Thomas Brück, Prof. Bernhard Rieger, Daniel Garbe, Felix Melcher, Nikita Reinhardt und Sophia Prem, welche im Besonderen in verschiedenster Weise die Projektlaufzeit mitgeprägt und bereichert haben. Die Zusammenarbeit war immer konstruktiv und produktiv. Ganz besonders bedanke ich mich bei Jonas Breitsameter. Danke Dir für die zahlreichen wissenschaftlichen Diskussionen, pragmatischen Lösungsansätze und Unterstützung in der Umsetzung vieler gemeinsamer Ideen. Ohne Deine Bemühungen im Labor und die stets tolle Zusammenarbeit wäre diese Arbeit nicht an diesem Punkt.

Ich danke meinem Mentor Dr. Thomas Michel und Heidi Holweck, die sich am Lehrstuhl um all die bürokratischen Angelegenheiten gekümmert haben, welche vorhergesehener oder auch unvorhergesehener Weise im Verlauf einer Dissertation auftauchen können. Weiterhin gilt mein aufrichtiger Dank an all meine Kollegen über die Jahre am Lehrstuhl: Philipp, Johanna, Thomas, Daniel, My, Tabea, Chris, Anne, Heike, Sebastian und Anna. Danke an Euch für die unzähligen fachlichen und nicht-fachlichen Diskussionen im Büro oder den Kaffeepausen. Ohne Euch hätte ich mir den Alltag am Lehrstuhl nicht vorstellen können. Die vielen Unternehmungen außerhalb des Lehrstuhlbetriebs oder auch auf den Konferenzen werden mir in Erinnerung bleiben.

In den letzten Jahren haben mich zahlreiche Studierende unterstützt, welche ich in Abschlussarbeiten, Forschungsberichten und Seminararbeiten betreuen durfte. Ich möchte mich bei Amedeo, Edwin, Fabian, Gözdem, Jan, Korbinian, Ong Dong, Yannick und Yosua bedanken für das Interesse, eine Arbeit bei mir zu schreiben und so auch im Kleinen zum Gelingen der Promotion beigetragen zu haben.

Mein abschließender und ganz besonderer Dank gilt meiner Familie und meiner Freundin. Danke, dass Du mir immer die Zeit und Motivation gegeben hast, den Endspurt durchziehen. Im Speziellen möchte ich meinen Eltern und meinem Bruder Dank aussprechen, die mich über all die Jahre in jeglicher Hinsicht unterstützt haben und mir immer den Rücken freigehalten und auch gestärkt haben, um meinen akademischen Weg zu bestreiten. Ich bin euch unendlich dankbar!

Abstract

The need for new, bio-based components to replace their fossil-derived counterparts is becoming increasingly urgent. The objective of transitioning to bio-based alternatives is not only to reduce carbon emissions and move towards environment-friendly solutions but also mitigate the health risks from hazardous substances. For a novel compound, developing a production strategy from laboratory synthesis involves a high investment and lengthy, rigorous testing. To address this challenge, kinetic modeling and process modeling can facilitate process development *in silico* based on first principles. The resulting process model allows for an initial assessment of the production design regarding technical and economic feasibility.

In this thesis, the synthesis of 1,2-epoxy-6-methyl-triglycidyl-3,4,5-cyclohexanetricarboxylate (EGCHC) serves as a case study to investigate the techno-economic viability of the novel sustainable epoxy resin. Therefore, this study sheds light on the synthesis path and presents a methodology to provide insights into the production, crucial for later scale-up decisions. EGCHC is formed from a four-step synthesis route starting from sorbic acid and allyl alcohol, which are both available as fully bio-based. Subsequently, maleic anhydride is added to the formed allyl sorbate. In the next step, further double bonds are introduced with the ring-opening and esterification reactions using allyl alcohol. The last reaction step epoxidizes the previously formed double bonds to generate four functional groups, leading to a dense cross-linked network in the cured resin. EGCHC shows a bio-based content of 53.8 %, taking a conservative approach of only including readily available bio-based resources on an industrial scale. All used components can be derived from natural feedstocks, but many synthesis routes are not implemented on a large scale. Comparing EGCHC to the industrial standard epoxy diglycidyl ether of bisphenol A (DGEBA), equivalent or even superior thermo-mechanical properties can be identified with minor drawbacks in the glass transition temperature.

As allyl sorbate is a commercial product, the initial reaction step starting from sorbic acid is excluded from kinetic and process modeling. Thus, the underlying synthesis route covers three reaction steps, which are scrutinized individually. Reaction models are derived for each step, and the representative kinetic models are regressed with experimental data gathered from batch experiments. Pre-exponential factors and activation energies are estimated with high accuracy and confidence for the three reaction steps: Diels-Alder

reaction, allylation, and epoxidation. The key findings cover not only kinetic parameters but also information about the respective reaction mechanism. Several models are postulated and compared based on statistical information theory for the allylation. Here, it is shown that the reaction proceeds as second order through two intermediates. Modeling the epoxidation reveals that the reaction mechanism can be simplified by two kinetic constants representing the epoxidation of a terminal or ring-bound double bond. Using that assumption, the network of reactions with six intermediates can be modeled with high precision.

Based on the findings from the kinetic modeling studies, a process is designed for large-scale EGCHC production. Therefore, the kinetic models are implemented in a process simulation environment in the respective reaction units. Furthermore, efficient purification and separation sections are developed for each synthesis step. Due to the exothermic characteristic of the Diels-Alder reaction, the reaction is carried out in a tubular reactor, ensuring adequate heat control. Process intensification is applied in the allylation section, as the reagent here also acts as the solvent. Thus, separation and reaction are combined within a reactive distillation column. Sensitivity studies are carried out, enabling optimal operation conditions for the column regarding energy demand and product purity. The epoxidation reaction is also modeled in a tubular reactor, allowing for a high conversion. The complete process is used to perform a techno-economic analysis to judge the feasibility of the novel epoxy EGCHC produced with a purity of 95 %. A competitive market price for EGCHC compared to other bio-based epoxies is derived using a recycling economy for the epoxidation agent.

Overall, this thesis showcases, based on the synthesis route towards the epoxy EGCHC, a comprehensive methodology that allows an initial assessment in respect to commercialization and scale-up of a novel molecule using preliminary laboratory measurements. Thus, process design, general feasibility, and further key economic metrics can be derived. With the help of the kinetic models, reaction sections can be sized and designed accurately. However, the resulting figures should allow for further decisions rather than direct design. Nevertheless, a variety of findings around and from kinetic and process modeling will greatly enhance and drive development of the postulated process design.

Kurzzusammenfassung

Die rasant wachsende Nachfrage nach nachhaltigen Alternativen zu konventionellen, fossilen Materialien treibt die Entwicklung neuartiger, biobasierter Moleküle voran. Diese Ersatzstoffe bieten immense Potenziale zur Reduzierung von CO₂-Emissionen, zum Schutz der Umwelt und zur Minimierung von Gesundheitsrisiken, die oft mit konventionellen Stoffen verbunden sind. Die Entwicklung einer Produktionsstrategie für neuartige Moleküle basierend auf Laborsynthesen ist mit hohen Investitionen, sowie langwierigen und aufwändigen Studien verbunden. Einen Lösungsansatz können kinetische und Prozessmodellierung liefern, welche die *in silico* Prozessentwicklung auf Basis fundamentaler physikalisch-chemischer Gesetzmäßigkeiten ermöglichen. Das resultierende Fließbild erlaubt es, das Prozessdesigns bereits in einem frühen Stadium hinsichtlich der technischen und wirtschaftlichen Machbarkeit zu bewerten.

In dieser Arbeit wird die Synthese von 1,2-Epoxy-6-Methyl-Triglycidyl-3,4,5-Cyclohexantricarboxylat (EGCHC) als Fallstudie zur Untersuchung der technischen und wirtschaftlichen Umsetzbarkeit des neuartigen und nachhaltigen Epoxidharzes herangezogen. Der Syntheseweg wird im Detail dargelegt und eine Methodik präsentiert, welche es erlaubt, tiefere Einblicke in den Produktionsprozess zu ermöglichen, um eine spätere Skalierbarkeit zu beurteilen. Die Synthese von EGCHC erfolgt ausgehend von den biobasierten Edukten Sorbinsäure und Allylalkohol in einem vierstufigen Prozess. An das im ersten Schritt gebildete Allylsorbat wird darauffolgend Maleinsäureanhydrid addiert. Anschließend werden durch Ringöffnung und Veresterung mit Allylalkohol weitere Doppelbindungen eingeführt. Im letzten Reaktionsschritt werden die gebildeten Doppelbindungen epoxidiert, was zu einer vierfachen Funktionalisierung des Produkts führt. Die Epoxidgruppen erlauben die Formation eines dichten Netzwerks im ausgehärteten Harz. EGCHC weist einen biobasierten Anteil von 53,8 % auf, welcher konservativ bestimmt ist und nur bereits im industriellen Maßstab verfügbare biobasierte Komponenten einbezieht. Alle verwendeten Stoffe können in der Theorie aus nachwachsenden Rohstoffen gewonnen werden, jedoch sind viele Syntheserouten noch nicht großtechnisch umgesetzt. Vergleicht man EGCHC mit dem industriellen Standard-Epoxidharz Diglycidylether von Bisphenol A (DGEBA), so lassen sich vergleichbare, teils sogar bessere thermo-mechanische Eigenschaften feststellen, wobei geringfügige Einbußen in der Glasübergangstemperatur bestehen bleiben.

Aufgrund der kommerziellen Verfügbarkeit von Allylsorbat wird der erste Reaktionsschritt - ausgehend von Sorbinsäure - für die kinetische und Prozessmodellierung nicht betrachtet. Damit ergibt sich ein Syntheseweg mit drei Reaktionsschritten, die jeweils einzeln im Detail analysiert werden. Für jeden Schritt werden Reaktionsmodelle entwickelt, experimentelle Daten erfasst und die aufgestellten kinetischen Modelle mit diesen regressiert. Die jeweiligen prä-exponentielle Faktoren und Aktivierungsenergien für die Diels-Alder-Reaktion, Allylierung und Epoxidierung werden mit hoher Genauigkeit und geringen Konfidenzintervallen bestimmt. Die zentralen Erkenntnisse aus den kinetischen Modellen umfassen nicht nur deren Parameter, sondern auch Informationen über die jeweiligen Reaktionsmechanismen. Für die Allylierung werden verschiedene Modelle postuliert und eine Modellauswahl anhand von Informationskriterien vorgenommen. Dabei wird gezeigt, dass die Allylierung in zweiter Ordnung und unter Bildung zweier Zwischenprodukte abläuft. Die Modellierung der Epoxidierungsreaktion legt offen, dass die Approximation des Reaktionsmechanismus durch zwei kinetische Konstanten gerechtfertigt ist. Die beiden Parameter beschreiben die Reaktionsgeschwindigkeit der Epoxidierung an einer terminalen oder ringgebundenen Doppelbindung im Molekül. Unter Berücksichtigung dieser Annahme kann das Reaktionsnetzwerk mit den sechs Zwischenprodukten modelliert werden.

Basierend auf den Ergebnissen aus der kinetischen Modellierung wird ein Verfahren für die großtechnische EGCHC-Produktion konzipiert. Dafür werden die Reaktionsmodelle mit den regressierten Parametern in einer Prozesssimulationsumgebung implementiert. Weiterhin werden für jeden Syntheseschritt effiziente Aufreinigungs- und Abtrennungsmethoden *in silico* entwickelt. Die Diels-Alder-Reaktion wird aufgrund der Exothermie in einem Rohrreaktor durchgeführt, um eine adäquate Wärmeabfuhr zu gewährleisten. Im darauffolgenden Abschnitt wird mit Hilfe von Prozessintensivierung Reaktion und Aufreinigung in einer einzelnen Reaktivdestillationskolonne kombiniert, da Allylalkohol gleichermaßen als Reagens und Lösungsmittel fungiert. Mit Hilfe von Sensitivitätsstudien werden optimale Betriebsbedingungen für die Rektifikation hinsichtlich Energiebedarfs und Produktreinheit ermittelt. Die Epoxidierung wird in einem weiteren Rohrreaktor simuliert, um einen hohen Umsatz zu ermöglichen. Der gesamte Prozess wird einer technoökonomischen Analyse unterzogen, um die Umsetzbarkeit des Herstellungsprozesses des neuartigen Epoxids zu beurteilen. EGCHC, welches eine Reinheit von 95 % aufweist, kann mit Hilfe einer Kreislaufwirtschaft für das verwendete Epoxidierungsmittel zu einem wettbewerbsfähigen Marktpreis hergestellt werden.

Die vorliegende Arbeit demonstriert eine umfassende Methodik zur initialen Bewertung der Marktfähigkeit und Skalierbarkeit eines neuartigen Moleküls anhand von leicht durchführbaren Labormessungen. Die Methodik kann für andere, neue Syntheserouten angewendet werden, sodass Prozessdesign, Umsetzbarkeit sowie weitere ökonomische Kenngrößen in kurzer Zeit abgeleitet werden können. Die resultierenden Ergebnisse dienen

jedoch eher als Entscheidungsgrundlage, denn als direkte Auslegungsrichtlinie. Dennoch wird die Vielzahl an Erkenntnissen aus den Studien zur kinetischen und Prozessmodellierung die Entwicklung eines möglichen Herstellungsprozesses maßgeblich fördern und vorantreiben.

Contents

Abstract	vii
Kurzzusammenfassung	ix
1 Introduction	1
1.1 Motivation	1
1.1.1 Bisphenol A: Health Concerns and Regulatory Change in the EU	2
1.1.2 Research on Bio-Based Alternatives to DGEBA	3
1.2 Outline	4
2 Theoretical Background	7
2.1 Kinetic Modeling	7
2.1.1 Reaction Kinetics	7
2.1.2 Parameter Estimation	9
2.1.3 Model Discrimination	12
2.2 Process Modeling	15
2.2.1 Physical Properties	15
2.2.2 Process Units	19
2.2.3 Techno-Economic Analysis	23
3 Synthesis of the Novel Epoxy and Properties of the Cured Resin	27
3.1 Background	27
3.2 Synthesis of EGCHC	29
3.3 Curing of EGCHC	30
3.4 Ecological Assessment	32
3.5 Conclusion	34
4 Kinetic Modeling of the Synthesis Steps	35
4.1 Introduction	36
4.2 Experimental	37
4.2.1 Materials	37
4.2.2 Kinetic Experiments	37

4.3	Model Development	39
4.3.1	Diels-Alder Reaction	39
4.3.2	Esterification	40
4.3.3	Epoxidation	42
4.4	Computational Methodology	45
4.4.1	Reactor Model	45
4.4.2	Regression	45
4.5	Results and Discussion	47
4.6	Conclusions	55
5	Process Development for the Production	67
5.1	Introduction	68
5.2	Methodology	69
5.2.1	Components	69
5.2.2	Physical Properties	70
5.2.3	Kinetic Models	74
5.2.4	Process Model	77
5.3	Results and Discussion	82
5.4	Conclusion	91
6	Summary	107
6.1	Conclusions	107
6.2	Outlook	109
A	UNIFAC Groups	111
A.1	UNIFAC	111
B	Bibliography	115
	Nomenclature	135
	List of Figures	141
	List of Tables	145
	List of Publications	147

1 Introduction

1.1 Motivation

Epoxy resins are ubiquitous in modern life, serving as important materials in a vast array of applications, from high-performance adhesives and coatings to composites used in construction and electronics [1, 2]. Their versatility and superior properties, including chemical resistance, low density, and mechanical strength, have led to an increased application in industry [3]. The worldwide market size for epoxy resins in 2019 is estimated at 3.1–3.2 million tons per year [4]. However, the market volume remains comparably small taking the total plastics production of 382 million tons in 2022 into consideration [5]. Figure 1.1 illustrates the annual production capacity of fossil and bio-based polymers worldwide from 1950 to 2022. Additionally, a forecast using component annual growth rates (CAGR) of 2 % and 17 % for fossil and bio-based derived polymers until 2028 is indicated [5]. Clearly, with less than 1 % of the total polymer production, the latter still only plays a minor role in the world’s plastics economy. However, the CAGR of bio-based polymers evidently shows that it is an emerging and valuable market.

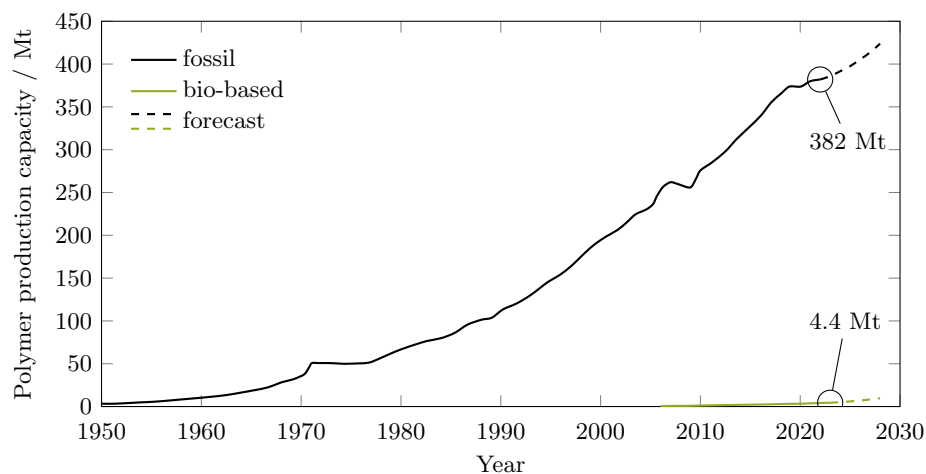


Figure 1.1: Development of the worldwide polymer production capacities for fossil and bio-based plastics from 1950 to 2022 and forecast until 2028. Modified after [5].

About 90 % of the commercial epoxy resin is based on bisphenol A diglycidyl ether (BADGE), also diglycidyl ether of bisphenol A (DGEBA) [6]. The widely-used resin is made from bisphenol A (BPA) and epichlorohydrin (ECH). Currently, only ECH holds the potential to be synthesized from renewable resources. Glycerol, a byproduct of bio-diesel production, is the starting point for the formation of green ECH [7, 8]. Thus, bio-based ECH can readily be acquired at an industrial scale [9]. Most commonly, the Epicerol® process developed by Solvay is used to produce renewable epichlorohydrin from green glycerol [10]. In 2023, bio-based ECH used for the synthesis of epoxy resins made up 30 % of the bio-based polymer production capacities [5]. This fraction considers partial bio-based products, as the second reagent BPA remains to be produced from fossil resources. Despite the availability of an ECH replacement, the toxicity and health impact of the component remain unchanged [11, 12].

1.1.1 Bisphenol A: Health Concerns and Regulatory Change in the EU

Growing concerns regarding the health implications of bisphenol A cast a shadow on their continued use. The chemical is linked to various health issues, including endocrine disruption [13, 14] and cardiometabolic or cardiovascular diseases [15, 16]. Consequently, regulatory bodies around the globe begun implementing stricter regulations on the use of BPA in specific applications, prompting the search for safer alternatives. Several restrictions already exist in the European Union to ban the use of BPA for the application in thermal paper [17], plastic infant feeding bottles, and food packaging for children under the age of three [18]. In 2015, the European Food Safety Authority (EFSA) postulated a temporary tolerable daily intake (TDI) of 4 µg/kg [19]. In April of 2023, the EFSA re-evaluated the TDI of BPA and significantly reduced the TDI to 0.2 ng/kg based on new scientific evidence [20]. Recently, the EU government published the results of a study targeting BPA levels in adult urine samples in different EU countries [21]. To translate a TDI to a concentration level, a human biomonitoring guidance value (HBM-GV) is developed for a certain substance, which was also established for BPA [22]. The human biomonitoring initiative (HBM4EU) revealed that BPA concentrations exceeded the HMB-GV in the samples of 92 % of the participants [23]. Noteworthy, the derived HMB-GV of 11.5 ng/L is below the analytical detection limit of BPA [21]. Therefore, it is likely that additional samples could have contained BPA levels above the HBM-GV, raising health concerns for the European population. Even if new restrictions in the use of BPA are being set, producers will likely introduce similar structural compounds like bisphenol F or bisphenol S. This poses the question of whether a ban of the entire class of chemicals might be more effective instead of targeting single structures [24].

1.1.2 Research on Bio-Based Alternatives to DGEBA

Health and environmental impacts have spurred significant research towards syntheses of novel, green alternatives to DGEBA. The replacement of the conventional resin with sustainable alternatives draws great attention in recent research. Figure 1.2 illustrates and compares the total number of journal articles published with the fraction of articles, which include the keywords "epoxy" and "bio-based" in their title or abstract. The general

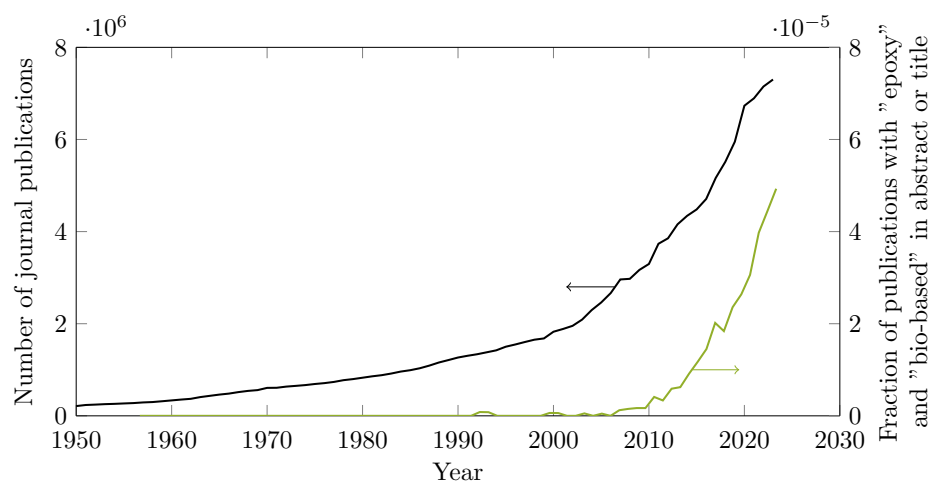


Figure 1.2: Development of the total number of journal articles published from 1950 to 2023 in comparison to the normalized fraction of number of articles published with the keywords "epoxy" and "bio-based" in the title or abstract. Data from [25].

volume of publications has risen exponentially since the 2000s. Nevertheless, articles with the focus on bio-based epoxies outgrow this trend starting from 2010. This underlines the urgency and interest of research groups in the field of sustainable resins. One frequently followed path is to mimic the aromatic properties of BPA with structurally similar natural molecules. Such starting materials can include but are not limited to cardanol [26–28], eugenol [29–32], vanillin [33–37], lignin derivatives [38–40], and other biogenic substances [41]. ECH is often added to form the desired glycidyl ethers. Similarly, cyclic aliphatic polyols derived from sugars can be used for the etherification [42–45]. Another strategy is to epoxidize the double bonds in highly unsaturated molecules derived from renewable feedstocks. Polyunsaturated fats and fatty acids serve as common starting materials [46–50]. *m*-Chloroperbenzoic acid is frequently utilized due to its ease of usage and separation on a laboratory scale [51]. Hydrogen peroxide can also function as an oxidizing agent, either in combination with metallic catalysts [52–54] or small chain carboxylic acids [55, 56]. In the context of bio-based materials, enzymatic epoxidations are increasingly recognized due to the environmentally friendly process conditions with low temperatures and pressures [57–59]. A challenge associated with the present oxidizing conditions is the rapid deactivation of enzymes, resulting in short lifetimes. Optimized operating principles can help mitigate this issue [60].

1.2 Outline

Many of the previously mentioned studies discussing novel bio-based molecules showcase their synthesis with laboratory experiments. Researchers then analyze the resulting epoxy resins' thermo-mechanical properties to compare and validate the materials. However, it often remains to be seen, whether an up-scaling of the synthesis is possible or feasible concerning technical and economic aspects. This thesis demonstrates a holistic approach towards the synthesis of a novel, bio-based epoxy resin with a strong focus on the necessary subsequent steps complementing laboratory research. From a depiction of the synthesis route developed within a collaboration in the "GreenCarbon" project [61, 62], kinetic and process modeling is employed to draw *a priori* conclusions on the complete production chain. The novel molecule with the name 1,2-epoxy-6-methyl-triglycidyl-3,4,5-cyclohexanetricarboxylate (EGCHC) is synthesized from sorbic acid, allyl alcohol, and maleic anhydride and thus does not rely on ECH or BPA [61]. All mentioned compounds are either bio-available [63–66] or routes were published to produce them abstaining from fossil resources [67, 68].

Therefore, a thorough understanding of the reaction steps can be established by utilizing state-of-the-art modeling techniques. This approach greatly reduces the efforts increasing production scale as information about the process design is already available. Thus, in an early development stage, not only details about the newly reported reaction steps, but also an assessment of the competitiveness of the proposed, novel structure can be given.

All parameter estimations and statistical analyses are performed in MATLAB® R2021a, due to the vast extent of toolboxes and advanced numerical solvers. Process modeling is conducted using Aspen Plus® V12 (38.0.0.380). Preliminary studies mainly related to bio-processes, which handle enzymes, are investigated using SuperPro Designer®. As the capabilities for the prediction of physical properties, especially for unknown components, are more pronounced in the Aspen Engineering Suite, all presented results in this thesis are generated with Aspen Plus®. The subsequent techno-economic assessment is carried out with Aspen Process Economic Analyzer® (APEA-V12), which estimates equipment costs assuming a first quarter 2019 pricing basis (CEPCI 618.7).

Chapter 2 lays the theoretical groundwork for the kinetic and process modeling employed throughout this work. A detailed examination of the methodologies used for parameter estimation and model discrimination is provided. Specifically, techniques within the framework of chemical reaction engineering are presented. Additionally, relevant physical property methods and unit operations that are directly connected to the studied process are discussed.

Chapter 3 presents the background of the upcoming chapters by introducing the synthesis route towards the novel epoxy EGCHC. This information is crucial for drawing a holistic picture. Starting with a description of all reaction steps, insights into thermo-mechanical results of the cured resins are given. The bio-based content of EGCHC and cured resins thereof are discussed in detail in an ecological assessment. This chapter summarizes the key findings of the works published in:

J. M. Breitsameter, N. Reinhardt, M. Feigel, O. Hinrichsen, K. Drechsler, B. Rieger, “Synthesis of a Sustainable and Bisphenol A-Free Epoxy Resin based on Sorbic Acid and Characterization of the Cured Thermoset”, *Macromol. Mater. Eng.* **2023**, 2300068, DOI 10.1002/mame.202300068.

Chapter 4 sheds light into the parameter estimation of the postulated reaction models. Therefore, the synthesis of the novel bio-based epoxy EGCHC is rapidly monitored using $^1\text{H-NMR}$ and multi-parameter fitting of non-linear regression functions is performed to obtain the reaction rate constants. The kinetic model variables are predicted using re-parameterization techniques. Additionally, model discrimination is applied to the reaction scheme using information theory where applicable. The described methodology provides a fast and efficient way to gather kinetic and mechanistic data about novel synthesis routes. This chapter was published in a similar way in:

M. Feigel, J. M. Breitsameter, K. Lechner, B. Rieger, O. Hinrichsen, “Kinetic Modeling of the Synthesis Path for the Production of a Sustainable Epoxy Resin based on Allyl Sorbate”, *Ind. Eng. Chem. Res.* **2023**, 62, 13389–13400, DOI 10.1021/acs.iecr.3c01317.

Chapter 5 presents a comprehensive and systematic process simulation for the production of the novel sustainable epoxy. The study successfully employs classical group contribution methods based on UNIFAC to accurately predict thermal separation processes and estimate physical properties of all relevant compounds. Sensitivity studies are performed to size and optimize the chosen equipment, with the results revealing the effects of crucial parameters on all stages of the process. A techno-economic analysis is conducted to assess the competitiveness of the proposed process design compared to representative epoxy resins. This chapter was published in a similar way in:

M. Feigel, J. M. Breitsameter, B. Rieger, O. Hinrichsen, “Bridging the Gap from Laboratory to Production: Kinetic Modeling-Guided Process Development for a Novel Epoxy Resin”, *Ind. Eng. Chem. Res.* **2024**, 63, 1271–1285, DOI 10.1021/acs.iecr.3c03339.

2 Theoretical Background

2.1 Kinetic Modeling

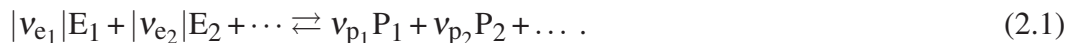
Understanding and predicting chemical reactions requires models representing the observed behavior. These models act as a theoretical approximation of reality, guiding researchers in understanding the reaction mechanism. Within the field of chemical reaction engineering, various approaches are employed to obtain reaction models. These models define the structure of a chemical conversion by describing the path reactants follow leading to the desired final product. Kinetics further investigate the reaction mechanism at a granular level, quantifying the rates and underlying mechanism associated with each elementary step within the pathway. Depending on the simulation method, the kinetic and reaction models can be separated or lumped. Aggregated approaches use empirical mathematical equations to predict specific observations without necessarily referencing, e.g., thermodynamics. Increased computational power has also advanced data-driven models using machine learning and neural networks in chemical engineering. While these can generate accurate predictions with large datasets, they risk acting as "black boxes", hindering fundamental understanding of the reactions.

This thesis focuses on reaction models based on first-principles power-law kinetics, providing a fundamental understanding of the reactions involved. Therefore, the approaches presented in the upcoming chapters instead follow a separate structure using reaction models and kinetics based on known and observable chemistry.

2.1.1 Reaction Kinetics

Kinetics play a pivotal role in chemical process design by providing a quantitative description of reaction rates while offering valuable insights into the reaction mechanisms themselves. To provide a focused context for the following studies, this chapter presents a brief introduction to reaction kinetics. For a comprehensive understanding of various aspects of this field, please refer to the extensive literature available [71–74].

In general, a reaction equation comprises educts E_i which are converted to products P_i



By convention, the stoichiometric coefficients v_i are positive for products and negative for educts. By summarizing Equation 2.1, it can be written

$$0 = \sum_i v_{e_i}E_i + \sum_i v_{p_i}P_i = \sum_i v_i C_i \quad (2.2)$$

for all components C_i . It is more practical to refer to "components" or "species" due to the often reversible nature of a reaction indicated by the double-sided arrow in Equation 2.1.

The rate of reaction for component i is defined as

$$r_i = \frac{1}{V} \frac{dn_i}{dt} \quad (2.3)$$

with the change in moles n_i . Assuming constant volume V , Equation 2.3 can be expressed with molar concentrations $c_i = n_i/V$

$$r_i = \frac{dc_i}{dt}. \quad (2.4)$$

The reaction rate r is represented by

$$r = v_i r_i. \quad (2.5)$$

The conversion at which an educt reacts to a product can generally be expressed as

$$r = kf(c_i) \quad (2.6)$$

with the reaction rate constant k and a function f , describing the dependency on the components present in the system. A frequent approach is to approximate $f(c_i)$ as

$$f(c_i) = \prod_i c_i^{\alpha_i} \quad (2.7)$$

with the reaction orders α_i [71]. The temperature dependency of the rate constant k can be described by the Arrhenius law

$$k = k_0 \exp\left(-\frac{E_A}{RT}\right) \quad (2.8)$$

with the pre-exponential factor k_0 , the activation energy E_A and the universal gas constant R . If the reaction consists of multiple reaction steps, Equation 2.3 needs to be adjusted to consider each step j :

$$\frac{dn_i}{dt} = \sum_j v_{j,i} r_j = \dot{R}_i. \quad (2.9)$$

Therefore, the introduced total rate of production $\dot{\mathbf{R}}$ is a matrix with dimensions of $j \times i$ and Equation 2.9 can be written as

$$\frac{dn}{dt} = \mathbf{v}^T r = \dot{\mathbf{R}}. \quad (2.10)$$

2.1.2 Parameter Estimation

Parameter estimation is the regression of selected model variables to find the minimum deviation between measured data and simulated model responses, typically using a minimum least-squares or maximum likelihood estimation (MLE). The underlying data, both in quantity and quality, determine the confidence of the parameter estimates. The total number of observations n_{tot} is defined as the sum of data sets n_{data} with their number of discrete experimental measurement points n_{exp} , where n_{exp} can have multiple responses n_{resp} :

$$n_{\text{tot}} = \sum_{m=1}^{n_{\text{data}}} \sum_{i=1}^{n_{\text{resp}}} \sum_{j=1}^{n_{\text{exp}}} . \quad (2.11)$$

The reaction in Equation 2.12 acts as an example with the task to find pre-exponential factor k_0 and activation energy E_A :



All three components a, b and c can be measured separately by an analysis method of choice. Assuming that batch experiments are performed at different temperatures, samples with distinct points in time are collected according to Table 2.1.

Table 2.1: Sampling protocol with the number of samples taken at temperatures T_i (example).

Temperatures	T_1	T_2	T_3	T_4
Number of samples	10	20	15	10

Each temperature run m represents one data set: $n_{\text{data}} = 4$. As all three components can be measured within one sample, the number of responses is $n_{\text{resp}} = 3$. Therefore, the total number of observations can be calculated:

$$n_{\text{tot}} = \sum_{m=1}^{n_{\text{data}}} \sum_{i=1}^{n_{\text{resp}}} \sum_{j=1}^{n_{\text{exp}}} = (10 + 10 + 10 + 20 + 20 + 20 + \dots) = 165. \quad (2.13)$$

In the field of parameter estimation measured data is segregated to predictors X and responses Y :

$$Y = f(X) \quad (2.14)$$

with f being the unknown model generating the responses. The function is described with parameters Φ which are the target values of the estimation. Therefore, it can be written as

$$Y = f(X, \Phi) + \varepsilon \quad (2.15)$$

with the parameter vector $\Phi = [\Phi_1, \dots, \Phi_{n_{\text{par}}}]$ and an error term ε . Writing Equation 2.15 with the corresponding dimensions introduced in Equation 2.11, it follows that:

$$\begin{bmatrix} Y_{1,1} & Y_{1,2} & \dots & Y_{1,n_{\text{resp}}} \\ Y_{2,1} & Y_{2,2} & \dots & Y_{2,n_{\text{resp}}} \\ \vdots & \vdots & \ddots & \vdots \\ Y_{n_{\text{exp}},1} & Y_{n_{\text{exp}},2} & \dots & Y_{n_{\text{exp}},n_{\text{resp}}} \end{bmatrix}_m = f \left(\begin{bmatrix} X_1 \\ X_2 \\ \vdots \\ X_{n_{\text{exp}}} \end{bmatrix}_m, \begin{bmatrix} \Phi_1 \\ \vdots \\ \Phi_{n_{\text{par}}} \end{bmatrix} \right) + \begin{bmatrix} \varepsilon_{1,1} & \varepsilon_{1,2} & \dots & \varepsilon_{1,n_{\text{resp}}} \\ \varepsilon_{2,1} & \varepsilon_{2,2} & \dots & \varepsilon_{2,n_{\text{resp}}} \\ \vdots & \vdots & \ddots & \vdots \\ \varepsilon_{n_{\text{exp}},1} & \varepsilon_{n_{\text{exp}},2} & \dots & \varepsilon_{n_{\text{exp}},n_{\text{resp}}} \end{bmatrix}_m \quad (2.16)$$

or in a compact notation form:

$$\mathbf{Y}_m = f(X_m, \Phi) + \varepsilon_m. \quad (2.17)$$

In the case of the example reaction given in Equation 2.12, the predictor vectors X_m consist of the sampling times and the response matrices \mathbf{Y}_m are the measured concentrations of each component at a time. The size of \mathbf{Y}_m is different for each temperature campaign. The parameter vector has two entries: $\Phi = [\Phi_1, \Phi_2] = [k_0, E_A]$.

Generally, the function f is neither linear nor analytically solvable. In the case of reaction kinetics, ordinary differential equations (ODEs) need to be solved.

It is tempting to linearize the Arrhenius equation (Equation 2.8) and evaluate k at each temperature which is a common approach [71, 72]:

$$\ln k = \ln(k_0) - \frac{E_A}{R} \frac{1}{T}. \quad (2.18)$$

Using a graphical analysis of $\ln(k)$ over $1/T$, the slope and intercept of the regression line facilitate to estimate $-\frac{E_A}{R}$ and $\ln(k_0)$, respectively. However, this fitting approach limits the statistical meaning of the results and thus, should be avoided [75].

Therefore, a simultaneous fitting of both parameters is favorable. The temperature dependency of the kinetic constant k described by an Arrhenius-type law imposes a strong correlation between pre-exponential factor k_0 and activation energy E_A . Several approaches are pursued to weaken the coupling thereof. The otherwise high correlation of the parameters to be estimated would lead to an increased computational effort or lower the efficiency of the optimization algorithm [76]. Different possibilities to re-parameterize the Arrhenius equation using a reference temperature T_{ref} have been published, which are listed in Equation 2.19a–Equation 2.19d [77–79]:

$$\Phi_k = \Phi_{k_0} \exp \left[-\frac{E_A}{R} \left(\frac{1}{T} - \frac{1}{T_{\text{ref}}} \right) \right] \quad (2.19a)$$

$$\Phi_k = \Phi_{k_0} \exp \left[\Phi_{E_A} \left(1 - \frac{T_{\text{ref}}}{T} \right) \right] \quad (2.19b)$$

$$\Phi_k = \exp \left[\Theta - \frac{E_A}{R} \left(\frac{1}{T} - \frac{1}{T_{\text{ref}}} \right) \right] \quad (2.19c)$$

$$\Phi_k = \exp \left[\Theta + \Phi_{E_A} \left(1 - \frac{T_{\text{ref}}}{T} \right) \right] \quad (2.19d)$$

with

$$\Theta = \ln(\Phi_{k_0}) \quad (2.20a)$$

$$\Phi_{k_0} = k_0 \exp[-\Phi_{E_A}] \quad (2.20b)$$

$$\Phi_{E_A} = \frac{E_A}{RT_{\text{ref}}} \quad (2.20c)$$

$$T_{\text{ref}} = \frac{1}{n_{\text{data}} + 1} \sum_{n=1}^{n_{\text{data}}} T. \quad (2.20d)$$

A good summary and review of the different forms and their sensitivity towards T_{ref} can be found from Schwaab et al. [75, 76, 80, 81]. The four re-parameterization strategies can be grouped into half- (Equation 2.19a, Equation 2.19b) and full-exponential (Equation 2.19c, Equation 2.19d) approaches. In this study, parameter estimation of the kinetic rate equations is performed using the half-exponential formulation of Equation 2.19b, which shows the best numerical stability.

2.1.3 Model Discrimination

Model selection is a crucial part of parameter estimation. This chapter introduces the principles of the information-theoretic approach to select and rate candidate models from data-based experiments. For an advanced understanding, reading detailed literature is recommended [82–85].

Einstein's assertion that "everything should be made as simple as possible, but no simpler" is widely cited [84, 85], yet its validity remains subject to an ongoing debate [86]. Nevertheless, this quote encapsulates the essence of model discrimination. The selection of a "best-fit" model, referred to as model discrimination, is of particular interest when the true function or first-order principle model is unknown. In chemical reaction engineering, representing all molecular steps involved in a reaction pathway may not always be essential. Otherwise, experimental data may not be sufficient to fully elaborate on intermediate steps present in a reaction. While various theories and reaction models can be proposed and tested against the gathered data, the challenge lies in determining which model best represents the data.

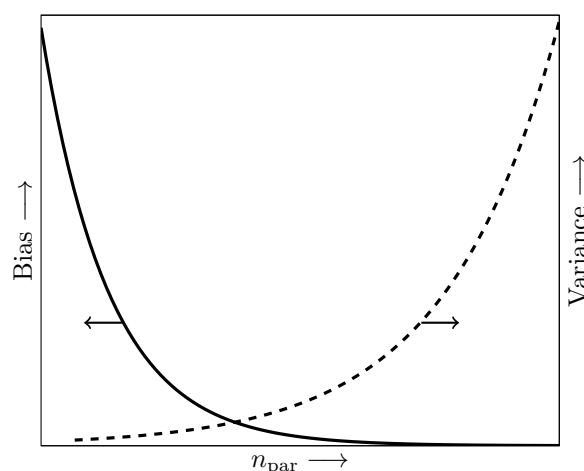


Figure 2.1: Schematic illustration of the principle of parsimony. Bias and variance as function of the number of parameters n_{par} . Modified after [85].

Information and likelihood theory provide a relative means to assess which candidate model is empirically most supported. However, information theory cannot give an absolute rating or propose an ideal model. Instead, it assists the applicant in deciding on a model that, based on the available data, possesses the highest empirical support while also being simple in terms of its parameter space. The latter is referred to as the principle of parsimony and is illustrated in Figure 2.1. Increasing the parameter space and thus reducing the bias will automatically result in a higher variance in the estimated parameters. Therefore, a trade-off is required to derive an optimal, minimal number of parameters necessary to describe the empirical observations. Wei demonstrated this principle in a humorous yet vivid example by asking, "How many parameters does it take to fit an

elephant?" [87]. A simplified two-dimensional drawing with 36 discrete points was fitted with a Fourier sine series where the number of terms was chosen as the fitting parameter. The author concluded that a 30-term series "may not satisfy the third-grade art teacher, but would carry most chemical engineers into preliminary design" [87].

Mathematically, the difference between the true model function g and a selected model f_i with set parameters $\Phi = [\Phi_1, \dots, \Phi_{n_{\text{par}}}]$ can be calculated by the Kullback-Leibler (K-L) distance $I(g, f_i)$ [88]:

$$I(g, f_i) = \int g(X) \ln \left(\frac{g(X)}{f_i(X, \Phi)} \right) dX. \quad (2.21)$$

The underlying data X are always bound to the truth g . However, the K-L distance cannot be directly applied in regression studies due to the inherent uncertainty in determining the true model function g . Rewriting Equation 2.21 gives:

$$I(g, f_i) = \int g(X) \ln(g(X)) dX - \int g(X) \ln(f_i(X, \Phi)) dX. \quad (2.22)$$

Equation 2.22 describes the K-L distance as two statistical expectations E_g referenced to the true function g . Thus, it can be written:

$$I(g, f_i) = E_g [\ln(g(X))] - E_g [\ln(f_i(X, \Phi))]. \quad (2.23)$$

The first term in Equation 2.23 is only dependent on the true function g which is unknown. Hence, it can be treated as a constant C [85]:

$$I(g, f_i) = C - E_g [\ln(f_i(X, \Phi))]. \quad (2.24)$$

The remaining expectation in Equation 2.24 represents the distance or measurable discrepancy between true model g and candidate model f_i up to the constant C . The quantitative expectations will rank the models in order of smaller distances. This marks the fundamentals of information theory, as the true function is unknown *a priori*. Thus, only a relative measure is available to decide within a set of models based on data samples which model is closest to g , i.e., has the least loss of information [85]. As still g is unknown, an estimation of the K-L distance $I(g, f_i)$ is required. Akaike took the expected value $E_{g'}$ of Equation 2.24 which in theory refers to a second sample taken out of the n_{data} [82, 89, 90].

$$E_{g'} [I(g, f_i)] = C' - E_{g'} E_g [\ln(f_i(X, \Phi))] \quad (2.25)$$

Akaike demonstrated that the key step lies in estimating the double expectation in the second term of Equation 2.25. This term represents the statistical expected values derived

from the true function g , evaluated across two independent data samples ($x_1, x_2 \in X$) denoted here by g and g' [82]. Akaike proposed an elegant method using the log-likelihood function \mathcal{L} at its maximum point as an unbiased estimator of the double expectation with a bias-correction term representing the number of estimated parameters n_{par} [82]:

$$\mathcal{L}(\Phi, X) - n_{\text{par}} = C' - E_{g'} [I(g, f_i)]. \quad (2.26)$$

In 1973, Akaike introduced an information criterion (*AIC*) by multiplying the left hand side of Equation 2.26 with -2 . More details on the emergence of the "magic number 2" can be found in [91]. Thus, the Akaike information criterion can be written as

$$AIC = -2\mathcal{L}(\Phi, X) + 2n_{\text{par}} \quad (2.27)$$

or in a simplified notation

$$AIC = -2\mathcal{L} + 2n_{\text{par}}. \quad (2.28)$$

While AIC can select the best model from a given set, the selected model may still be inadequate if the set itself is poor. Therefore, ensuring that the model selection is comprehensive and well-founded is crucial. Adding more known parameters to an approximating model can reduce the relative K-L distance. However, adding more estimated parameters will introduce uncertainty to the estimation and potentially increase the relative K-L distance due to overfitting. This trade-off between complexity and accuracy is reflected in the information criterion being minimized. For least-squares estimation, the general likelihood function \mathcal{L} can be replaced by regression statistics, i.e, estimated residuals of a model assuming normally distributed errors [85]. Using the introduced notation, if least-squares fitting is applied to the model responses \mathbf{Y}_m and experimental observations $\hat{\mathbf{Y}}_m$, *AIC* can be calculated as:

$$AIC = n_{\text{exp}} \ln \left(\frac{\sum (\mathbf{Y}_m - \hat{\mathbf{Y}}_m)^2}{n_{\text{exp}}} \right) + 2n_{\text{par}}. \quad (2.29)$$

2.2 Process Modeling

2.2.1 Physical Properties

Regardless of the chemical process studied, the initial stage of each simulation is to define the components that should be handled throughout the model and their physical properties. Here, critical decisions are made, ultimately influencing the generation of the flowsheet in the next stage. Also, prior understanding of the phases and units to be designed can significantly reduce the complexity of the physical property methods.

The accurate description of the vapor-liquid-equilibrium (VLE) of a pure component or a mixture of components is of high interest. Precise VLE calculations provide a crucial foundation for the design of thermal separation units. At equilibrium the liquid phase fugacity $f_{i,l}$ can be equated with the fugacity of the vapor phase $f_{i,v}$:

$$f_{i,l} = f_{i,v}. \quad (2.30)$$

Physical property methods can be grouped into two main categories, each defined by the calculation method for fugacities in each phase. Either an equation of state model or an activity coefficient model can be selected. Details will be given on models that will be used in the later stage of the process simulation in chapter 5.

2.2.1.1 Equation of State Method

Equation of state (EOS) methods derive an algebraic correlation between the state variables temperature T , pressure p , and volume V . The simplest EOS model is the ideal gas law. Other prominent EOS models are the cubic equations of Peng-Robinson [92] and Soave's modifications [93] to Redlich-Kwong [94] or the virial type models Benedict-Webb-Rubin [95] and Hayden-O'Connell [96].

The fugacity in each phase can be calculated using the fugacity coefficient ϕ , which describes the deviation from ideal behavior.

$$f_{i,l} = \phi_{i,l} x_i p \quad (2.31a)$$

$$f_{i,v} = \phi_{i,v} y_i p \quad (2.31b)$$

Redlich-Kwong

The Redlich-Kwong model is an equation of state method valid for systems at low pressures [94]. The EOS is defined as

$$p = \frac{RT}{V_m - b} - \frac{a}{\sqrt{T}V_m(V_m + b)} \quad (2.32)$$

with

$$a = \sum_i x_i \sqrt{a_i} \quad \text{and} \quad a_i = \frac{1}{9(\sqrt[3]{2}-1)} \frac{R^2 T_c^{1.5}}{p_c} \quad (2.33a)$$

$$b = \sum_i x_i b_i \quad \text{and} \quad b_i = \frac{\sqrt[3]{2}-1}{3} \frac{RT_c}{p_c}. \quad (2.33b)$$

Therefore, only knowledge about the critical properties of pressure p_c and temperature T_c of each component and their molar volume V_m is required.

2.2.1.2 Activity Coefficient Method

In activity coefficient methods, the liquid phase fugacity is determined using an activity coefficient γ_i and a standard liquid fugacity $f_{i,l}^0$. Equation 2.34b is the same as Equation 2.31b. This means that in cases where both vapor and liquid phases are present, the activity coefficient method will be used for the liquid phase, while for the gas phase, an EOS is still required.

$$f_{i,l} = \gamma_i x_i f_{i,l}^0 \quad (2.34a)$$

$$f_{i,v} = \Phi_{i,v} y_i p \quad (2.34b)$$

Important activity coefficient models are Wilson [97], NRTL [98], UNIQUAC [99], and UNIFAC [100, 101]. For systems that deviate strongly from ideal behavior, activity coefficient methods are recommended to use. Predictions depend heavily on the accuracy of the known or estimated pure component or interaction parameters. Thus, Wilson, NRTL, or UNIQUAC are suitable for calculating the liquid phase behavior in non-ideal systems for components listed in one of the established databases.

In the case of novel structures or mixtures of molecules that are not available in common databases, predictive physical property methods, such as UNIFAC or PSRK [102], are required.

UNIFAC

The UNIFAC model uses the same approach as the UNIQUAC model but generalizes the physical property method using functional groups instead of distinct molecules. Hence, with a relatively small number of functional groups, the physical properties of almost any molecule can be predicted [100, 101]. The UNIFAC model calculates the liquid activity factor γ_i based on a combinatorial $\gamma_{i,c}$ and residual term $\gamma_{i,r}$:

$$\ln \gamma_i = \ln \gamma_{i,c} + \ln \gamma_{i,r}. \quad (2.35)$$

Each term is defined in Equation 2.36a and Equation 2.36b, respectively.

$$\ln \gamma_{i,c} = \ln \frac{\Phi_i}{x_i} + 1 - \frac{\Phi_i}{x_i} - \frac{z}{2} \left(\ln \frac{\Phi_i}{\theta_i} + 1 - \frac{\Phi_i}{\theta_i} \right) \quad (2.36a)$$

$$\ln \gamma_{i,r} = \sum_k^{n_{\text{group}}} v_{k,i} (\ln \Gamma_k - \ln \Gamma_{k,i}) \quad (2.36b)$$

The combinatorial term calculated with Equation 2.36a is based on a molecular volume fraction Φ_i and a molecular surface fraction θ_i for component i in a system with a total fixed number of molecules n_{comp} . Volume and surface fraction are determined with Equation 2.37a and Equation 2.37b, respectively. The coordination number z is frequently set to 10 [103].

$$\Phi_i = \frac{x_i r_i}{\sum_j^{n_{\text{comp}}} x_j r_j} \quad (2.37a)$$

$$\theta_i = \frac{x_i \frac{z}{2} q_i}{\sum_j^{n_{\text{comp}}} x_j \frac{z}{2} q_j} \quad (2.37b)$$

The used parameters r_i and q_i are derived from tabulated group volume R_k and group area values Q_k with the total number of functional groups in the mixture n_{group} and the number of occurrences $v_{k,i}$ of a group of type k in molecule i .

$$r_i = \sum_k^{n_{\text{group}}} v_{k,i} R_k \quad (2.38a)$$

$$q_i = \sum_k^{n_{\text{group}}} v_{k,i} Q_k \quad (2.38b)$$

In Equation 2.36b, the residual term $\gamma_{i,r}$ is calculated with the activity coefficient of group k at the mixture composition Γ_k . $\Gamma_{k,i}$ is defined as the activity coefficient of group k in a mixture of only molecule i present, i.e., a pure component mixture. Both coefficients can be calculated with the help of Equation 2.39:

$$\ln \Gamma_k = Q_k \left[1 - \ln \sum_m^{n_{\text{group}}} \Theta_m \Psi_{m,k} - \sum_m^{n_{\text{group}}} \left(\frac{\Theta_m \Psi_{k,m}}{\sum_n^n \Theta_n \Psi_{n,m}} \right) \right]. \quad (2.39)$$

Here, Θ_m is the area fraction of group m , similar to θ_i in Equation 2.37b, but calculated with a group mole fraction X_k . X_k is defined as the fraction of a functional group of type k in a molecule divided by the total number of functional groups in the mixture.

$$\Theta_m = \frac{\frac{z}{2} Q_m X_m}{\sum_n^n \frac{z}{2} Q_n X_n} \quad (2.40a)$$

$$X_k = \frac{\sum_j^{n_{\text{comp}}} v_{k,j} x_j}{\sum_j^{n_{\text{comp}}} \sum_m^{n_{\text{group}}} v_{m,j} x_j} \quad (2.40b)$$

$\Psi_{m,k}$ is a binary interaction parameter between two groups m and k , which is temperature dependent and calculated from tabulated parameters $a_{m,k}$.

$$\Psi_{m,k} = \exp\left(-\frac{a_{m,k}}{T}\right) \quad (2.41)$$

An overview of published and available binary interaction parameters of the UNIFAC model is given in Figure A.1 ($a_{m,k} \neq a_{k,m}$). In total, 1400 parameters are listed in public literature, while additional and updated values are only available within the UNIFAC consortium.

UNIFAC (Dortmund)

In 1987, Weidlich and Gmehling introduced a modified version of the original UNIFAC method to achieve higher prediction accuracy of vapor-liquid-equilibria [104]. The adjusted and improved version of the UNIFAC model, cited as Dortmund due to the affiliation of the authors, differs slightly in the calculation of the combinatorial term:

$$\ln \gamma_{i,c} = \ln \frac{\Phi_i^*}{x_i} + 1 - \frac{\Phi_i}{x_i} - \frac{z}{2} \left(\ln \frac{\Phi_i}{\theta_i} + 1 - \frac{\Phi_i}{\theta_i} \right) \quad (2.42)$$

with

$$\Phi_i^* = \frac{x_i r_i^{\frac{3}{4}}}{\sum_j n_{\text{comp}} x_j r_j^{\frac{3}{4}}}. \quad (2.43)$$

The main advantage is the enhanced temperature dependency of the binary interaction parameter $\Psi_{m,k}$:

$$\Psi_{m,k} = \exp \left(-\frac{a_{m,k} + b_{m,k}T + c_{m,k}T^2}{T} \right). \quad (2.44)$$

This allows the calculation of excess enthalpies with improved accuracy, which is not possible in the original UNIFAC model [104].

2.2.2 Process Units

This chapter provides some conceptual insights into key process units used throughout this work. Modern process simulation tools are equipped with a vast selection of unit operation models that can easily be aggregated to complex flowsheets. Heat and mass balances are solved in the background, and the user has to take care of the specifications, such as the thermal mode of operation, pressure, dimensions, and the set of reactions. A short introduction to the mass balances of each reactor type is presented in the next section. As reactor design and engineering is not within the scope of this work, a complete but brief overview is given. Similarly, some basics for the simulation of distillation columns based on theoretical stages are introduced. Excellent literature on chemical reaction engineering and process technology has been published over the last decades, covering all relevant reactor and process design topics [71–74, 105–108].

2.2.2.1 Reactors

At the heart of any chemical plant lie the reactors, where the educts undergo transformations that yield the desired products. While other unit operations like feed conditioning and product purification might have larger dimensions and visibility of a plant, reactors remain the very essence of chemical production. From a modeling perspective, understanding and simulating reactor behavior is crucial. Mass transport limitations play a minimal role in the homogeneous liquid-liquid reactions studied in this thesis due to the inherent mixing occurring at the molecular level. In contrast, heterogeneous catalyzed reactions require a deep understanding of mass transport and diffusion processes to adequately design and size the respective reaction equipment.

Batch Reactor

In this thesis, all experiments for kinetic studies are conducted in stirred glass vessels in batch operation. Due to vigorous stirring and a large heat sink in the form of oil or ice baths, the system can be treated as homogeneous and isothermal $\frac{dT}{dt} \approx 0$. Hence, the mass balance can be set up as follows:

$$\frac{dn_i}{dt} = V_R \dot{R}_i \quad (2.45)$$

with the formation rate of each species \dot{R}_i , the reaction volume V_R and the time derivative of the molar amount n_i . The mass balance is valid for closed systems, which is assumed throughout the conducted experiments.

For the conversion X follows

$$X = \frac{n_{i,0} - n_i}{n_{i,0}}. \quad (2.46)$$

If isochor behavior ($\frac{dV}{dt} = 0$) is assumed, the molar amounts can be exchanged with molar concentrations c_i

$$X = \frac{c_{i,0} - c_i}{c_{i,0}}. \quad (2.47)$$

Even though all experiments in this thesis were conducted in batches, it is inevitable that continuously operated reactors are necessary for a successful commercialization. The disadvantage of batch reactors lies in the comparably small throughput due to the lead and

cleaning times necessary to fill the reactor, perform a reaction, and discharge the products. Thus, batch reactors are only applied in high-value product formulation or processes that are infeasible to run continuously [74].

Continuously Stirred Tank Reactor

The main property of a continuously stirred tank reactor (CSTR) is the homogeneity in the reaction phase. Therefore, no gradients exist in any reactor dimension, and outlet conditions represent the reaction phase. The mass balance can be written as:

$$\frac{dn_i}{dt} = \dot{n}_{i,0} - \dot{n}_i + V_R \dot{R}_i. \quad (2.48)$$

Similarly to the batch reactor, the conversion can be calculated with

$$X = \frac{\dot{n}_{i,0} - \dot{n}_i}{\dot{n}_{i,0}}. \quad (2.49)$$

Ideal Plug Flow Reactor

The ideal plug flow reactor is characterized by neglecting radial profiles within the tube and dispersion in the axial direction. Assuming stationary behavior, the mass balance over the axial domain z can be derived as:

$$\frac{dc_i u}{dz} = V_R \dot{R}_i \quad (2.50)$$

with the superficial velocity u . Conversion can be calculated using Equation 2.49 with the molar inlet flowrate of component $\dot{n}_{i,0}$ and the molar flow at the outlet \dot{n}_i .

2.2.2.2 Distillation Columns

Component separation and purification are essential in chemical production. Various techniques exist, while thermal separation is one of the most critical methods. The concept of an ideal theoretical stage represents the foundation for several thermal separation systems. Due to the benefits of continuous operation in large-scale chemical production, separation methods must also be capable of processing these flows. For a rigorous analysis, the concept of theoretical stages is a well-suited approach [106, 109]. Figure 2.2 illustrates a respective equilibrium stage j . The mass balance involves vapor and liquid flows entering

and leaving the system to the next stage. Additionally, a feed flow \dot{n}_j^f and vapor $\dot{n}_{S,j}^v$ or liquid $\dot{n}_{S,j}^l$ side stream flows might be present.

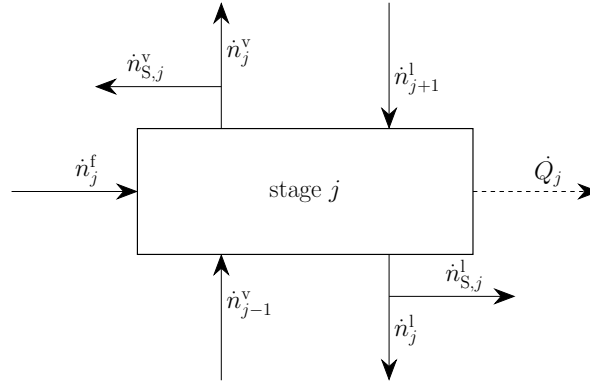


Figure 2.2: Schematic representation of the mass balance on a theoretical stage.

Loss or provision of heat is represented by \dot{Q}_j , while enthalpies need to be balanced for the complete stage additionally. The system can be described by the so-called MESH (material-equilibrium-summation-heat) equations. The material balance for a component i is set up as:

$$M_{i,j} = \dot{n}_{j+1}^l x_{i,j+1} + \dot{n}_{j-1}^v y_{i,j-1} + \dot{n}_j^f z_{i,j} - (\dot{n}_j^l + \dot{n}_{S,j}^l) x_{i,j} - (\dot{n}_j^v + \dot{n}_{S,j}^v) y_{i,j} = 0 \quad (2.51)$$

with liquid mole fraction x_i and vapor mole fraction y_i . All stages are assumed to be at equilibrium condition. Hence,

$$E_{i,j} = y_{i,j} - x_{i,j} K_{i,j} = 0 \quad (2.52)$$

with an equilibrium constant $K_{i,j}$. Additionally, summation of molar fraction must be conserved:

$$S_{x,j} = \sum x_{i,j} = 1 \quad \text{and} \quad S_{y,j} = \sum y_{i,j} = 1. \quad (2.53)$$

Lastly, the heat balance needs to be closed for the theoretical stage:

$$H_j = \dot{n}_{j+1}^l H_{j+1}^l + \dot{n}_{j-1}^v H_{j-1}^v + \dot{n}_j^f H_j^f - (\dot{n}_j^l + \dot{n}_{S,j}^l) H_j^l - (\dot{n}_j^v + \dot{n}_{S,j}^v) H_j^v - \dot{Q}_j = 0. \quad (2.54)$$

If reactions occur in the theoretical stage, the influence on heat and mass balance must be considered. The system of equations is solved for all stages, which can be computationally demanding if many stages and components are present. Available software nowadays provides efficient solution methods and solvers tackling the design of distillation columns [73]. Aspen Plus applies the inside-out method by default but offers various other solver algorithms [110]. Further details on solution methods, design, and simulation of distillation columns can be found in the literature [106].

2.2.3 Techno-Economic Analysis

Economic figures are crucial metrics for deciding on further development and investment at all stages of designing a chemical process. Depending on the conceptualization stage, ballpark numbers can be derived for the project with uncertainties narrowing down to $\pm 10\%$ in the best case [107]. Higher confidence can be achieved if data about comparable processes or similar plants with different capacities are accessible [73]. For novel processes, widespread uncertainties are typical and must be coped with short payback periods or higher return on investment rates.

To gather information about the total annual cost TAC of a plant, the total capital investment TCI and the total operating costs TOC need to be calculated. The fundamental relation is given in Equation 2.55

$$TAC = \frac{TCI}{t_P} + TOC \quad (2.55)$$

with the payback time t_P . Thus, fixed and reoccurring costs are taken together and spread over a period of time. This simple description shall be sufficient for understanding the calculations performed in this thesis. Detailed financial mathematics are required to accurately determine project costs, considering as many external impacts as possible, which can be found in related literature [105, 107, 108, 111, 112]. Software tools like the Aspen Process Economic Analyzer (APEA) greatly reduce the efforts to estimate the key cost indices. A pre-built process flowsheet can be directly imported, allowing mapping and sizing of all relevant process units. Furthermore, additional equipment can be connected and sized if required. A detailed cost analysis can be performed, compared, and refined in simple steps by specifying important input parameters such as raw material and utility prices, tax rate, interest, or depreciation method. [110]

2.2.3.1 Total Capital Investments

The following two chapters shed light on the main contributions to Equation 2.55. The TCI is a fixed amount representing the equipment costs, including land and auxiliaries, referred to as fixed-capital investment and working capital [111]. The fixed-capital investment covers the costs for all plant manufacturing and non-manufacturing parts. The first part includes equipment necessary for the process, typically consisting of the process units, piping, insulation, and instrumentation. Everything unrelated to the production

process is categorized as the non-manufacturing fixed-capital. Examples are the land, buildings for administration or offices, warehouses, laboratories, and permanent installations for transporting or receiving of goods [111]. A certain amount of money must be held back to cover production costs. The working capital marks the second fraction of the *TCI* and includes raw materials and products in stock and cash required to pay salaries, materials, or utilities. Typically, the working capital covers the operation costs for a one-month period [111].

Each contribution to the *TCI* must be either known *a priori* or approximated. Different methods exist to estimate costs for equipment. One frequent approach is the use of a costing index *CI*. Cost indices facilitate historical data to determine recent prices of the sought equipment. If an unit's capacity is different to the original design ($V_1 \neq V_0$), a correction can be applied using an exponent α :

$$C_1 = C_0 \left(\frac{CI_1}{CI_0} \right) \left(\frac{V_1}{V_0} \right)^\alpha . \quad (2.56)$$

Commonly used cost indices are the Chemical Engineering Plant Cost Index (CEPCI), the Nelson Farrer Refinery Construction Index (NF-Index), or the Marshall and Swift Index (M&S) [112]. APEA uses the CEPCI as a basis for calculating equipment prices published and updated yearly by Chemical Engineering.

2.2.3.2 Total Operating Costs

Besides the investment costs, the second contribution to the total annual cost of a plant covers the operating or production costs. One large portion is manufacturing costs, which include all costs related to the actual production. Operating and supervisory labor, raw materials, utilities, and catalysts are examples.

To accurately estimate the total costs, reasonable estimates of the operating costs are required. Labor costs can be assigned to unit operations within the process. Tools such as APEA offer workforce requirement information for each primary equipment type to estimate the number of workers necessary to operate the plant [110]. Another possibility to calculate the costs for each labor type is to use rule-of-thumb percentages to narrow down the operating labor costs to supervision, supply, laboratory, and other charges [109]. For common chemicals, tabulated data can be found indicating labor hours per ton of chemical produced [111].

The raw materials account for up to 50 % of the product costs. Often, it remains challenging to gather recent chemical prices from public sources or literature. Direct quotations are preferred when the highest accuracy is required [111]. Examples of sources for

estimating chemical market prices are *Chemical Week* or *ICIS Chemical Business*. For non-commodity chemicals, fluctuations can be higher and reported market prices might not be available or only for small quantities.

Process utilities are required to provide electricity and energy, which can be supplied by fired heat, steam, cooling water, and refrigerants, among others. The accuracy of cost estimation varies depending on the development stage of the process. While electricity, natural gas, and water prices can be derived from the respective local stock exchange or other sources, the amount of heat needed and the price of steam heavily depends on the level of detail in heat management. Furthermore, steam can be produced on-site or bought from external sources. Generally, a steam network consists of three pressure regimes to provide heat for different temperature levels. Prices for electricity, cooling water, refrigerants, and low, medium, and high-pressure steam can be derived from APEA, allowing for coherence of the cost estimate basis in accordance to the equipment [110].

3 Synthesis of the Novel Epoxy and Properties of the Cured Resin

This chapter summarizes key aspects of J. M. Breitsameter, N. Reinhardt, M. Feigel, O. Hinrichsen, K. Drechsler, B. Rieger, “Synthesis of a Sustainable and Bisphenol A-Free Epoxy Resin based on Sorbic Acid and Characterization of the Cured Thermoset”, *Macromol. Mater. Eng.* **2023**, 2300068, DOI 10.1002/mame.202300068. Respective figures and tables are reprinted with permission.

3.1 Background

Even though the range of applications for epoxy resins has increased in the last years due to their unique material properties, the need to replace their components with environmentally friendly and sustainable alternatives has risen recently. Moving away from fossil resources is one apparent reason. Moreover, in the case of diglycidyl ether of bisphenol A, which is present in around 90 % of epoxy resins [6], also health concerns are a driving force. As discussed in Chapter 1, these are mainly related to using of bisphenol A in the thermosets. Also, the toxicity of epichlorohydrine is to be considered [11, 12]. Despite the plethora of literature on new sustainable epoxy resins [26–43, 50, 113], the aromatic structure of DGEBA permits high thermo-mechanical properties necessary for many applications, which most of the reported alternatives lack. Especially the high glass transition temperature T_g of epoxy thermosets based on DGEBA is crucial in structural applications in the automotive or aerospace sector [114]. Even though some cases achieve desirable T_g -values using natural aromatic building blocks, the epoxy groups are still introduced by reaction with ECH [30, 38, 41]. The proposed, novel molecule 1,2-epoxy-6-methyl-triglycidyl-3,4,5-cyclohexanetri-carboxylate (EGCHC), which is based on bio-based available sorbic acid and allyl alcohol, abstains from the use of BPA or ECH completely [61]. A detailed ecological assessment of the molecule is given in Section 3.4. The conducted synthesis route covering all reaction steps is illustrated in Figure 3.1.

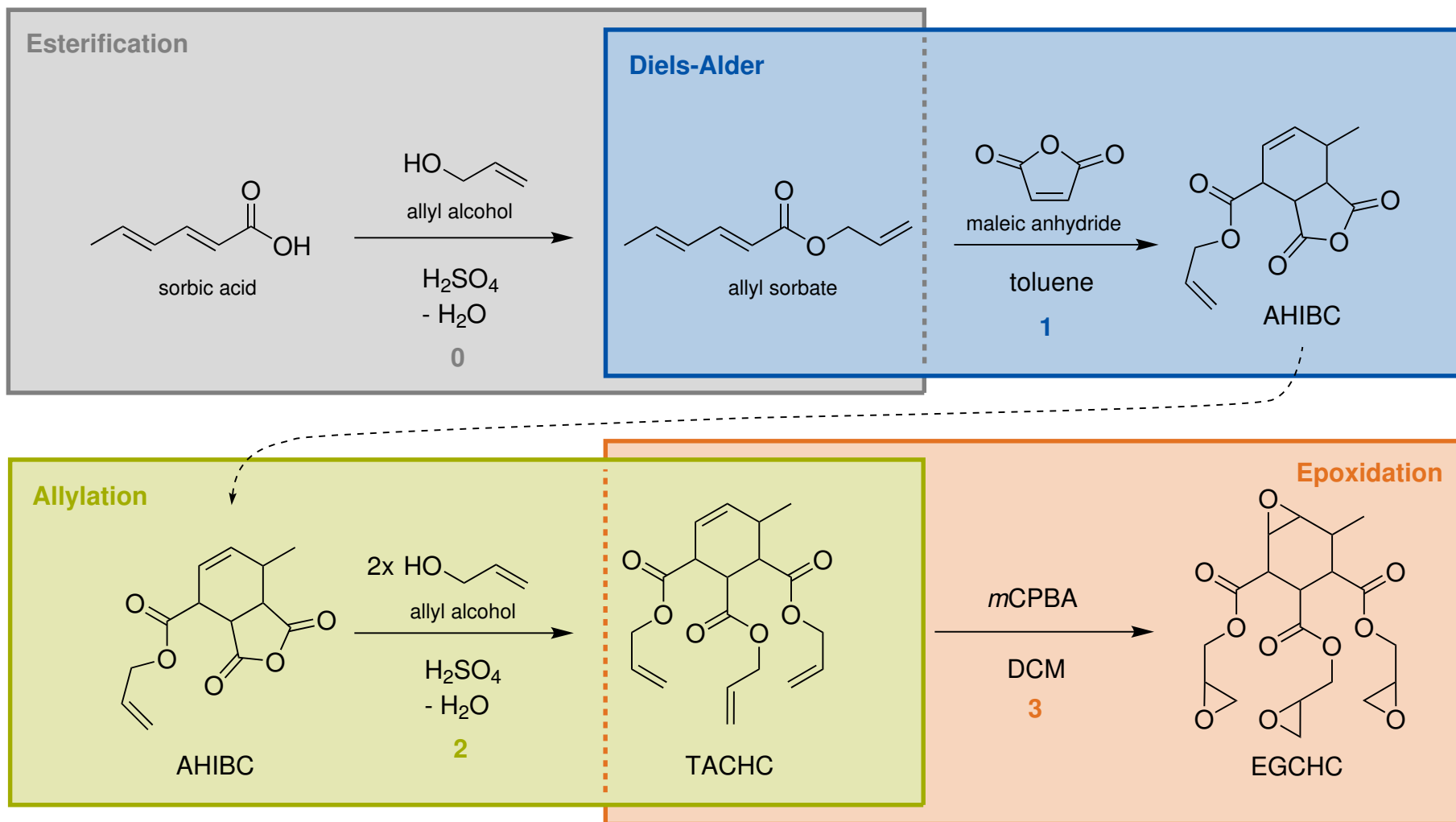


Figure 3.1: Reaction steps for the synthesis of the epoxy EGCHC starting from sorbic acid. Modified from [61].

3.2 Synthesis of EGCHC

Starting from bio-available sorbic acid, four reaction steps are proposed to synthesize EGCHC [61]. The steps will be referred to with numbers from **0–3**. The initial esterification (**0**) is later excluded from kinetic and process modeling as allyl sorbate is a commercially available product used as a food flavoring agent [115–117]. Hence, reaction **0** is only depicted to gain a whole view of the synthesis route starting from sustainable educts. Steps **1–3** are the main focus of the kinetic and process modeling study in Chapter 4 and Chapter 5.

The synthesis procedure is shortly summarized according to Breitsameter et al. [61]. For a detailed synthesis and purification protocol, the original publication is recommended [61]. Reaction progress is monitored by $^1\text{H-NMR}$. Details on the analysis are given in the Supporting Material of Chapter 4 and [61].

Solid sorbic acid is dissolved in allyl alcohol and heated to reaction temperature. The reaction is started by adding catalytic amounts of sulfuric acid (0.5 vol%) and performed under reflux and isothermal conditions by applying continuous stirring. After extraction and purification using distillation, allyl sorbate is obtained as a colorless liquid. In synthesis step **1**, a Diels-Alder reaction between previously formed allyl sorbate and maleic anhydride is conducted. Toluene is used as a solvent and heated to reflux conditions. Maleic anhydride, which was beforehand dissolved, undergoes a [4 + 2]-cycloaddition with the conjugated double bonds of allyl sorbate. The product allyl 7-methyl-1,3-dioxo-1,3,3a,4,7,7a-hexahydroisobenzofuran-4-carboxylate (AHIBC) is received after crystallization. The collected solid AHiBC is then dissolved in allyl alcohol and heated until reflux is reached. With the addition of catalytic amounts of sulfuric acid, the ring-opening and condensation reaction **2** is started. The product triallyl-6-methylcyclohex-4-ene-1,2,3-tricarboxylate (TACHC) is obtained as a colorless oil after extraction from the solvent and purification using column chromatography. In the last step **3**, TACHC and *meta*-chloroperbenzoic acid (*m*CPBA) are added together with DCM as a solvent at room temperature. Formed *meta*-chlorobenzoic acid (*m*CBA) is not soluble in DCM and precipitates out of solution. After filtration, solvent removal, and drying, the epoxy 1,2-epoxy-6-methyl-triglycidyl-3,4,5-cyclohexanetricarboxylate (EGCHC) is received. The concentrations and weight yields from each synthesis step are summarized in Table 3.1.

Table 3.1: Synthesis summary with concentrations and mass yields of each reaction step [61].

#	Reagent 1	c_1^a / mol/L	Reagent 2	c_2^a / mol/L	Solvent	Yield Y^b / %
0	sorbic acid	2.23	allyl alcohol	-	allyl alcohol ^c	82
1	allyl sorbate	10.00	maleic anhydride	10.20	toluene	84
2	AHIBC	0.84	allyl alcohol	-	allyl alcohol ^c	81
3	TACHC	0.23	<i>m</i> CPBA	1.84	DCM	78

^aconcentration here defined as mole component divided by volume solvent.

^bmass yield.

^cwith catalytic amounts of H₂SO₄ (0.5 vol%).

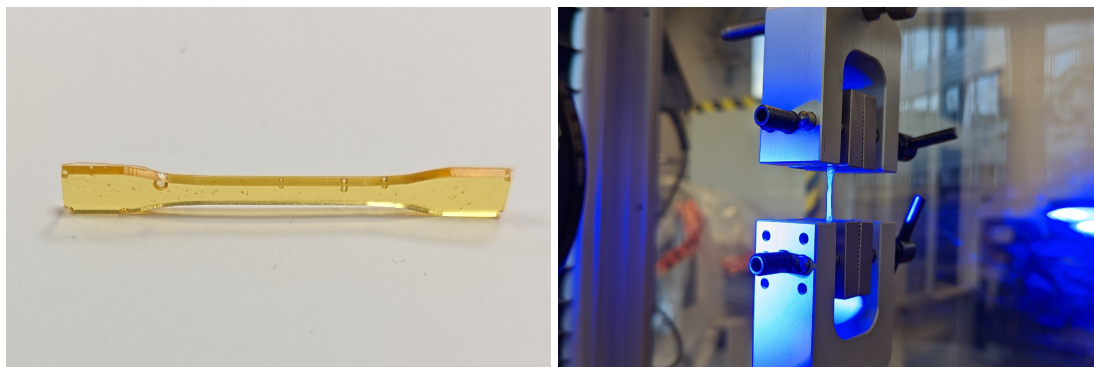
3.3 Curing of EGCHC

As the mechanical properties of the cured resins are a crucial parameter, the curing procedure of EGCHC is explained. Additionally, DGEBA samples were cured with identical hardeners to compare the novel, sustainable epoxy resin with an industrial standard resin. Two commonly used amine-based curing agents are selected: isophorone diamine (IPD) and commercially available Jeffamine®T-403 [118, 119]. The samples are transferred into silicone molds and cured in an oven after rigorous mixing of the epoxy and the respective curing agent in an equimolar ratio. The curing procedures are summarized in Table 3.2. Details and process parameters can be extracted from Breitsameter et al. [61]. For mechanical testing, i.e., tensile strength and modulus, dog-bone structures are

Table 3.2: Summary of curing procedure conditions for EGCHC and DGEBA samples [61].

Sample	Molar mixing ratio / -	Curing time / h	Curing temperature / °C	Post-curing time / h	Post-curing temperature / °C
EGCHC + IPD	1.0	0.5	45	0.5	120
EGCHC + T-403	1.0	2.0	60	2.0	100
DGEBA + IPD	1.0	2.0	60	2.0	160
DGEBA + T-403	1.0	3.0	80	2.0	120

prepared as shown in Figure 3.2a following the small geometry 1BB from DIN EN ISO 527-2 [120]. The geometry is chosen as the structure volume is minimal and produced sample masses are limited. Care needs to be taken so that the structures show no defects that could alter the measurement results. Defects comprise air inclusions, as seen in Figure 3.2a. Measurements are performed in an Inspekt 100 (Hegewald & Peschke, Germany) displayed in Figure 3.2b in accordance to [61]. Tensile testings are repeated five times with an elongation speed of 0.125 mm/min.



(a) Dog-bone structure of EGCHC cured with IPD with air inclusions. (b) Cured EGCHC sample with IPD after tensile testing.

Figure 3.2: Tensile testing after DIN EN ISO 527-2 of cured EGCHC and DGEBA samples [120].

Glass transition temperatures T_g are measured using dynamic mechanical analysis (DMA). Three samples are tested for each epoxy and curing agent combination. The specimen is heated with a constant heating ramp of 2 K/min under an oscillating tensile load. For details, the original publication is recommended [61].

Table 3.3 summarizes the key results of the thermo-mechanical analyses of the cured resins. The glass transition temperature T_g together with the tensile modulus and strength are tabulated for the four samples. The curing agent IPD shows superior material properties for all samples compared to T-403 if stiffness at high temperatures is required. Due to the cycloaliphatic structure of IPD, a more rigid cross-linked network can be established [61]. As EGCHC also has more oxirane functionalities, the cross-link density is increased for resins consisting of the novel epoxy. Thus, the EGCHC-containing samples are stiffer compared to the respective samples with DGEBA. However, T_g is lower in EGCHC-based resins. Because of the aromatic structure of DGEBA, strong π - π interactions are formed, leading to very high glass transition temperatures compared to EGCHC [61].

Table 3.3: Glass transition temperature, tensile modulus and tensile strength for the four cured samples [61].

Sample	T_g / °C	Tensile modulus / MPa	Tensile strength / MPa
EGCHC + IPD	129.8 ± 6.2	3964.5 ± 285.3	75.5 ± 17.1
EGCHC + T-403	56.5 ± 1.3	3622.1 ± 166.5	51.7 ± 6.1
DGEBA + IPD	161.7 ± 0.4	3138.6 ± 184.2	67.5 ± 3.7
DGEBA + T-403	82.0 ± 1.2	2926.5 ± 153.4	54.0 ± 5.5

3.4 Ecological Assessment

The ecological assessment of the synthesis route illustrated in Figure 3.1 is based conservatively on readily available components on a larger scale. Alternatives or published bio-based syntheses are mentioned where applicable. The calculations utilize a carbon balance applying the standard ASTM D6866 [121].

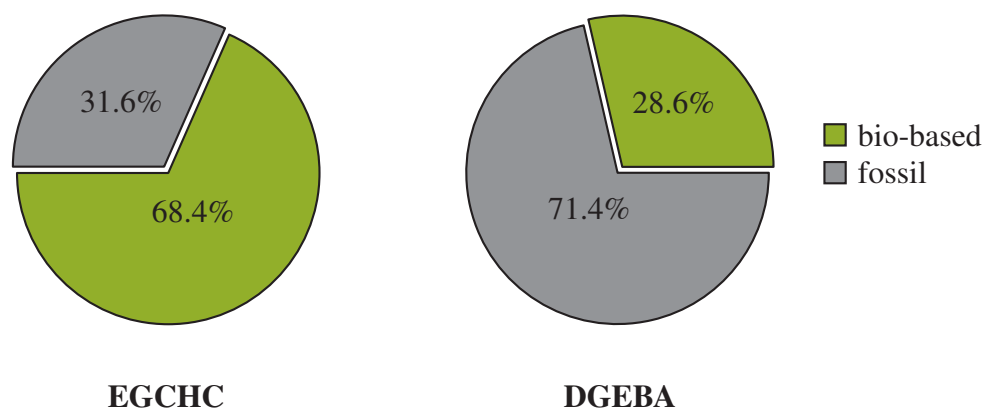


Figure 3.3: Comparison of bio-based carbon content between epoxy EGCHC (left) and industrial standard DGEBA (right) using ASTM D6866 [121].

In principle, both components in the esterification step **0** are bio-based. Sorbic acid can be derived as a natural feedstock from rowan berries [63, 64]. However, the industrial production of the preserving agent is performed using malonic acid and crotonaldehyde [122]. The latter is readily bio-available [123, 124], leading to a total bio-based content of 66.7 % for sorbic acid. Allyl alcohol can fully be derived from natural resources [65, 66]. Hence, the calculated bio-based fraction of the intermediate allyl sorbate is 77.8 %. In step **1**, maleic anhydride is added to the diene forming AHIBC in a Diels-Alder reaction. Maleic anhydride is a fossil commodity chemical produced on an industrial scale from partial oxidation of *n*-butane [125–128] or benzene [126, 128]. Even though plenty of bio-based routes have been published, no realized pilot or industrial-scale plants are operating [67, 68, 129–132]. Therefore, fossil-originating maleic anhydride is taken into consideration, reducing the bio-based content to 53.8 % for AHIBC. As now allyl alcohol is added twice in reaction step **2**, the bio-based content of TACHC increases to 68.4 %. This also marks the final bio-based content for the epoxy EGCHC since only oxygen atoms are incorporated in the epoxidation step, which is not tracked by the ASTM method. A best-case scenario is pursued to compare EGCHC with the industrial standard epoxy DGEBA. Thus, 100 % bio-based epichlorohydrin is assumed in the synthesis of DGEBA. Green ECH can readily be acquired in large quantities from the Epicerol® process [9, 10]. Consequently, the bio-based content of DGEBA can be improved up to 28.6 %.

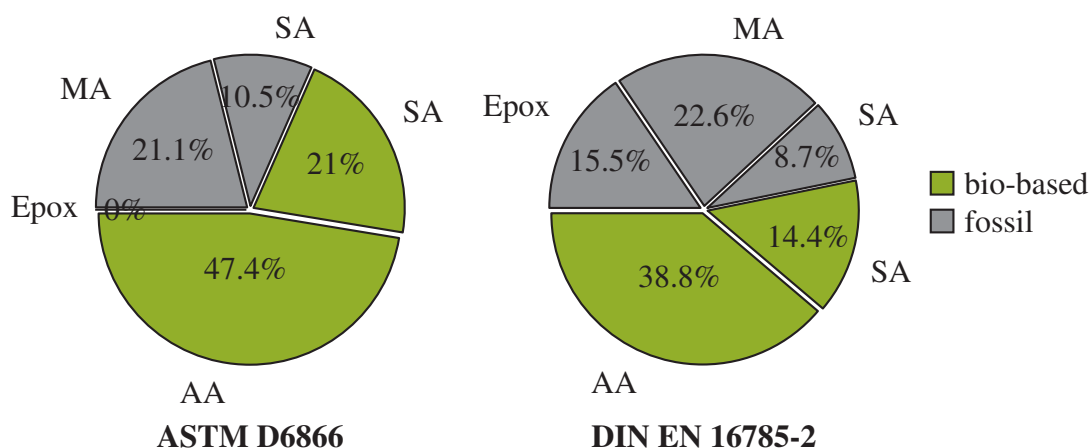


Figure 3.4: Contribution of different components to the total bio-based content of EGCHC calculated using ASTM D6866 [121] (left) and DIN EN 16785-2 [133] (right). SA: sorbic acid, AA: allyl alcohol, MA: maleic anhydride, Epox: epoxidation with *m*CPBA.

Analyzing the bio-based content of EGCHC over the synthesis route applying DIN EN 16785-2 leads to 53.2% [133]. The slightly lower reported content stems from a more extended approach than only a carbon balance, which also considers H-, N-, and O-atoms. Thus, the epoxidation step lowers the bio-originating content as fossil-based *m*CPBA is taken as an oxidizing agent. To better visualize the contributions of each reaction step and component on the total bio-based content of EGCHC, Figure 3.4 illustrates the shares for both standards. Sorbic acid contributes to both contents due to the assumption being derived partially bio-based.

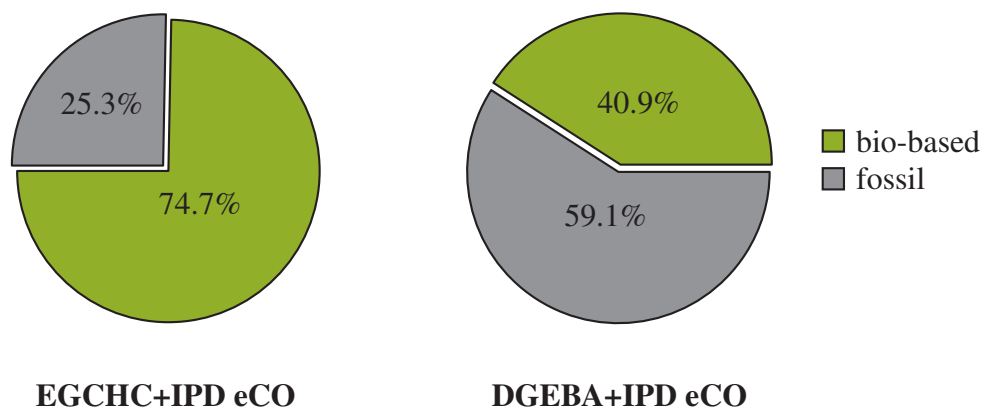


Figure 3.5: Comparison of bio-based carbon content of cured resins EGCHC and IPD eCO (left) and DGEBA and IPD eCO (right) using ASTM D6866 [121].

The cured samples are also compared using their bio-based theoretical content, as the total bio-based content of a resin consisting of epoxy and curing agent is often given. The curing agent of interest for the ecological assessment is isophorone diamine (IPD). IPD

is a common amine-based curing agent produced from acetone [118]. Despite the conventional fossil availability, EVONIK recently launched sustainable amine-based cross-linkers [134]. Renewable IPD (90 % bio-based carbon) is sold under the trade name VESTAMIN® IPD eCO [135]. Figure 3.5 illustrates the achievable bio-based contents for EGCHC and DGEBA. As the curing agent is assumed to have 90 % bio-based carbon, the content of renewable carbon rises in comparison to Figure 3.3 for both cases. The cured resin containing EGCHC shows a minor increase due to the larger molecular mass of EGCHC compared to DGEBA and an equimolar curing ratio.

3.5 Conclusion

A novel, highly sustainable molecule, derived from easily obtainable building blocks, is introduced. EGCHC, which is completely BPA- and ECH-free, shows promising thermo-mechanical properties while maintaining a high bio-based carbon content. Starting from natural available sorbic acid and allyl alcohol, a synthesis route is presented, covering four major reaction steps. After an esterification of the respective components, maleic anhydride is added in a [4 + 2]-cycloaddition. The intermediate molecule AHIBC is then again reacted with allyl alcohol, forming TACHC, which has distinct terminal double bonds that are epoxidized in the last step. The resulting compound EGCHC has four oxirane functionalities and is, therefore, capable of acting as a cross-linking agent. Even though some of the components and solvents used are of fossil origin, alternatives or published bio-based routes to these molecules are shown. Hence, the presented structure could be produced fully bio-based once these alternatives become technically and economically feasible. The cured resins with IPD show auspicious thermo-mechanical properties. EGCHC exceeds the measured values of the industrial standard DGEBA for tensile modulus and strength. The slightly lower T_g still allows the EGCHC systems to be employed in various applications. The ecological assessment revealed a high bio-based content of EGCHC of 68.4 %, which makes the epoxy a promising alternative to its fossil competitors. Additionally, the synthesis completely abstains from the use of BPA or ECH.

4 Kinetic Modeling of the Synthesis Steps

Abstract

The homogeneous catalytic reaction steps for the production of 1,2-epoxy-6-methyl-triglycidyl-3,4,5-cyclohexanetricarboxylate (EGCHC) starting from allyl sorbate were studied. The promising largely bio-based bisphenol A and epichlorohydrine-free epoxy compound was synthesized with a three-step reaction network consisting of a Diels-Alder reaction with maleic anhydride, an esterification with allyl alcohol, and an epoxidation with 3-chloroperbenzoic acid. All reactions were performed batchwise in defined temperature ranges between 2 and 103 °C depending on the respective reaction. Reaction progress was monitored with ¹H-NMR spectroscopy. For all studied reactions, kinetic models were established and regressed with acquired experimental data to gather information about pre-exponential factors and activation energies. A model comparison for the esterification using both maximum likelihood and parsimony showed that the reaction is second order and proceeds through two intermediates toward the product. Moreover, the reactivity of the different double bond types in the epoxidation is compared and discussed. The postulated models fitted well with the experimental measurements and thus were found to accurately describe the underlying reaction mechanisms.

Bibliographic Information

M. Feigel, J. M. Breitsameter, K. Lechner, B. Rieger, O. Hinrichsen, "Kinetic Modeling of the Synthesis Path for the Production of a Sustainable Epoxy Resin based on Allyl Sorbate", *Industrial & Engineering Chemistry Research* **2023**, 62, 13389–13400.

Copyright Notice

©2023 American Chemical Society. This is an accepted version of this article published in doi:10.1021/acs.iecr.3c01317. Clarification of the copyright adjusted according to the guidelines of the American Chemical Society.

4.1 Introduction

Epoxy resins are an important material crucial in various applications and across different industry sectors ranging from construction over electronics to coatings due to their easy handling and processing [1–3]. In general, the resin consists of a two component system: the polyepoxide containing multiple oxirane oxygen and a curing agent. The strength and nature of the forming network of cross-links depend on the curing agent's functional groups, which can be amines, acids, alcohols, and mercaptanes among others. The most common epoxy thermoset is synthesized using the bisphenol A (BPA) and epichlorhydrine (ECH) route. Concerns about the toxicity of bisphenol A arouse in the past and are still today a relevant topic [13, 136]. The risks and hazardous characteristics of bisphenol A led to a ban of BPA in certain food and beverage contact materials and restricted limits in other applications in the European Union [14, 17, 18]. Ultimately, as research is still ongoing and public opinion shifts due to "BPA-free" marketing campaigns, a ban of BPA-based chemicals in other fields could follow. Furthermore, as the commercial production of both BPA and ECH is mostly based on fossil resources, a transition to bio-based alternatives is indispensable. Epichlorhydrine can readily be synthesized from sustainable resources using bio-based glycerin. This route is already conducted industrially on a kiloton scale and constitutes 20 % of the total bio-based platform chemicals in Europe [9]. For BPA no such route exists. Therefore, the production of the commonly used bisphenol A diglycidyl ether (DGEBA) leads to a total bio-based fraction of 33.5 % using green ECH. Advancing towards climate-friendly and sustainable alternatives is a vital part of present research as the most commonly used epoxy resins rely on fossil resources and toxic raw materials. The availability of commercially distributed so-called bio-based epoxy resins is limited both in number and maximum stated bio-based content [137]. While these products try to increase their ecological footprint, they still rely on BPA.

Previously, we reported a novel synthesis route to an epoxy compound which can readily be produced with a bio-based content of > 68 % and also is completely BPA free [61]. Additionally, the chemicals used in the current synthesis strategy can reportedly be produced with renewable resources [67, 68, 138] or alternatives are at hand [52, 59]. Furthermore, synthesized 1,2-epoxy-6-methyl-triglycidyl-3,4,5-cyclohexanetricarboxylate (EGCHC) cured with isophorone diamine (IPD) shows promising mechanical properties with high glass transition temperatures up to 131 °C and a tensile stress of up to 50 MPa. IPD is available with a bio-based carbon content of up to 90 % [135] further increasing in that case the total bio-based carbon content of the cured resin to 75 %, exceeding competitors [137] while maintaining the required thermo-mechanical properties [61].

As the proposed novel molecule shows promising properties, details on the reaction should pave the way for further elaboration on the production. Thus, reaction models of

the crucial reaction steps are postulated. Thereby gathered kinetic models are fitted with experimental data to get insights on the different reactions. The production of the epoxy EGCHC consists of four main reactions starting from sorbic acid and allyl alcohol. As the first step comprises the esterification to allyl sorbate, which is already commercially available as a flavouring agent [115, 116], this step is excluded from the kinetic modeling. Thus, starting from allyl sorbate, each of the three subsequent reaction steps is kinetically modeled in detail. Therefore, the reaction progress is examined on a laboratory scale in a batch reactor, and adequate reaction models are regressed with therein gathered data. Non-linear parameter fitting using a standard least squares approach is applied as a regression tool due to the stiff nature of the underlying differential equations. A total number of 652 experimental observations are used for kinetic modeling. Model discrimination is performed using classical information criteria if applicable.

4.2 Experimental

4.2.1 Materials

All chemicals were purchased from Sigma-Aldrich unless otherwise noted and were used as received: sorbic acid ($\geq 99.0\%$), allyl alcohol ($\geq 98.5\%$), maleic anhydride ($\geq 99.0\%$), sulfuric acid (H_2SO_4 , ACS reagent, 95.0 to 98.0%), toluene (ACS reagent, $\geq 99.5\%$), diethyl ether ($\geq 99.9\%$, suitable for HPLC, inhibitor free), 3-chloroperbenzoic acid (*m*CPBA, $\geq 77\%$), methylene chloride (DCM, suitable for HPLC, $\geq 99.8\%$, contains 40 to 150 ppm amylene as stabilizer), $\geq 99.5\%$), methyl 3,5-dinitrobenzoate (99%), sodium thiosulfate ($\text{Na}_2\text{S}_2\text{O}_3$, ACS reagent, 99%).

4.2.2 Kinetic Experiments

4.2.2.1 General Procedure

All experiments were conducted in a laboratory-scale three-necked-flask equipped with a magnetic stirrer, a condenser, and thermocouples. If not described differently, samples of roughly 0.1 mL were taken with the help of a syringe and diluted to 0.5 mL in a NMR-tube with chloroform- d_3 . The reaction progress of each reaction was monitored with ^1H -NMR: δ . Detailed information on the analysis method and synthesis procedure can be found in the Supplementary Information and our previous publication [61]. Total sample

volumes were kept < 5 % of the reaction volume. Thus, all reactions are modeled in batch with the assumption of constant volume over reaction time. Ideal mixtures are assumed which was realized by rigorous stirring. Isothermal conditions were achieved using oil or cooling baths, respectively. The temperature was continuously monitored with the help of thermocouples.

4.2.2.2 Diels-Alder Reaction

Allyl sorbate was prepared by dissolving sorbic acid (50 g) in allyl alcohol (200 mL) with catalytic amounts of H_2SO_4 (1 mL). The product was extracted with diethyl ether and purified by distillation. Maleic anhydride (13.40 mmol, 1.31 g, 1.02 eq) was dissolved in toluene (100 mL) and heated to the desired temperature. The reaction was started with the addition of allyl sorbate (13.14 mmol, 2 g). The Diels-Alder product with the name allyl 7-methyl-1,3-dioxo-1,3,3a,4,7,7a-hexahydroisobenzofuran-4-carboxylate (AHIBC) was gathered as a white solid after crystallizing.

4.2.2.3 Esterification

The product of the Diels-Alder reaction (1.0 g, 4.0 mmol) was dissolved in allyl alcohol (5 mL). The mixture was heated to the desired temperature and the reaction started by the addition of the catalyst sulfuric acid (0.025 mL, 0.5 vol%). Samples were either measured immediately or cooled to $-30\text{ }^\circ\text{C}$ to prevent further reaction. The yielded triester with the name triallyl-6-methylcyclohex-4-ene-1,2,3-tricarboxylate (TACHC) was further functionalized in an epoxidation reaction.

4.2.2.4 Epoxidation

TACHC (0.5 g, 1.44 mmol) and 3,5-dinitrobenzoate (standard for quantification in NMR-spectroscopy) were diluted in DCM (30 mL) and heated to the desired temperature. In the case of the reaction at $1.6\text{ }^\circ\text{C}$ the mixture was cooled with the help of an ice-bath. The reaction was started by the addition of *m*CPBA (3.54 g, 2.05 mmol, 10 eq). Samples were prepared by quenching an aliquot of roughly 0.3 mL with a saturated solution of $\text{Na}_2\text{S}_2\text{O}_3$ to remove excess *m*CPBA. The organic phase was then concentrated *in vacuo*, and the residue was dissolved in chloroform- d_3 .

4.3 Model Development

The models used in this report are regressed with the experimental data which are acquired with the beforehand stated procedures and analysis methods. For each of the three reactions, an adequate reaction model is chosen which is described in the following sections.

4.3.1 Diels-Alder Reaction

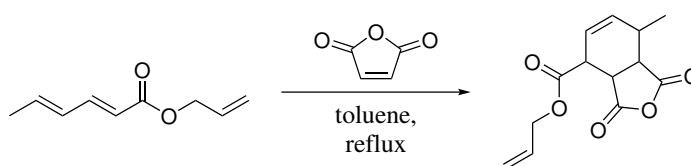


Figure 4.1: Diels-Alder reaction of allyl sorbate and maleic anhydride to AHIBC.

For the implementation of the Diels-Alder reaction between allyl sorbate (AS) and maleic anhydride (MA), which is displayed in Figure 4.1, an irreversible reaction second order is assumed [139–141]. The possible retro Diels-Alder reaction is neglected since only low to medium temperatures are used in the performed experiments. Due to the high exothermicity of the reaction ($\Delta_r H^0 = -185.5 \text{ kJ/mol}$), educt concentrations are in a limited range with enough solvent to ensure isothermal conditions. The reaction rate of each component can thus be described with the help of Equation 4.1:

$$\frac{dc_i}{dt} = -k_{\text{DA}} c_{\text{AS}} c_{\text{MA}} \quad (4.1)$$

with the reaction rate constant k_{DA} and the molar concentration c_i of component i . This second order reaction can readily be solved analytically. The solution for the case $c_{\text{AS},0} \neq c_{\text{MA},0}$ ($\alpha \neq 0$) is shown in Equation 4.2:

$$\alpha = c_{\text{AS},0} - c_{\text{MA},0} \quad (4.2a)$$

$$c_{\text{AS}} = \frac{\alpha}{1 - \left(1 - \frac{\alpha}{c_{\text{AS},0}}\right) \exp(-k_{\text{DA}} t \alpha)} \quad (4.2b)$$

The conversion of allyl sorbate X_{AS} is then calculated with Equation 4.3.

$$X_{\text{AS}} = 1 - \frac{c_{\text{AS}}}{c_{\text{AS},0}} \quad (4.3)$$

The AS conversion X_{AS} is directly measured by $^1\text{H-NMR}$ as shown in Figure 4.13. Therefore, the progress of the Diels-Alder reaction of AS with MA can be tracked by analysing the timely resolved spectra displayed in Figure 4.14. Hence, a single response variable is regressed. In contrast to the other reactions, the simplicity of the underlying rate law in Equation 4.1 allows the direct regression of its analytical solution shown in Equation 4.2.

4.3.2 Esterification

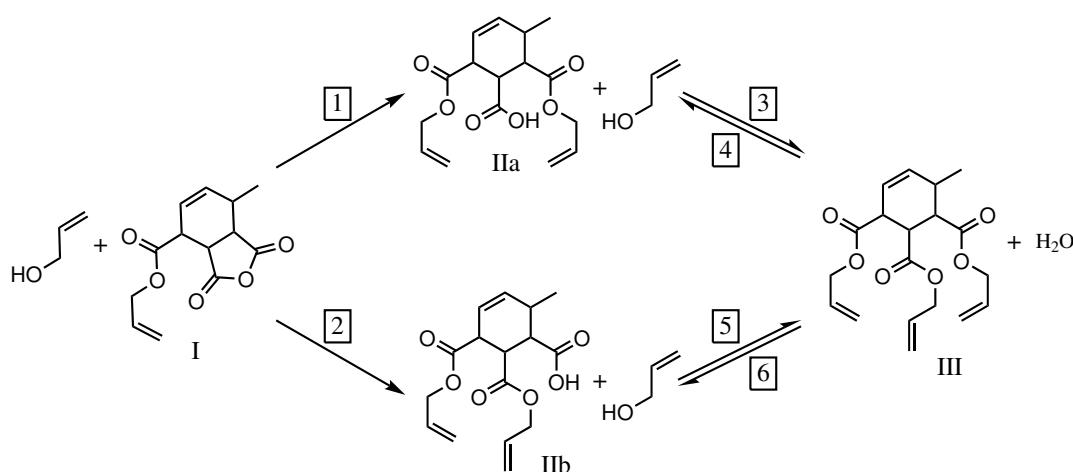


Figure 4.2: Acid catalyzed reaction path of the esterification reaction starting from the Diels-Alder product (I) to TACHC (III) via the two intermediates IIa and IIb.

The mechanism of the esterification reaction is displayed in Figure 4.2. The first reaction step opens the anhydride of structure I (AHIBC, Diels-Alder product) and leads to the diester IIa or IIb, respectively. The reaction is acid catalyzed and can be assumed to be irreversible [142]. Due to the fact that the initial reactant is not symmetric, two different possibilities for the addition of allyl alcohol exist. It is expected that the electronic configuration with the proximate carboxylate group influences the opening of the anhydride ring and therefore preferably builds intermediate IIb. Thus, two different reactivities and consequently kinetic constants need to be considered. Subsequently, allyl alcohol reacts with the free acid functionality of the opened anhydride ring in a condensation reaction to form product III and water. As sulfuric acid acts as a catalyst, the concentration of the mineral acid is supposed to be constant. Therefore, the reactions are modeled with $k_i^* = k_i \cdot c_{\text{H}_2\text{SO}_4}$. Thus, a reaction scheme can be drawn with the to be considered kinetic constants. From Figure 4.2 the number of kinetic constants required to describe the reaction paths towards TACHC can be extracted with the above stated considerations. In total six reactions are distinguished while for this reaction different models will be tested due to the plethora of variables. Parameter reduction is performed by equal reactivity assumptions. All forward

reactions are second order with allyl alcohol (AA) as the second reagent. The reverse reactions 4 and 6 are second order with the condensation product water as the second component.

The formation rate of each species can therefore be set up. The system of differential equations is shown in Equation 4.4 comprising all four reaction paths and six kinetic constants k_i as illustrated previously in Figure 4.2.

$$\frac{dc_I}{dt} = -(k_1 + k_2)c_I c_{AA} \quad (4.4a)$$

$$\frac{dc_{IIa}}{dt} = +k_1 c_I c_{AA} - k_3 c_{IIa} c_{AA} + k_4 c_{III} c_{H_2O} \quad (4.4b)$$

$$\frac{dc_{IIb}}{dt} = +k_2 c_I c_{AA} - k_5 c_{IIb} c_{AA} + k_6 c_{III} c_{H_2O} \quad (4.4c)$$

$$\frac{dc_{III}}{dt} = +k_3 c_{IIa} c_{AA} + k_5 c_{IIb} c_{AA} - (k_4 + k_6) c_{III} c_{H_2O} \quad (4.4d)$$

The change in concentration c_i of the species I, IIa, IIb, and III is monitored by $^1\text{H-NMR}$. A detailed description of the spectra and procedure is given in the Supplementary Information. The reaction progress can be extracted from the timely measured spectra as seen in Figure 4.16. The areas F_i from the spectra are direct proportional to the concentration of each component and are referenced to the signal area F_{tot} which includes all components as illustrated in Figure 4.15. The concentrations are determined using the initial concentration of component I $c_{I,0}$ known from weighed portion as illustrated in Equation 4.5.

$$c_i(t) = f_i \cdot c_{I,0} = \frac{F_i}{F_{\text{tot}}} \cdot c_{I,0} \quad (4.5)$$

Similarly, the initial concentration of AA is calculated from the known amount added as described in the experimental procedure. Thereof collected concentration data of components I, IIa, IIb and III are employed for fitting the postulated models. Due to only narrow shifts between the resonance signals of IIa and III, the areas can in some cases not be solely integrated leading to a sum of $c_{IIa} + c_{III}$.

Different models are tested and compared using best likelihood and maximum parsimony. Mathematical details can be extracted from the Statistical Analysis section in the Supplementary Information. The applied models are listed in Table 4.1 and are based on Figure 4.2. The number of parameters n_{par} includes both pre-exponential factor and activation energy. Hence, the value is twice the number of regarded reactions or can be deduced from the number of equal reactivity assumptions: $(6 - n_{\text{assum}}) \cdot 2$. Even though already neglected, model 1 treats reactions 1 and 2 as reversible leading to a total number of 16 parameters. Model 2 represents the scheme drawn in Figure 4.2 with individual kinetic constants for each reaction. In contrast to that, model 3 assumes both reverse reactions to be kinetically equal ($k_4 = k_6$), while model 4 sets forward and backward

reaction of the second step equal. In model 5, all forward reactions of each path are treated equally. Furthermore, model 6 simplifies the reaction network by taking identical reactivity of forward and backward reactions for all steps into consideration.

Table 4.1: Selection of different tested models for the esterification reaction of the Diels-Alder product with allyl alcohol.

Model number	n_{par}	Assumption
1	16	reversible reactions for the first step
2	12	irreversible reactions for the first step
3	10	$k_4 = k_6$
4	8	$k_3 = k_5; k_4 = k_6$
5	8	$k_1 = k_3; k_2 = k_5$
6	6	$k_1 = k_2; k_3 = k_5; k_4 = k_6$

4.3.3 Epoxidation

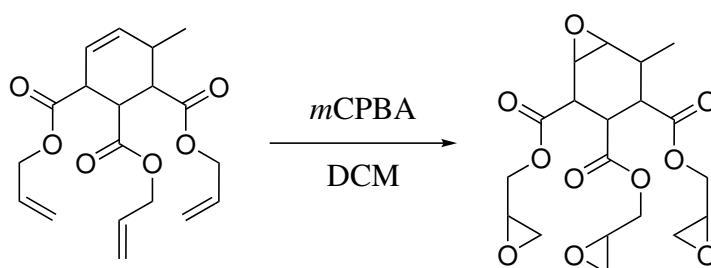


Figure 4.3: Simplified epoxidation reaction of TACHC with *m*CPBA forming EGCHC.

The product of the esterification step TACHC has two distinct sites for epoxidation. The double bond in the hexene ring, which stems from the [4 + 2] cycloaddition, and three terminal double bonds. The terminal bonds belong to the former AA. All reactions are irreversible, first-order in each reactant and bimolecular as generally considered for the epoxidation of alkenes [143–146]. In the following, the single double bond within the ring will be referred to as R, whereas a terminal bond with T. It is assumed that each bond T behaves equally in the epoxidation reaction and therefore cannot be distinguished. As a result, a reaction scheme can be developed which depicts each possible route from TACHC to EGCHC. Figure 4.4 illustrates the reaction paths with all potential components named after the number and type of double bond which are converted. The product EGCHC is equivalent to RTTT. For better visibility, *m*CPBA is not shown as a reactant in the scheme due to its presence in all pathways. As a consequence of the similar structure of the terminal bonds and equal reactivity assumption the reaction scheme is defined by two rate constants k_r and k_t , respectively. The rate constant k_t , which describes the epoxidation of terminal bonds T, is adjusted by a probability factor taking into account the number of

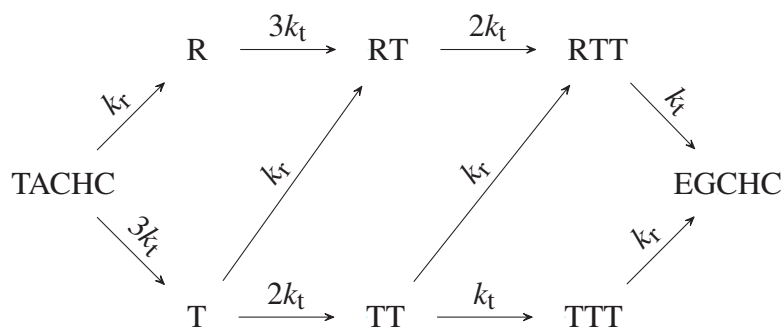


Figure 4.4: Possible reaction paths of the step-wise epoxidation of TACHC with indication of the respective rate constants for terminal k_t or ring-bound double bonds k_r .

possible victim double bonds. In the beginning, either R or T can first be epoxidized. As there are three terminal bonds available, the kinetic constant is multiplied by a factor of three. If the terminal bond reacts first (species T), again two possibilities exist: epoxidation of R (species RT) or again introducing a terminal oxirane functionality (species TT). All further reaction steps can be described in an analogous way. Equation 4.6a–Equation 4.6h define the rate laws for the kinetic model resulting from Figure 4.4.

$$\frac{dc_{\text{TACHC}}}{dt} = c_{m\text{CPBA}}(-k_r c_{\text{TACHC}} - 3k_t c_{\text{TACHC}}) \quad (4.6a)$$

$$\frac{dc_R}{dt} = c_{m\text{CPBA}}(+k_r c_{\text{TACHC}} - 3k_t c_R) \quad (4.6b)$$

$$\frac{dc_T}{dt} = c_{m\text{CPBA}}(+3k_t c_{\text{TACHC}} - k_r c_T - 2k_t c_T) \quad (4.6c)$$

$$\frac{dc_{\text{RT}}}{dt} = c_{m\text{CPBA}}(+k_r c_T + 3k_t c_R - 2k_t c_{\text{RT}}) \quad (4.6d)$$

$$\frac{dc_{\text{TT}}}{dt} = c_{m\text{CPBA}}(+2k_t c_T - k_r c_{\text{TT}} - k_t c_{\text{TT}}) \quad (4.6e)$$

$$\frac{dc_{\text{RTT}}}{dt} = c_{m\text{CPBA}}(+2k_t c_{\text{RT}} + k_r c_{\text{TT}} - k_t c_{\text{RTT}}) \quad (4.6f)$$

$$\frac{dc_{\text{TTT}}}{dt} = c_{m\text{CPBA}}(+k_t c_{\text{TT}} - k_r c_{\text{TTT}}) \quad (4.6g)$$

$$\frac{dc_{\text{EGCHC}}}{dt} = c_{m\text{CPBA}}(+k_t c_{\text{RTT}} + k_r c_{\text{TTT}}) \quad (4.6h)$$

The used analysis method $^1\text{H-NMR}$ only allows to examine the depletion of double bonds with a distinction in terminal T or ring-bound R. This is shown in a characteristic spectrum drawn in Figure 4.18. As it is not possible to distinguish the individual terminal double bonds, the model is regressed with the conversion of each type of double bond X_i . The conversions X_R and X_T are defined in Equation 4.7 and Equation 4.8 with respect to the reaction species of Figure 4.4 and the initial concentration of the educt $c_{\text{TACHC},0}$:

$$X_R = 1 - \frac{1}{c_{\text{TACHC},0}} \left[c_{\text{TACHC}} + c_T + c_{\text{TT}} + c_{\text{TTT}} \right] \quad (4.7)$$

$$X_T = 1 - \frac{1}{c_{\text{TACHC},0}} \left[c_{\text{TACHC}} + c_R + \frac{2}{3}(c_T + c_{\text{RT}}) + \frac{1}{3}(c_{\text{TT}} + c_{\text{RTT}}) \right], \quad (4.8)$$

where c_i denotes the molar concentration of species i . The measured values for X_R and X_T are used as the response variables for the fitting approach. Hence, both pre-exponential factor $k_{0,r}$, $k_{0,t}$ and activation energies $E_{A,r}$, $E_{A,t}$ can be determined.

An important property of epoxy resin components is their oxirane oxygen content OOC which is defined as the molar mass of epoxy group oxygen atoms divided by the total molar mass of the molecule M_{tot} :

$$OOC = \frac{N_{\text{OO}} \cdot M_{\text{O}}}{M_{\text{tot}}} \quad (4.9)$$

with the number of oxirane oxygen atoms N_{OO} and the molar mass of oxygen M_{O} . In the model, OOC is calculated with Equation 4.10:

$$OOC = \frac{1}{c_{\text{TACHC},0}} \cdot \left[\left(\frac{c_R + c_T}{\omega + 1} \right) + 2 \left(\frac{c_{\text{RT}} + c_{\text{TT}}}{\omega + 2} \right) + 3 \left(\frac{c_{\text{RTT}} + c_{\text{TTT}}}{\omega + 3} \right) + 4 \left(\frac{c_{\text{EGCHC}}}{\omega + 4} \right) \right] \quad (4.10)$$

with the dimensionless ratio of educt and oxygen molar mass ω

$$\omega = \frac{M_{\text{TACHC}}}{M_{\text{O}}}. \quad (4.11)$$

The maximum oxirane value can be calculated by the known molecular mass of the product EGCHC and a total number of oxirane oxygen atoms of $N_{\text{OO}} = 4$. Hence, a relative progress of epoxidation η can additionally be determined which is defined in Equation 4.12.

$$\eta = OOC \cdot \left(\frac{1}{4} \omega + 1 \right). \quad (4.12)$$

Note that the oxirane oxygen content for the measured values was calculated based on the experimentally derived conversions X_R and X_T .

4.4 Computational Methodology

4.4.1 Reactor Model

The used batch reactor is modeled as an isothermal, isochoric, and homogeneous system. Therefore, the net formation rate of each species \dot{R}_i can be calculated with the reaction volume V_R and the time derivative of the molar amount n_i :

$$\frac{dn_i}{dt} = V_R \dot{R}_i \quad (4.13)$$

For better numerical stability, Equation 4.13 is transformed to a dimensionless form by multiplying the net formation rate with the total experimental time $t_{\text{end},m}$ and initial molar amount $n_{\text{tot},m}$ of experiment m .

$$\frac{dY_m}{dt} = \frac{t_{\text{end},m}}{n_{\text{tot},m}} V_R \dot{R}_i \quad (4.14)$$

The differential equations describing the reaction rates are solved numerically by applying a variable-step, variable-order solver suited for these stiff systems [147].

4.4.2 Regression

As all systems comprise of ordinary differential equations or their solutions, the respective regression functions f to fit the kinetic parameters to the experimental data are nonlinear. In general, the used nonlinear regression models can be described as in Equation 4.15:

$$\mathbf{Y}_m = f(X_m, \Phi) + \varepsilon_m \quad (4.15)$$

with the response matrix \mathbf{Y}_m , the predictor vector X_m , the parameter vector $\Phi = [\Phi_1, \dots, \Phi_{n_{\text{par}}}]$ and an error term ε_m . \mathbf{Y}_m is sized by the number of responses n_{resp} and measurement points n_{exp} , respectively. The regression is performed by a standard least squares approach applying the well-established Levenberg-Marquardt algorithm [148–150]. Hence, Equation 4.16 is minimized numerically with the experimental measurement points $\hat{\mathbf{Y}}_m$ of data set m for the number of data sets n_{data} .

$$\min_{\Phi} \sum_{m=1}^{n_{\text{data}}} \sum_{i=1}^{n_{\text{resp}}} \sum_{j=1}^{n_{\text{exp}}} (f(X_m, \Phi) - \hat{\mathbf{Y}}_m)^2 \quad (4.16)$$

The total number of observations n_{tot} , which is used for least squares minimisation, is therefore equal to the sum of the data sets, i.e., the experimental runs at a given temperature, together with the number of experimental measurements contained therein, i.e., the time-resolved samples, and the number of responses obtained from a taken sample.

$$n_{\text{tot}} = \sum_{m=1}^{n_{\text{data}}} \sum_{i=1}^{n_{\text{resp}}} \sum_{j=1}^{n_{\text{exp}}} \quad (4.17)$$

The parameters to be fitted are the kinetic constants k , which can be described by an Arrhenius law:

$$k = k_0 \exp\left(-\frac{E_A}{RT}\right). \quad (4.18)$$

Thus, a simultaneous regression of pre-exponential factors k_0 and activation energies E_A is performed. Due to the sensitive nature of the exponential equation, Equation 4.18 is transformed for better numerical stability using a half-exponential approach with the following Φ -function:

$$\Phi_k = \Phi_{k_0} \exp\left[\Phi_{E_A} \left(1 - \frac{T_{\text{ref}}}{T}\right)\right] \quad (4.19a)$$

$$\Phi_{E_A} = \frac{E_A}{RT_{\text{ref}}} \quad (4.19b)$$

$$\Phi_{k_0} = k_0 \exp(-\Phi_{E_A}) \quad (4.19c)$$

with the respective transformed parameters ($\Phi_{k_0}, \Phi_{E_A} \in \Phi$) and a reference temperature T_{ref} defined as the arithmetic mean of the experiment temperatures. After the minimization of squared residuals is converged, the variables are re-parameterized and values for k_0 and E_A are obtained. Due to the number of potential models in the esterification of the Diels-Alder product, further statistical analysis is performed to rate and compare these models. For model discrimination, information criteria are used which rate the reaction models based on number of parameters and likelihood. Two different criteria are applied to assess the models, the Akaike information criterion AIC in Equation 4.20 [82] and the Bayesian information criterion BIC in Equation 4.21 [151]:

$$AIC = -2\mathcal{L} + 2n_{\text{par}} \quad (4.20)$$

$$BIC = -2\mathcal{L} + \log(n_{\text{exp}}) \cdot n_{\text{par}} \quad (4.21)$$

with the log-likelihood function \mathcal{L} . Further details can be extracted from the Supplementary Information. Regression of kinetic parameters and thereby fitting of experimental data are performed with MATLAB® R2021a.

4.5 Results and Discussion

Model Evaluation

Diels-Alder Reaction

The Diels-Alder reaction was conducted at different temperatures ranging from 70 to 103 °C. Figure 4.5 displays the linear parity plot gathered for several batch experiments at the various temperatures ($n_{\text{tot}} = 141$).

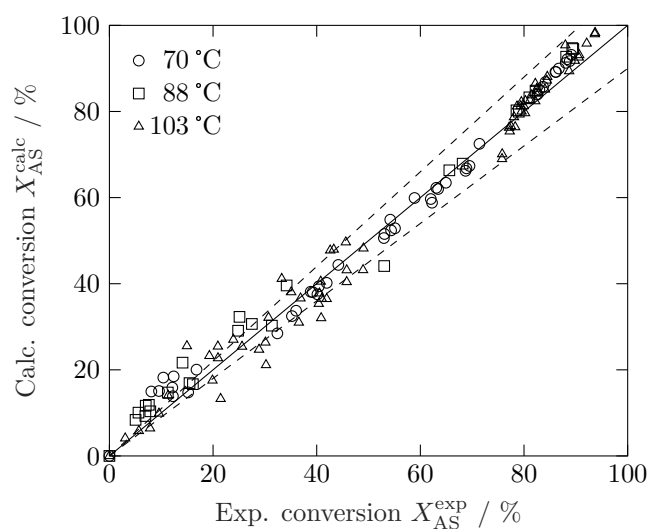


Figure 4.5: Linear parity plot of the allyl sorbate conversion for all measurements. Dashed lines mark the $\pm 10\%$ region.

The simple reaction model allows to fit the analytical solution stated in Equation 4.2 to the response values which accurately describes the reaction conversion. This procedure diminishes computational time to a fraction of the numerical solution of the differential equation. Separate conversion plots for the batch experiments can be found in Figure 4.19 in the Supplementary Information section. In Figure 4.6, the distribution of the residuals (Figure 4.6a) and the corresponding lag plot (Figure 4.6b) for all measurements are drawn. Additionally, the residuals are fitted with a Gaussian distribution function $\mathcal{N}(\mu, \sigma^2)$ for better visualization. The residuals follow a normal distribution and no identifiable structure in the lag plot which concludes random error in the data points and thus no correlation of the measurements. The total coefficient of determination for all experiments is $R^2 = 0.9861$ which further endorses the applied model and measurement approach.

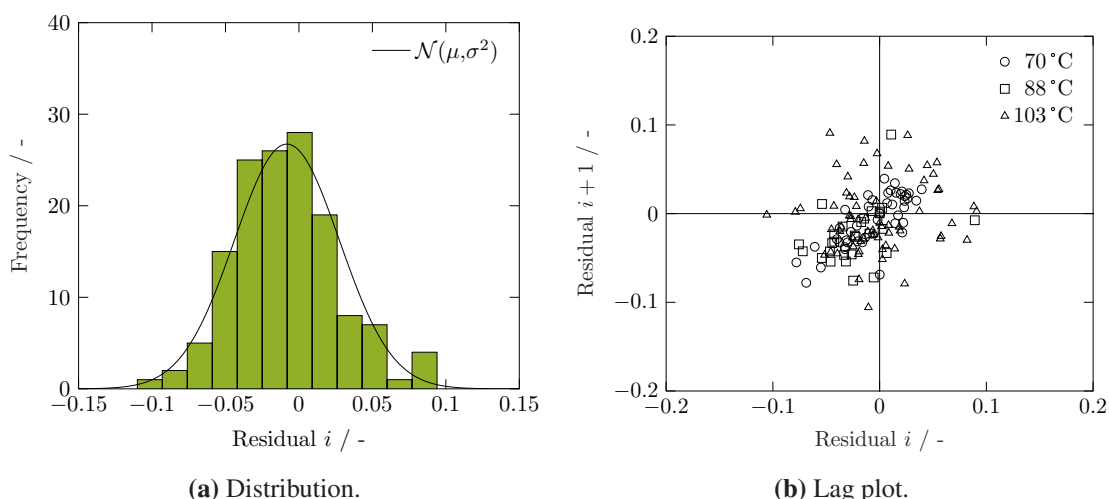


Figure 4.6: Distribution with normal distribution curve approximation ($\mu = -0.0082$, $\sigma^2 = 0.0013$) and lag plot of the residuals of fitting the Diels-Alder reaction at different temperatures.

The resulting parameters with 95 % confidence intervals are $\Phi_{k_0} = (0.405 \pm 0.014) \text{ L}/(\text{mol s})$ and $\Phi_{E_A} = 20.016 \pm 0.818$. Corresponding pre-exponential factor and activation energy are re-parameterized from the respective Φ -values at a reference temperature of 360.15 K and determined to be $6.904 \cdot 10^4 \text{ L}/(\text{mol s})$ and 59.93 kJ/mol using the half-exponential transformation of the Arrhenius equation. As a comparison, similar activation energies between 56.3 and 58.5 kJ/mol have been found for the Diels-Alder reaction of MA with isoprene [152, 153].

The most critical parameter in the kinetic study is the temperature control to ensure isothermality. Due to the strong exothermic character of the reaction, a rise in temperature can be seen, if the educt concentrations are chosen too high. Diels and Alder also experienced this exothermic behavior, when describing the reaction between MA and sorbic acid [139]. By performing the reaction without solvent, our studies showed a temperature increase from initially 100 to 200 °C within 30 s which leads to quick decarboxylation if temperatures rise above 150 °C [140]. An adequate amount of solvent as presented in this report in combination with the oil bath therefore suffocates to execute the Diels-Alder reaction under nearly perfect isothermal conditions.

Esterification

In Table 4.2, the various tested models are compared using the Akaike AIC and Bayesian BIC information criterion calculated with the number of parameters n_{par} and model likelihood. Additionally, corrected Akaike values AIC_c , differences Δ_{AIC} , and total coefficients

of regression R_{tot}^2 are tabulated. Akaike differences show that model 4 with eight parameters performs best, indicating substantial level of empirical support. In contrast to that, the other models show considerably less or essentially no support. [85] Furthermore, the confidence intervals are increased for the other tested models as displayed in Table 4.5. Thus, model 4 is selected as the candidate model. All shown regression and error plots are computed with the underlying candidate model with eight parameters.

Table 4.2: Total coefficient of determination, Akaike and Bayesian information criteria for the different tested models for the esterification reaction of the Diels-Alder product with allyl alcohol.

Model number	n_{par}	R_{tot}^2	AIC	AIC_c	BIC	Δ_{AIC}
1	16	0.9948	32.24	39.40	72.77	15.97
2	12	0.9943	24.27	28.17	54.66	7.99
3	10	0.9942	20.27	22.96	45.60	4.00
4	8	0.9942	16.28	17.99	35.54	0
5	8	0.9477	18.48	20.19	38.74	2.20
6	6	0.8478	19.28	20.26	34.48	3.01

Table 4.3 depicts the resulting values for Φ_i and the re-parameterized variables for pre-exponential factor and activation energy. Additionally, 95 % confidence intervals are shown. Activation energies are in a reasonable range. Even though the uncertainty of the reversible reaction towards the intermediates is high, considering the reaction improves the model fits. Figure 4.20 shows that an equilibrium is reached at each temperature, which otherwise would lead to a complete consumption of IIa or IIb in the case of an irreversible reaction.

Table 4.3: Estimated parameters Φ_i with 95 % confidence intervals and re-parameterized variables $k_{0,i}$ and $E_{A,i}$ for a reference temperature of $T_{\text{ref}} = 348.16$ K for candidate model 4.

Reaction i	$\Phi_{k_{0,i}} / \text{L}/(\text{mol s})$	$k_{0,i} / \text{L}/(\text{mol s})$	$\Phi_{E_{A,i}} / -$	$E_{A,i} / \text{kJ/mol}$
1	12.212 ± 0.418	$1.14 \cdot 10^7$	21.93 ± 0.54	62.76
2	2.830 ± 0.137	$1.66 \cdot 10^6$	23.77 ± 0.89	68.03
3,5	0.747 ± 0.020	$1.14 \cdot 10^9$	29.34 ± 0.59	83.96
4,6	0.632 ± 0.099	$3.07 \cdot 10^3$	16.68 ± 4.74	47.72

Figure 4.7 illustrates the linear parity plots for the esterification reaction with individual sub figures for each measured component. The parity plots comprise all experimental data points gathered between 48 and 97 °C ($n_{\text{tot}} = 341$). High agreement between calculated and measured concentrations is achieved.

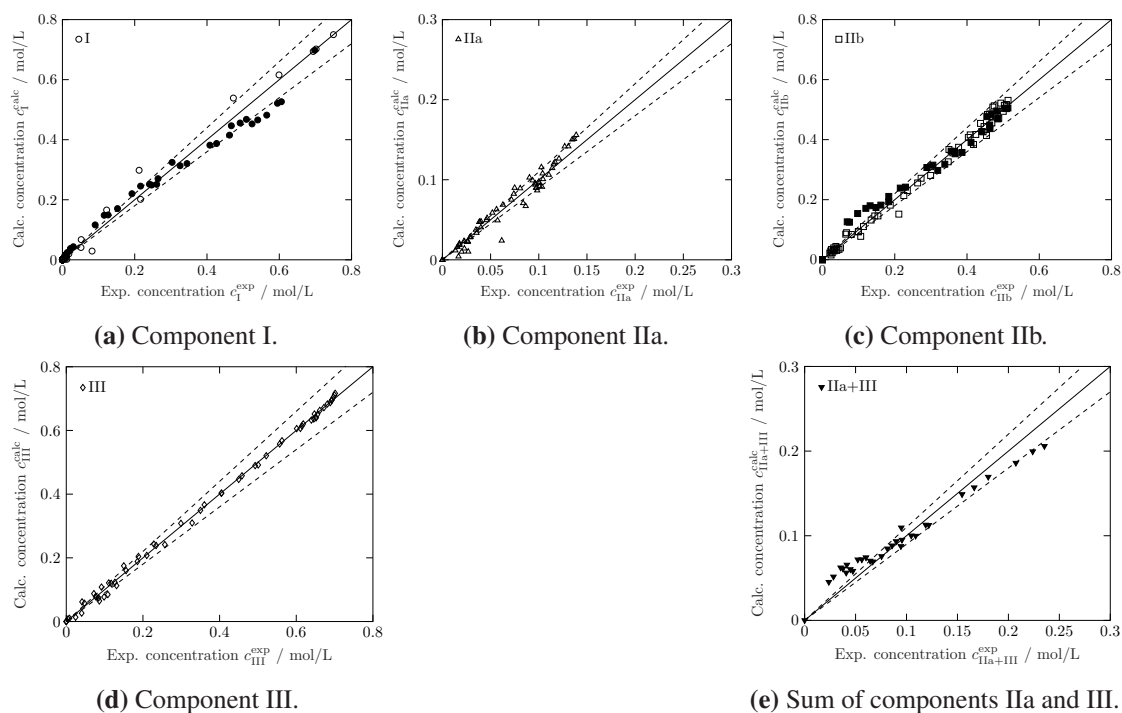


Figure 4.7: Linear parity plots of the esterification reaction of the Diels-Alder reaction (I) to TACHC (III) for each component. Experiments with only three responses are indicated by closed symbols. Dashed lines mark the $\pm 10\%$ region.

Mostly, outliers representing more than 10% deviation stem from the measurement at 48 °C indicated by closed symbols in Figure 4.7a, Figure 4.7c and Figure 4.7e. The less accurate fitting of that particular experiment can be deduced from the respective parity plots. The recorded $^1\text{H-NMR}$ spectrum which could not resolve the individual concentrations of IIa and III was evaluated so that the sum of $(c_{\text{IIa}} + c_{\text{III}})$ could be fitted. As only the sum of both components was accessible, a degree of freedom is yielded for that particular data set leading to an underdetermined system of equations. Although this adds measurement points prone to larger errors for regression, the data are included in the overall regression of the parameters to enhance the validity of the results for an increased temperature range. In addition to the parity plots, measured batch concentration experiments of the esterification of the Diels-Alder product with AA can be found in Figure 4.20 for the different temperatures with corresponding model fits represented by lines. The candidate model 4 agrees well with the measurements. Both fast formation of primary products and equilibrium are in accordance to the data. While the Diels-Alder product reacts rapidly to zero concentration within a short time, the synthesis of TACHC (III) is rather slow. The assumption of an irreversible reaction for the first reaction step is justified taking the quick vanishing of I into consideration. This further disproves model 1 which comprises reversible reaction steps for the formation of the intermediates. The formation of intermediate IIb is enhanced for all experiments leading to a higher maximum in concentration than IIa. If steric hindrance of the carboxylic group would

determine the progress of reaction, the result of equal reactivity could not hold true. Rather, the inductive effects of groups in educt I lead to the difference in reactivity of reactions 1 and 2. As the ester group induces a -I-effect and the methyl group induces a +I-effect, the electron density at the carbon atom in the anhydride ring adjacent to the ester group is decreased. Hence, the attack of the nucleophile proceeds more likely with the ring-opening toward the neighboring ester group and thus, forming component IIb. Equilibrium of product III and intermediates IIa and IIb is reached at the end of each experiment. Due to the chosen candidate model with identical equilibrium constants, the end concentrations of the intermediates is equal ($K_{\text{eq}} = k_3/k_4 = k_5/k_6$). This broadly matches with the measurement data.

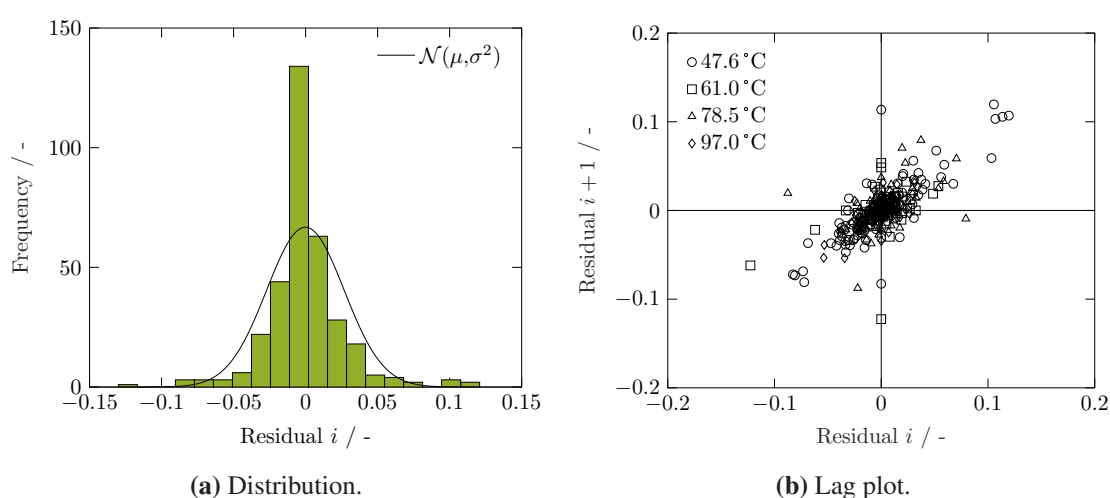


Figure 4.8: Residual distribution with normal distribution curve approximation ($\mu = -0.0002$, $\sigma^2 = 0.0007$) and lag plot of the residuals of fitting the esterification reaction at different temperatures. Residuals are normalized by $c_{1,0}$.

Figure 4.8 illustrates the distribution and lag of errors. The histogram follows a normal distribution with an accumulation of residuals at zero stemming from regression of educt I. The Diels-Alder product rapidly reacts and, thus, the concentration reaches zero for the majority of the measurement time. Hence, model and experiment align with high agreement and calculated errors are minimal. Figure 4.8b displays the lag of the residuals for the four measured temperatures. The spreading and pattern of the lag plot suggests randomness of the errors without correlation between subsequent points. Mostly, outliers in Figure 4.8b are contributed from the measurement at the lowest temperature due to the fitting of both IIa and III. Though, residuals and distribution of errors are in an acceptable range.

Epoxidation

Figure 4.9 displays the linear parity plot of the epoxidation reaction for the various batch experiments performed ($n_{\text{tot}} = 170$). Each temperature is indicated by a different symbol. Additionally, the type of double bond is distinguished by the symbols being closed or open. A general high agreement between experimental and model values is achieved. Conversion plots for the batch epoxidation can be found in the Supplementary

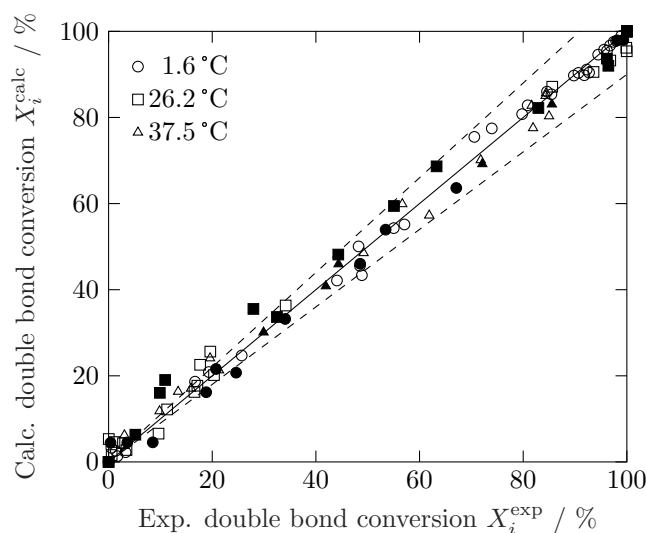


Figure 4.9: Linear parity plot of the epoxidation of TACHC. Double bond in ring is represented by closed symbols, terminal double bonds by open symbols. Dashed lines mark the $\pm 10\%$ region.

Information section. Figure 4.21 shows the experimental data points of X_R and X_T , and the respective model fit. Both conversions reach 100% when all double bonds of type R or T are epoxidized. Thus, X_T represents the reaction conversion of all three terminal double bonds. Note that the time scale differs greatly from Figure 4.21a to Figure 4.21c. In other words, a temperature increase in the considered range leads to a more than 20-fold faster conversion of each double bond. The temperature used in the experiments is limited to the normal boiling point of the solvent DCM ($T_b = 39.6^\circ\text{C}$) as a pressurization of the glass reaction vessels is not possible. Figure 4.10 displays the residual distribution and lag plot, respectively. The histogram in Figure 4.10a shows a normal distribution with an accumulation of residuals at close to zero. The aggregation stems from the underlying analysis method. Due to the fast reaction of the ring-bound double bond, the remaining peak diminishes rapidly to zero within the noise of the signal as seen in Figure 4.21. Hence, after only 10% of the measurement time, experimental values for X_R are noted to be fully converted showing high agreement with the model and, thus, residuals are minimal. The initial measurement values in the beginning are prone to error because of the fast reaction and therefore, steep slope of the profile. The data points of X_R

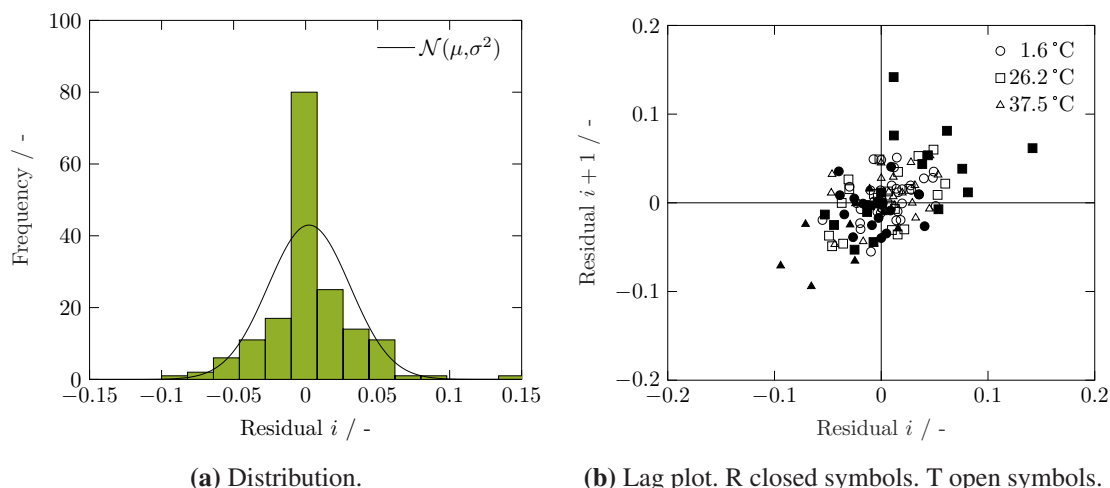
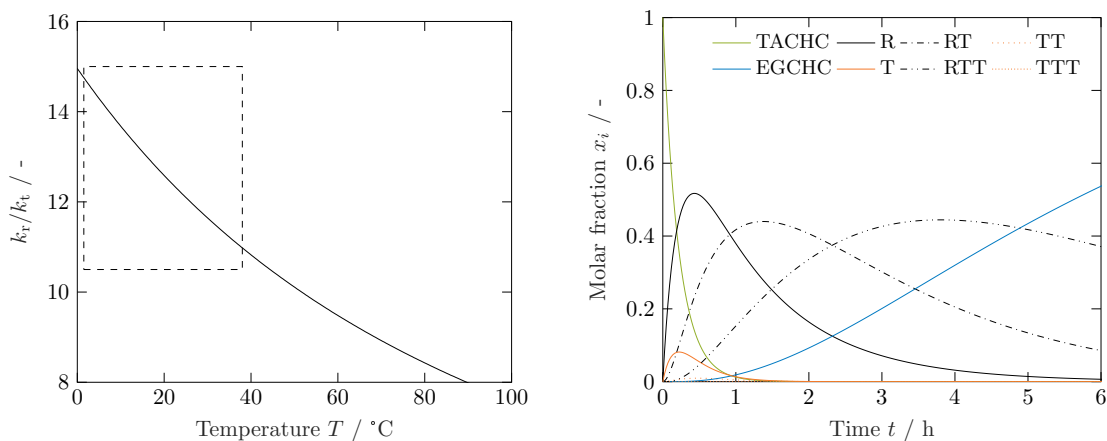


Figure 4.10: Residual distribution with normal distribution curve approximation ($\mu = 0.0024$, $\sigma^2 = 0.0008$) and lag plot of the residuals of fitting the epoxidation reaction at different temperatures.

tend to show a kink in the curve at high turnovers due to the uncertainty of the values close to 100 %, which can be lost in the signal noise (reciprocal trend of peak area and conversion). As a result, the residuals of X_R are spread at the beginning and concentrated around zero for residuals determined at long measurement times. This trend can be seen in Figure 4.22 illustrating a residual versus predictor plot for X_R . Nevertheless, with no identifiable structure in the lag plot, independent errors can be assumed. Furthermore, the normal distribution of residuals assures that the random errors are drawn from a Gaussian distribution validating stated confidence intervals. The regressed Φ -functions with their respective 95 % confidence intervals and re-parameterized pre-exponential factors and activation energies are listed in Table 4.4. The confidence intervals are in a narrow range. Furthermore, a total coefficient of determination of $R^2 = 0.9952$ is achieved which justifies the underlying reaction scheme.

Table 4.4: Estimated parameters Φ_i with 95 % confidence intervals and re-parameterized variables pre-exponential factor $k_{0,i}$ and activation energy $E_{A,i}$ for a reference temperature of $T_{\text{ref}} = 294.92$ K.

Reaction i	$\Phi_{k_{0,i}} / \text{L}/(\text{mol s})$	$k_{0,i} / \text{L}/(\text{mol s})$	$\Phi_{E_{A,i}} / -$	$E_{A,i} / \text{kJ/mol}$
R	0.760 ± 0.030	$2.15 \cdot 10^7$	24.395 ± 0.831	59.82
T	0.061 ± 0.002	$1.81 \cdot 10^7$	26.744 ± 0.566	65.57



(a) Ratio of kinetic constants for epoxidation of ring and terminal double bond k_r/k_t . Dotted line indicates measured temperature range.

(b) Molar fraction profiles for all possible components in epoxidation reaction scheme. $T = 37.5^\circ\text{C}$.

Figure 4.11: Comparison of ring and terminal double bond epoxidation and reaction progress of the modeled epoxidation scheme.

To get an insight on the relative reactivity of each type of double bond Figure 4.11a depicts the ratio of the obtained kinetic constants against the temperature. As expected, the terminal bonds are less likely to react. The higher activation energy of the terminal epoxidation reveals a preferred reaction of the ring-bound double bond. Thus, in the measured temperature range, the ring-bound double bond is converted 11–15 times faster than a terminal bond whereas this difference becomes less pronounced at higher temperatures. To achieve a high oxirane oxygen content, either sufficient reaction times or high temperatures need to be ensured. The limiting temperature of 40°C can be exceeded by increasing the reaction pressure according to the vapor pressure of DCM. The proposed model allows to predict the course of each species in contrast to a total double bond conversion. This will later be used to determine the oxirane oxygen content. Figure 4.11b displays the timely development of each possible species derived from the reaction model in Figure 4.4 for 37.5°C . The initial development of the reactant composition is shown for the first 6 h. As a result of the implemented reaction network, species R and T are primary products which can be deduced by their non-zero slope through the origin. All other intermediates and the product have a slope of zero at $t = 0\text{h}$. Furthermore, the difference in reactivity between the two double bond types illustrated in Figure 4.11a is evident in Figure 4.11b. The maximum molar fraction of T is slightly more than 0.08 whereas R peaks at a molar fraction of more than 0.50. A continued terminal epoxidation is very unlikely ($\max(x_{\text{TT}}) < 0.01$). The production of TTT is negligible. It is apparent that the main route in the epoxidation reaction comprises a preliminary conversion of the ring-bound double bond and a subsequent gradual epoxidation of the three terminal bonds. This behavior is in accordance to the typically low reactivity of terminal double bonds [154, 155].

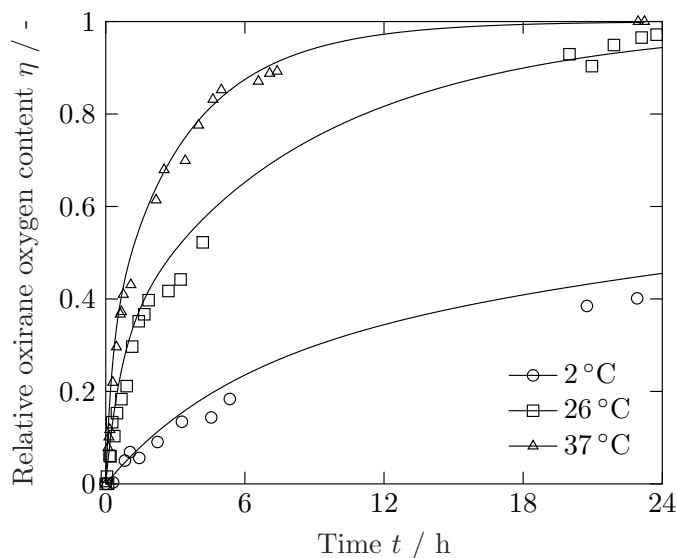


Figure 4.12: Simulated versus experimental determined relative oxirane oxygen content η over time for all measured temperatures.

The theoretical oxirane oxygen content of EGCHC is $OOC = 15.5\%$. The commercial standard epoxy component DGEBA yields 9.4% . The difference in OOC results from the higher density of epoxy groups per mass in EGCHC than in DGEBA which leads to a lower epoxy equivalent weight in the sustainable epoxy [61]. Though, in the present study, only theoretical observations are made to interpret the model results and expand the model predictions. Figure 4.12 shows the relative progress in oxirane oxygen formation η for the different tested reaction temperatures within 1 day. The model predicts well the measured OOC . While only the total OOC can be determined with the laboratory data, the model allows statements to be made about the concentration of each individual species and consequently their contribution to the mixture OOC at any point in time. This could be used to optimize a process model for a maximum of OOC at reasonable process times to ensure high functionality, and thus, cross-linkage of the resin.

4.6 Conclusions

In this study, the previously described and published route to the partly bio-based epoxy resin EGCHC was further kinetically investigated. The main reaction steps were conducted on a laboratory scale while sampling and analysing the reaction progress with the use of $^1\text{H-NMR}$. The chosen analysis method proves to be suitable to rapidly generate the necessary batch profile data. Due to the simplicity of sample preparation and fast measurement time, experimental data of high accuracy could be achieved.

The Diels-Alder reaction between AS and MA is shown to be of second order and irreversible. These results simplify the rate law to an analytical solution of the underlying differential equations. The model accurately fits the AS conversion while errors proved to be random and independent. Thus, reliable values for pre-exponential factor and activation energy of $6.904 \cdot 10^4 \text{ L}/(\text{mol s})$ and 59.93 kJ/mol could be derived.

The further esterification of the received product is successfully described by a model comprising two different intermediates. The two diesters stem from the opening of the anhydride ring in either way. Model discrimination was performed with the help of information criteria and maximum likelihood. The selected candidate model with the assumption of equal reactivity of the two intermediates towards EGCHC fits well the measurements. It could be shown that the difference in reactivity in opening the anhydride ring and the resulting different intermediate concentrations are caused by the proximity of the carboxylate group.

The last reaction step toward the epoxy resin component EGCHC was regressed with a model describing in detail the development of the successive epoxidation of each double bond. In total, eight components are tracked including educt and product. Despite the various reaction paths, a data regression using two different kinetic constants proves to be sufficient to accurately depict the reaction progress. The different reactivity of the two reaction types, epoxidation of terminal or ring-bound double bonds, agrees with the expected lower reactivity of terminal double bonds.

In general, all of the postulated models precisely fitted the experimental values and can therefore be assumed to describe the respective reactions in a meaningful way. Statistical analyses showed random error and no correlation in the collected data. Hence, the results pave the way to a preliminary process implementation which allows to get insights into a possible production process with information about material and energy consumption and a better general overview of the process. Consequentially, a process simulation of the individual steps and the complete production of the well-performing sustainable epoxy needs to follow.

Supplementary Material

Analytical Solution of a Bi-Molecular Reaction

This chapter shows the analytical solution to the reaction equation of the type $a + b \xrightarrow{k_1} c$. Writing this chemical reaction in forms of differential equations results in:

$$\frac{dc_a}{dt} = -k_1 c_a c_b \quad (4.22a)$$

$$\frac{dc_b}{dt} = -k_1 c_a c_b \quad (4.22b)$$

with the reaction rate constant k_1 and the concentrations $c_i > 0$. Since $\frac{dc_a}{dt} = \frac{dc_b}{dt}$, it can be written:

$$\frac{d}{dt}(c_a - c_b) = 0. \quad (4.23)$$

This has the solution

$$c_a(t) - c_b(t) = c_{a,0} - c_{b,0} \quad (4.24)$$

with the initial concentrations $c_{i,0}$. Defining the initial concentration difference $\alpha = c_{a,0} - c_{b,0} \neq 0$ and using previous expression, the ordinary differential equations (ODE) can be decoupled, which yields for component a:

$$\frac{dc_a}{dt} = -k_1 c_a (c_a - \alpha). \quad (4.25)$$

Rearranging the ODE leads to

$$\frac{dc_a}{c_a(c_a - \alpha)} = -k_1 dt, \quad (4.26)$$

from which the solution can analytically be obtained by integration:

$$c_a(t) = \frac{\alpha}{1 - \left(1 - \frac{\alpha}{c_{a,0}}\right) \exp(-k_1 t \alpha)} \quad (4.27a)$$

$$c_b(t) = \frac{\alpha \left(1 - \frac{\alpha}{c_{a,0}}\right) \exp(-k_1 t \alpha)}{1 - \left(1 - \frac{\alpha}{c_{a,0}}\right) \exp(-k_1 t \alpha)}. \quad (4.27b)$$

For the special case that $\alpha = 0$, the solution is:

$$c_a(t) = \frac{c_{a,0}}{1 + c_{a,0}k_1t} = c_b(t). \quad (4.28)$$

Statistical Analysis

For the evaluation of the chosen models and reaction pathways statistical analysis is performed both on whole models and for individual fitting parameters. To describe the deviance of model values and responses, calculation of sum of squares error SSE and sum of squares total SST is a basic approach to gather information about the coefficient of determination R^2 :

$$R^2 = 1 - \frac{SSE}{SST} = 1 - \frac{\|f(X_m, \Phi) - \hat{Y}_m\|^2}{\|\hat{Y}_m - \mu\|^2} \quad (4.29)$$

with the mean of the observed values μ

$$\mu = \frac{\sum_{j=1}^{n_{\text{exp}}} \hat{Y}_m}{n_{\text{exp}}}. \quad (4.30)$$

Confidence intervals are calculated based on the estimated coefficient variance matrix **COV**

$$\mathbf{COV} = \frac{SSE}{dof_{\text{res}}} \cdot (\mathbf{J}^T \cdot \mathbf{J})^{-1} \quad (4.31)$$

with the residual degree of freedom dof_{res} , which is defined as

$$dof_{\text{res}} = n_{\text{exp}} - n_{\text{par}}. \quad (4.32)$$

J is the Jacobian matrix. The confidence intervals CI can thus be deduced to:

$$CI_{1-\alpha} = \Phi \pm t^{-1} \left(1 - \frac{\alpha}{2}, dof_{\text{res}} \right) \cdot \sqrt{\text{diag}(\mathbf{COV})} \quad (4.33)$$

with the reverse Student's t -distribution t^{-1} and $\alpha = 0.05$ for 95 % confidence intervals. A more detailed description and further reading can be found in literature [156].

In contrast to accurately fit the observations with a model of choice the particular model should be as simple as possible. This overfitting of gathered data and thus goal to minimize the parameter space is referred to as principle of parsimony. A trade off is often required to regress the proposed model with the smallest possible number of parameters achieving an adequate fit. Several estimation and rating criteria have been proposed in literature to

evaluate and compare different models. Most rely on the log-likelihood function \mathcal{L} which can readily be related to the regression process based on a minimization of the negative log-likelihood function.

The values of the maximum likelihood estimates can be correlated to the maximum of the log-likelihood function. Together with the number of parameters n_{par} and number of experiments n_{exp} the Akaike and Bayesian information criteria can be defined (c.f. Equation 4.20 and Equation 4.21). In the case of minimization of least squares and for the case of normally distributed errors, the likelihood function and thus AIC can be calculated as

$$AIC = n_{\text{exp}} \log \left(\frac{\sum_{m=1}^{n_{\text{data}}} \sum_{i=1}^{n_{\text{resp}}} \sum_{j=1}^{n_{\text{exp}}} (f(X_m, \Phi) - \hat{Y}_m)^2}{n_{\text{exp}}} \right) + 2n_{\text{par}} . \quad (4.34)$$

Often, if the available data are over dispersed or in other words few responses are recorded, a corrected AIC is calculated, denoted as AIC_c :

$$AIC_c = AIC + \frac{2n_{\text{par}}(n_{\text{par}} + 1)}{n_{\text{exp}} - n_{\text{par}} - 1} . \quad (4.35)$$

Equation 4.35 should be used if $n_{\text{exp}}/n_{\text{par}} < 40$ [85]. Of general interest are the differences of the gained AIC as the absolute values are not interpretable:

$$\Delta_{AIC} = AIC_i - \min(AIC) . \quad (4.36)$$

Burnham and Anderson suggest as a rule of thumb ranges of 0–2, 4–7 and < 10 which indicate the level of empirical support of model i in comparison as substantial, considerably less and essentially none, respectively [85].

Characterization

Nuclear magnetic resonance (NMR) spectra are recorded on a Bruker Ascend 400 MHz spectrometer. All spectra are referenced on the proton signal of the respective solvent. Complete spectra and referenced signals can be found in detail in literature [61]. The ^1H -NMR spectra are taken for different reaction times and stacked chronologically in the following figures. Though, the time difference between subsequent ^1H -NMR varies due to logarithmic distributed sampling times. Furthermore, the concentration of the components, which is proportional to the area of a signal, is mapped with the shading of a color to better visualize the development of the reaction.

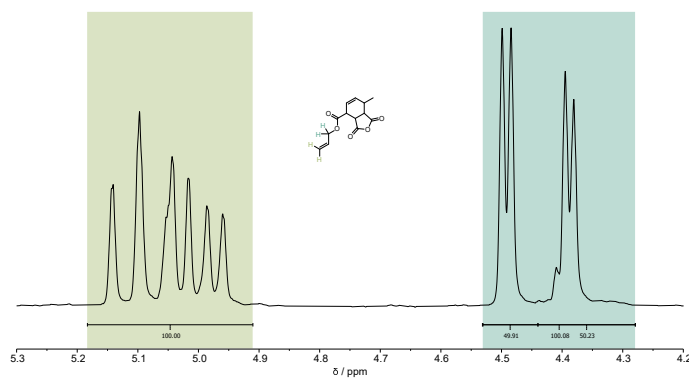


Figure 4.13: Section of the $^1\text{H-NMR}$ spectrum of the Diels-Alder reaction between maleic anhydride and allyl sorbate at a conversion of 49.9% after a reaction time of 15 min at 103 °C. Displayed values denote the area of the peaks for conversion determination.

Figure 4.13 shows a characteristic section of a $^1\text{H-NMR}$ spectrum of the reaction mixture. The indicated signals at 4.9 to 5.2 ppm and 4.3 to 4.5 ppm are used to identify and determine the allyl sorbate conversion.

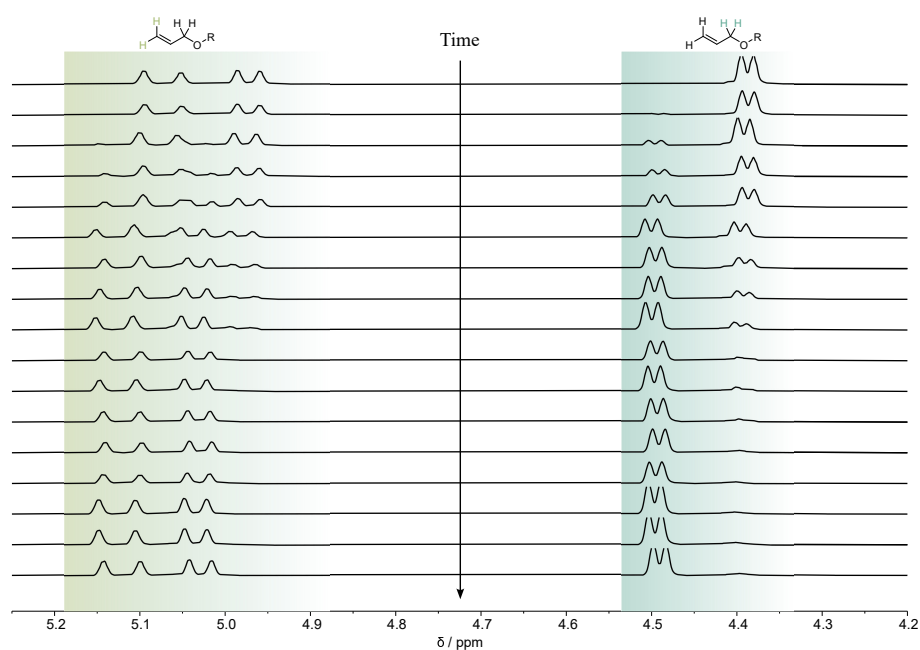


Figure 4.14: Progress of the Diels-Alder reaction at 103 °C in $^1\text{H-NMR}$.

Figure 4.14 illustrates the progress of the reaction at 103 °C. The stacked plot with increasing time from top to bottom clearly indicates the formation of the Diels-Alder product and thus the diminishing of allyl sorbate.

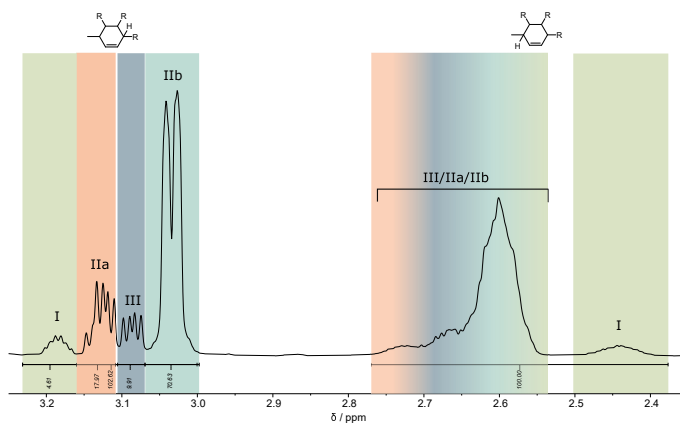


Figure 4.15: Exemply $^1\text{H-NMR}$ after 8 min reaction time of the allylation reaction at $78.5\text{ }^\circ\text{C}$.

In Figure 4.15 the characteristic section used to determine the concentration of the components in the esterification reaction is shown. The resonance signals in the $^1\text{H-NMR}$ spectrum between 3.0 to 3.2 ppm determine the fraction of I, IIa, IIb, and III. The areas are correlated with the signal area between 2.4 ppm and 2.8 ppm which is used as a reference area. This procedure allows to directly calculate the fraction and thus the concentration taking the initial concentration $c_{I,0}$ into consideration.

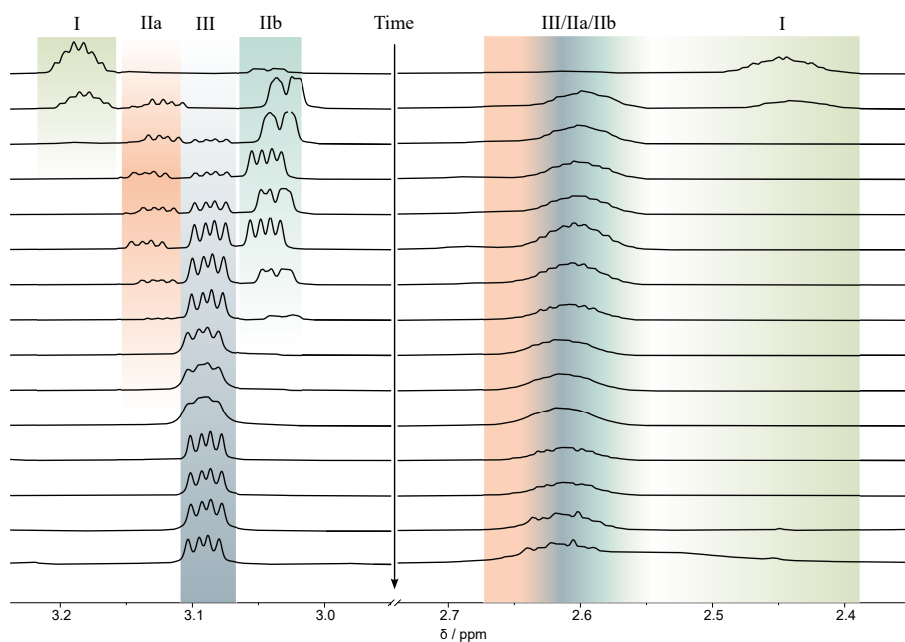


Figure 4.16: Progress of the allylation reaction at $78.5\text{ }^\circ\text{C}$ in $^1\text{H-NMR}$.

Figure 4.16 illustrates the reaction progress on the basis of timely taken $^1\text{H-NMR}$ spectra. While signal I decreases rapidly to zero, the signals IIa and IIb slowly increase, pass a maximum and diminish for longer times. The product III is generated throughout the reaction.

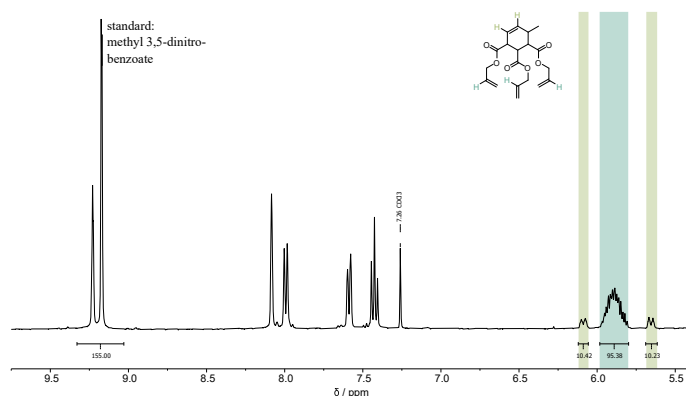


Figure 4.17: Section of the $^1\text{H-NMR}$ spectrum of the epoxidation reaction of TACHC after a reaction time of 48 min at 26.2 °C.

In Figure 4.17, the relevant section of a $^1\text{H-NMR}$ spectrum to analyse the epoxidation reaction is drawn. Signals at 9.2 to 9.3 ppm refer to the signals of the used standard methyl 3,5-dinitrobenzoate. Both signals shifting at 5.6 ppm and 6.1 ppm are introduced by the resonance of the protons located at the hexene double bond. The signal at 5.8 to 5.9 ppm can be referenced to the hydrogen atoms attached to the terminal double bonds. The resonance signal does not differ, and therefore, the signal shifts are identical. The signal area corresponding to all three protons is used for the calculation of X_T . All calculated areas are referenced with the signal area of the standard, which has a constant concentration over the course of the reaction.

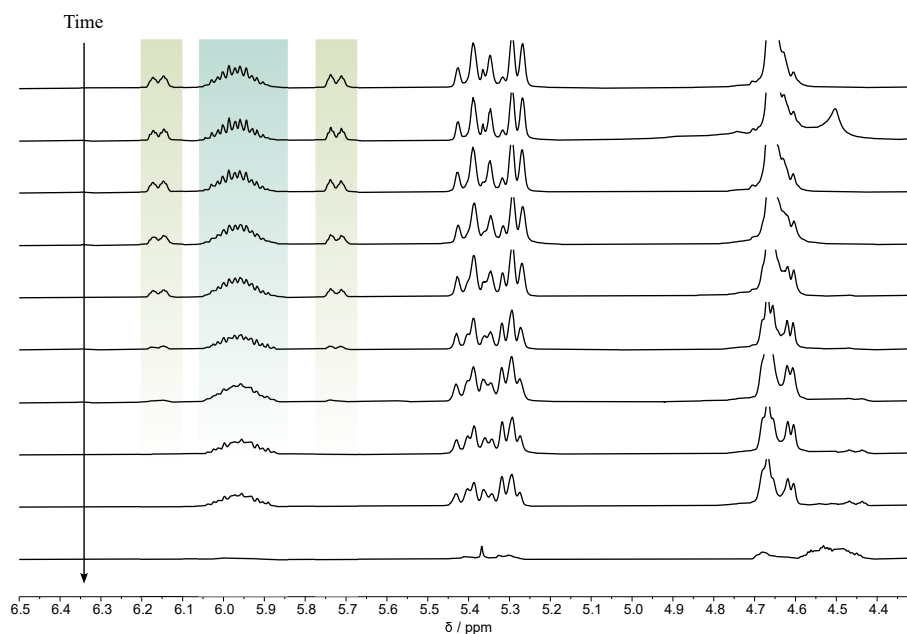


Figure 4.18: Progress of the epoxidation reaction at 26.2 °C in $^1\text{H-NMR}$.

Figure 4.18 shows the reaction progress successfully tracked by $^1\text{H-NMR}$. Thus, the conversion of terminal or ring-bound double bonds can be examined. These generated batch reaction data are used for fitting the kinetic model of the epoxidation.

Additional Model Results

This section further illustrates the model results gathered by fitting the experimental data or gives additional insights into the statistical analysis of the parameters.

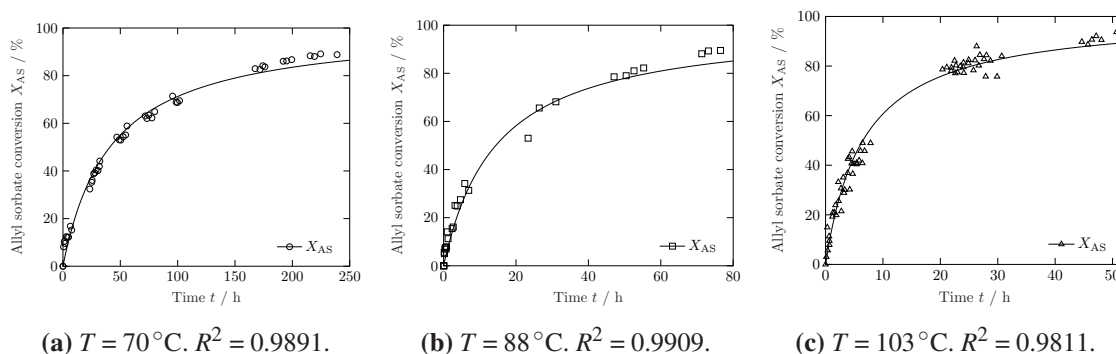


Figure 4.19: Fit of the experimental allyl sorbate conversion data at various temperatures. Experimental points as markers, model fits as lines. Total coefficient of determination $R_{\text{tot}}^2 = 0.9861$.

The Diels-Alder reaction batch experiment results are displayed in Figure 4.19. Additionally, model fits are shown with lines. Accurate regression of the measurements can be seen for all temperatures resembling an adequate model assumption for the Diels-Alder reaction of maleic anhydride and allyl sorbate. Total coefficient of determination is $R_{\text{tot}}^2 = 0.9861$.

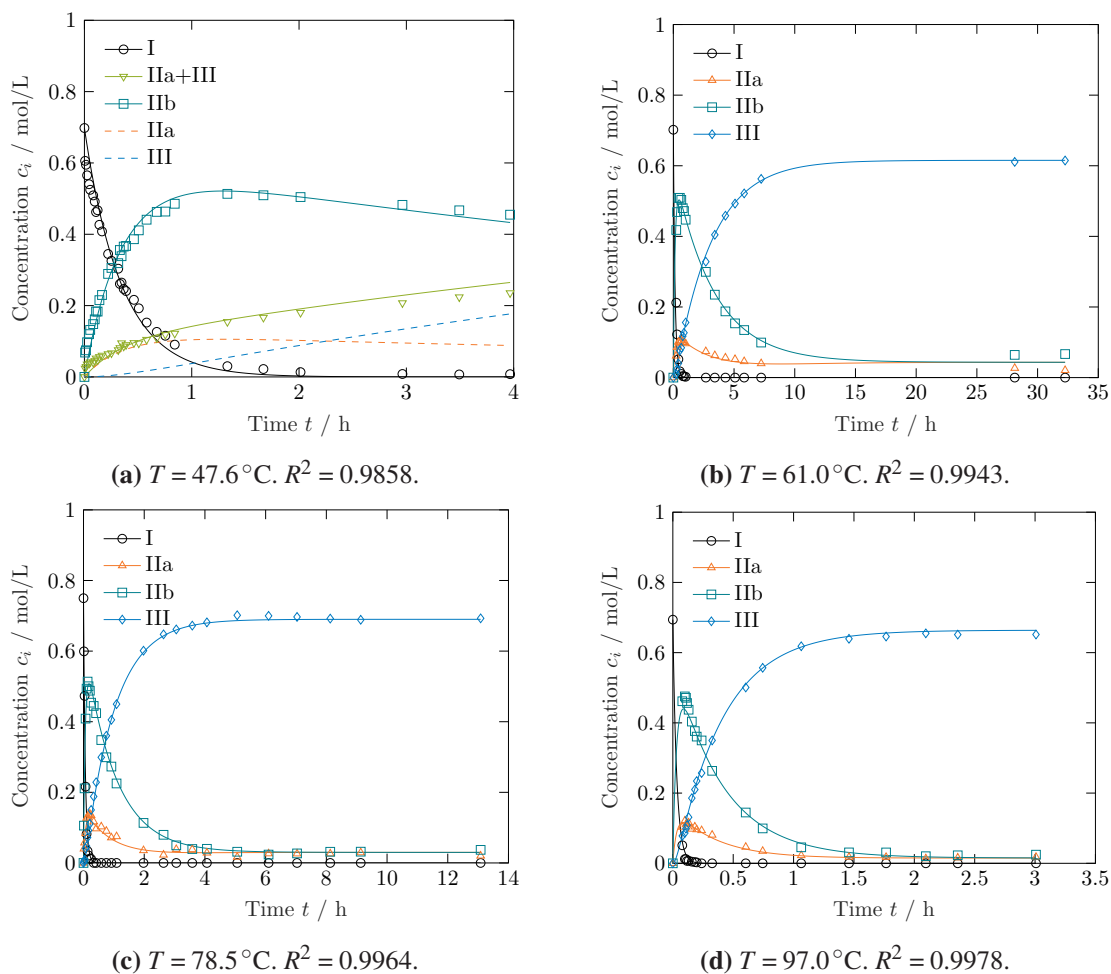


Figure 4.20: Measured concentration values with model fits denoted as lines for the allylation of the Diels-Alder product (I) over the two intermediates IIa and IIb towards TACHC (III). Experimental points as markers, model fits as lines (Model 4). Dashed lines show individual model results from fitting the sum of IIa+III. Total coefficient of determination $R_{\text{tot}}^2 = 0.9942$.

Figure 4.20 shows the concentration profiles for the batch experiments of the Diels-Alder product with allyl alcohol. In Figure 4.20b–Figure 4.20d all components could be tracked individually as shown in the $^1\text{H-NMR}$ reaction progress spectra in Figure 4.16. Though, due to the small shifts between component IIa and III in the recorded $^1\text{H-NMR}$ spectra (cf. Figure 4.15) and thus an overlapping of the peaks in some measurements, a separation of the individual peaks was not possible in these cases. Therefore, structures IIa and III are fitted as a sum. Using this method, only the concentrations of species I and IIb can directly be determined, whereas the remainder comprises the sum of IIa and III. As a result, the experimental obtained concentrations c_{I} , c_{IIb} and $(c_{\text{IIa}} + c_{\text{III}})$ are fitted with Equation 4.4a – Equation 4.4d. This is illustrated in Figure 4.20a which shows experimental data points and model fits at 48°C .

A comparison of estimated parameters with 95 % confidence intervals and re-parameterized variables is displayed in Table 4.5. Models 2, 3, 5 and 6 are tabulated with their respective *AIC* and *BIC* values.

Table 4.5: Estimated parameters Φ_i with 95 % confidence intervals and re-parameterized variables $k_{0,i}$ and $E_{A,i}$ for a reference temperature of $T_{\text{ref}} = 348.16\text{K}$ for models 2, 3, 5 and 6. Akaike and Bayesian information criteria for model comparison.

i	$\Phi_{k_{0,i}}$ / L/(mol s)	$k_{0,i}$ / L/(mol s)	$\Phi_{E_{A,i}}$ / -	$E_{A,i}$ / kJ/mol	<i>AIC</i> / -	<i>BIC</i> / -
1	12.288 ± 0.422	$1.23 \cdot 10^7$	22.01 ± 0.54	62.98	24.27	54.66
2	2.746 ± 0.153	$1.19 \cdot 10^7$	23.47 ± 1.05	67.16		
3	0.768 ± 0.027	$1.35 \cdot 10^9$	29.48 ± 0.77	84.36		
4	0.767 ± 0.149	$1.24 \cdot 10^2$	13.27 ± 6.27	37.98		
5	0.613 ± 0.119	$6.52 \cdot 10^8$	28.97 ± 4.20	82.91		
6	0.365 ± 0.182	$1.10 \cdot 10^6$	23.11 ± 13.14	66.12		
1	12.251 ± 0.422	$1.21 \cdot 10^7$	21.99 ± 0.54	62.94	20.27	45.60
2	2.801 ± 0.148	$1.19 \cdot 10^7$	23.45 ± 0.99	67.10		
3	0.752 ± 0.023	$1.53 \cdot 10^9$	29.62 ± 0.70	84.77		
4,6	0.634 ± 0.106	$8.08 \cdot 10^2$	15.34 ± 5.02	43.90		
5	0.736 ± 0.109	$1.06 \cdot 10^8$	26.98 ± 3.41	77.20		
1	12.429 ± 0.532	$1.51 \cdot 10^7$	22.20 ± 0.67	63.53	16.43	36.69
2	2.698 ± 0.178	$6.90 \cdot 10^6$	22.94 ± 1.21	65.66		
1,3	0.751 ± 0.027	$2.42 \cdot 10^9$	30.08 ± 0.81	86.08		
2,5	0.413 ± 0.086	$1.15 \cdot 10^8$	27.63 ± 4.55	79.08		
1,2	5.916 ± 0.763	$1.51 \cdot 10^7$	19.41 ± 2.11	55.56	19.28	34.48
3,5	0.579 ± 0.086	$2.42 \cdot 10^9$	32.57 ± 3.36	93.19		
4,6	0.377 ± 0.393	$1.15 \cdot 10^8$	24.32 ± 29.06	69.60		

Figure 4.21 shows the epoxidation progress data from the batch experiments using *m*CPBA as an epoxidation agent for the different examined temperatures. The conversion of both types of double bonds, ring-bound or terminal, is displayed. Conversion data was deduced from $^1\text{H-NMR}$ spectra as illustrated in Figure 4.18.

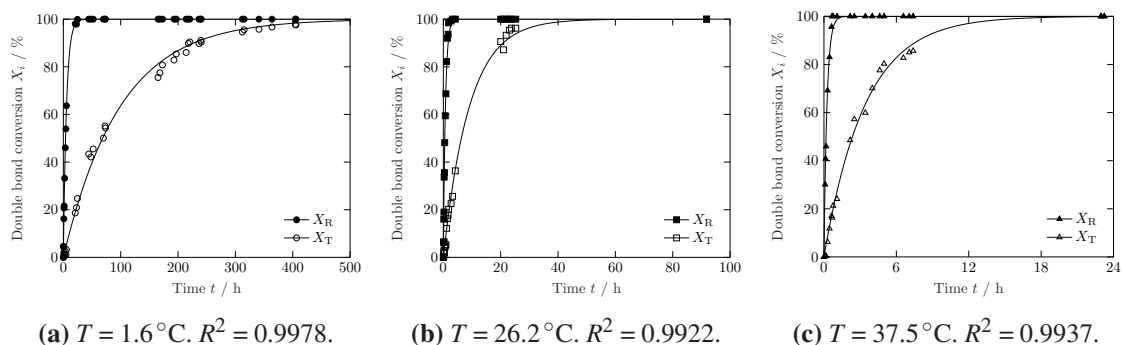


Figure 4.21: Double bond conversion of ring-bound double bond X_R and terminal bond X_T for different temperatures. Experimental points as markers, model fits as lines. Total coefficient of determination $R_{\text{tot}}^2 = 0.9952$.

In Figure 4.22 the residuals of the double bond conversion X_R are displayed versus the measurement time. Due to the large difference in the time scale between the experiments, the x -axis is scaled logarithmically.

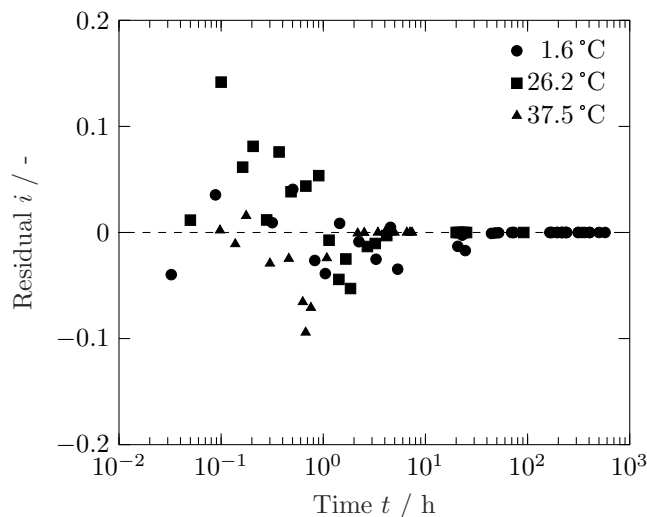


Figure 4.22: Residuals of ring-bound double bond conversion versus time. Abscissa scaled logarithmically.

5 Process Development for the Production

Abstract

The development of a production process of the sustainable epoxy resin 1,2-epoxy-6-methyl-triglycidyl-3,4,5-cyclohexanetricarboxylate (EGCHC) is presented. The three main sections of the suggested process flowsheet follow the reaction steps beginning with allyl sorbate and maleic anhydride. The Diels-Alder, allylation, and epoxidation reactions are simulated in Aspen Plus V12 and connected to form a single process train. To size and establish key process parameters, simulations supported by kinetic data for each reaction are performed. The [4 + 2]-cycloaddition and epoxidation are implemented in multitubular plug flow reactors with downstream crystallizers for product purification. The allylation reaction is carried out in a reactive distillation column to separate the heavy boiling product from the condensate/allyl alcohol mixture which is further processed to regain allyl alcohol. To decrease the intake of raw materials, recycle streams are added to each sections. EGCHC is achieved with a purity of 95 %, which can be employed with standard curing agents to form densely cross-links due to an average number of epoxy groups > 3.96 in the product stream. Furthermore, a techno-economic analysis is performed showcasing a competitive market price for EGCHC with the given process design in the segment of bio-based epoxy resins. The study demonstrates a comprehensive strategy that allows for rapid implementation of a novel synthesis process based on preliminary laboratory measurements and rating thereof.

Bibliographic Information

M. Feigel, J. M. Breitsameter, B. Rieger, O. Hinrichsen, "Bridging the Gap from Laboratory to Production: Kinetic Modeling-Guided Process Development for a Novel Epoxy Resin", *Industrial & Engineering Chemistry Research* **2024**, 63, 1271–1285.

Copyright Notice

©2024 American Chemical Society. This is an accepted version of this article published in doi:10.1021/acs.iecr.3c03339. Clarification of the copyright adjusted according to the guidelines of the American Chemical Society.

5.1 Introduction

Epoxy resins are widely used due to their versatility and ease of processing in various fields. Most commonly, commercial epoxy production relies on the bisphenol A (BPA) and epichlorohydrin (ECH) route to form bisphenol-A-diglycidylether. However, the use of BPA has raised environmental and health concerns. As BPA is a known endocrine disruptor, there are growing calls to restrict or ban its use in consumer products [157]. Furthermore, the reliance on fossil resources for both BPA and ECH production highlights the urgent need to rely on more sustainable alternatives. While bio-based epoxy resins have emerged as potential alternatives, they face limitations in their bio-based content, so epoxy production and still often relies on BPA [4, 113, 137, 158]. Nevertheless, it is inevitable to replace fossil-based epoxy systems in the future and therefore further advancement and expansion of scientific research in that field is required.

Previously, we presented a novel synthesis route to an epoxy resin which can readily be produced with a bio-based content of > 68% and also is completely BPA-free [61]. The production of the epoxy with the name 1,2-epoxy-6-methyl-triglycidyl-3,4,5-cyclohexanetricarboxylate (EGCHC) consists of four main reactions. The synthesis steps are illustrated in Figure 5.1. Allyl sorbate is prepared according to reaction **0a** by esterification of sorbic acid and allyl alcohol. The latter is available as a bio-based product from glycerol and formic acid through reaction **0b** [65, 66]. Sorbic acid is a natural product and can be extracted from rowan berries [64]. It is used in large quantities in the food industry as a preserving agent [159] and is produced from crotonaldehyde and fossil-derived malonic acid [122]. Crotonaldehyde is already available bio-based [124], leading to a conservative approximated bio-based content of allyl sorbate of 67%. The synthesis and process modeling of the production of allyl sorbate are not within the scope of this study since the compound is already commercially available due to its application as a food flavoring agent [115–117]. Hence, the focus is on the process simulation of reactions **1–3**. Additionally, in our earlier work, the reaction progress thereof was measured to facilitate kinetic modeling of the particular reactions [69]. The derived kinetic data are used to build the process model illustrated in the present study.

In total, a complete picture can be drawn starting from laboratory synthesis towards kinetic analysis and finally process modeling providing the starting point for a techno-economic analysis. It should be noted that the process model was developed closely to laboratory works and thus does not claim to be optimized in either scale or unit operations used in an industrial sense. Instead, the approach intended to show a methodology which allows to give access to *a priori* information crucial for further development. Additionally, a short techno-economic analysis was performed based on the gathered process data to rate the competitiveness of the molecule. In the context of the herein shown application

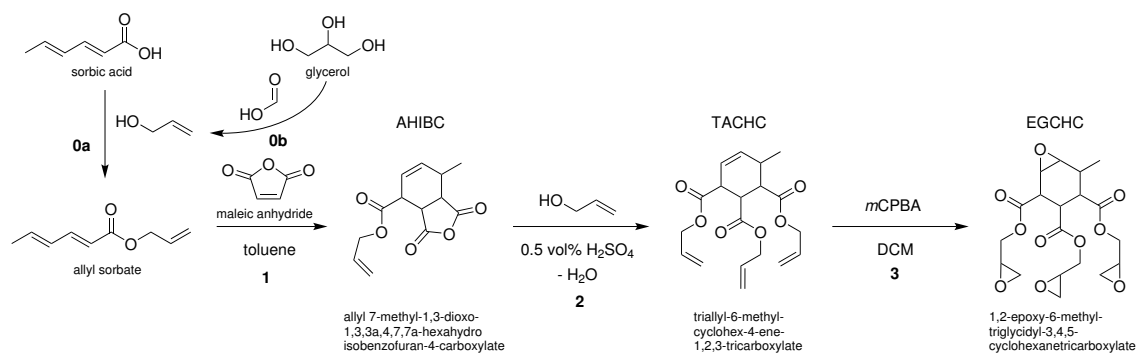


Figure 5.1: Reaction steps for the production of EGCHC starting from sorbic acid and allyl alcohol.

as a resin, only few similar methods can be found in the literature which deal with process design from initial kinetic modeling [160–164]. However, as these studies consider existing molecules and alternative production routes, the presented process model and the simulation approach in our work should demonstrate a methodology to assess the feasibility of the production of a novel resin component.

5.2 Methodology

5.2.1 Components

An overview over all components required for building the process model is given in Table 5.1 with reference to the data origin. Properties retrieved within Aspen Plus were taken from the APV120 PURE38 databank. IUPAC names and structures of all relevant reaction intermediates are given in the Supplementary Information section in Table 5.11.

Table 5.1: Components with names and formula included in the model. Source of their respective physical properties indicated.

component	name	formula	properties
AA	allyl alcohol	C ₃ H ₆ O	Aspen
AS	allyl sorbate	C ₉ H ₁₂ O ₂	Estimated
MA	maleic anyhydride	C ₄ H ₂ O ₃	Aspen
MCBA	<i>m</i> -chlorobenzoic acid	C ₇ H ₅ O ₂ Cl	Aspen
MCPBA	<i>m</i> -chloroperoxybenzoic acid	C ₇ H ₅ O ₃ Cl	Aspen
NMP	<i>N</i> -methyl-2-pyrrolidone	C ₅ H ₉ NO	Aspen
TOL	toluene	C ₇ H ₈	Aspen
DCM	dichloromethane	CH ₂ Cl ₂	Aspen
H ₂ O	water	H ₂ O	Aspen
AHIBC	allyl 7-methyl-1,3-dioxo-1,3,3a,4,7,7a-hexahydroisobenzofuran-4-carboxylate	C ₁₃ H ₁₄ O ₅	Estimated
Ia	†	C ₁₆ H ₂₀ O ₆	Estimated
Ib	†	C ₁₆ H ₂₀ O ₆	Estimated
TACHC	triallyl-6-methylcyclohex-4-ene-1,2,3-tricarboxylate	C ₁₉ H ₂₄ O ₆	Estimated
R	†	C ₁₉ H ₂₄ O ₇	Estimated
RT	†	C ₁₉ H ₂₄ O ₈	Estimated
RTT	†	C ₁₉ H ₂₄ O ₉	Estimated
T	†	C ₁₉ H ₂₄ O ₇	Estimated
TT	†	C ₁₉ H ₂₄ O ₈	Estimated
TTT	†	C ₁₉ H ₂₄ O ₉	Estimated
EGCHC	1,2-epoxy-6-methyl-triglycidyl-3,4,5-cyclohexanetricarboxylate	C ₁₉ H ₂₄ O ₁₀	Estimated

† Name and structure of component in Supplementary Information.

5.2.2 Physical Properties

To set up the process simulation, the required physical properties of all components present in the process must be known. If not stated otherwise, physical properties are taken from the Aspen Plus databases. For most of the structures presented in the synthesis route, physical properties are not available. Thus, a parameter estimation using a standard group contribution approach is employed. Either the UNIFAC or the modified UNIFAC (Dortmund) group contribution method (GCM) is applied to predict missing component properties. For details on calculation and further reading, the original publications are recommended [100, 101, 165]. The estimation of physical properties based on the group contribution method UNIFAC/UNIFAC-DMD is depicted for the components AHIBC, Ia, Ib, TACHC, and EGCHC in detail in Table 5.2.

Table 5.2: List of UNIFAC groups used in the model to determine physical properties of unknown structures. Breakdown of groups required to build the structures of AHIBC, IIa, IIb, TACHC and EGCHC.

main group number	group symbol	description	# of occurrences				
			AHIBC	IIa	IIb	TACHC	EGCHC
1	CH ^a	alkane group	-	-	-	-	-
1	CH2	alkane group	1	2	2	3	3
1	CH3	alkane end group	1	1	1	1	1
2	CH=CH	alkene group	1	1	1	1	-
2	CH=CH2	alkene group	1	2	2	3	-
20	COOH	acid group	-	1	1	-	-
41	COO	acrylate	1	2	2	3	3
42	cCH ^b	cyclic alkane group	4	4	4	4	4
53	H2COCH	epoxy	-	-	-	-	3
53	HCOCH	epoxy	-	-	-	-	1
54	O=COC=O ^c	anhydride	1	-	-	-	-

^aused in UNIFAC if cyclic group is not available.

^bmodified UNIFAC (Dortmund) only.

^cadded from literature [166].

All other components which require a GCM-approach are structured in a similar way and can easily be derived from the given examples. The list of groups for all structures is given in the Supplementary Information in Table 5.11 together with Table 5.12. From the set of required groups, only the anhydride group is not available in the Aspen Plus database. The volume parameter R_k , surface parameter Q_k , and required interaction parameters are listed in Table 5.3 and are taken from the literature [166]:

Table 5.3: Volume parameter R_k and surface parameter Q_k of the anhydride group O=COC=O [166].

group	R_k	Q_k
O=COC=O	1.5200	1.7732

With the help of the group parameters, the activity coefficients are estimated, which are made up of a combinatorial and a residual term. For the latter, binary interaction parameters are needed which are partly published and partly distributed between the UNIFAC consortium members. These interaction parameters are in most cases regressed from vapor-liquid equilibrium data and due to the extensive required number of experimental

data available only for certain groups. In the case of the modified UNIFAC GCM, the temperature dependency of the parameters is enhanced.

$$\Psi_{ij} = \exp\left(-\frac{a_{ij}}{T}\right) \quad (5.1a)$$

$$\Psi_{ij} = \exp\left(-\frac{a_{ij} + b_{ij}T + c_{ij}T^2}{T}\right) \quad (5.1b)$$

Equation 5.1a and Equation 5.1b depict the difference between the calculation methods to determine the binary interaction parameters Ψ_{ij} for two groups i and j . For the original UNIFAC method, in Equation 5.1a, only a single parameter a_{ij} is used. If no interaction

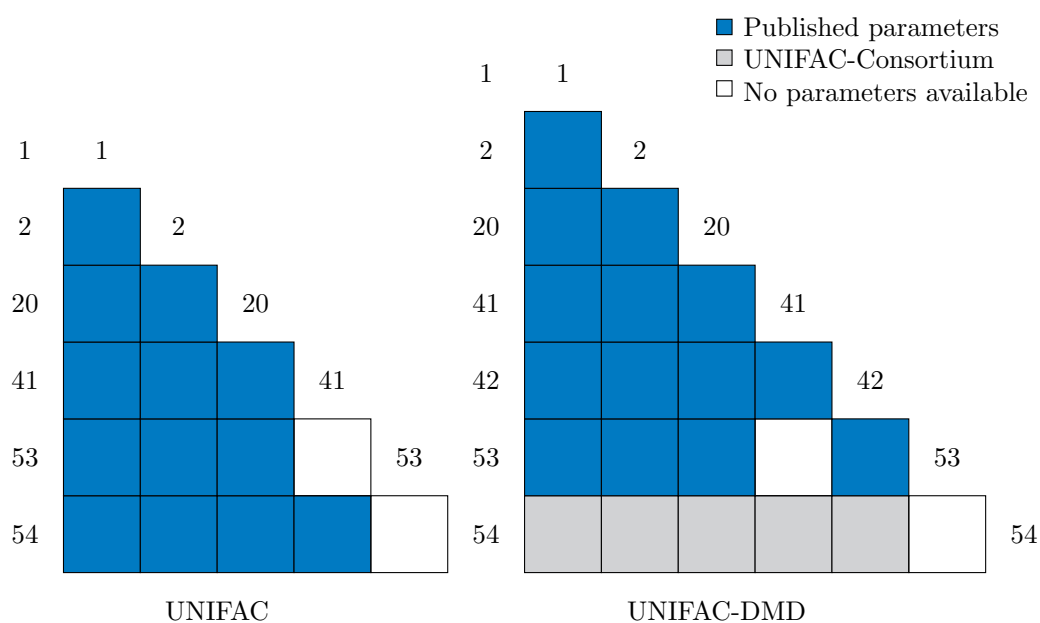


Figure 5.2: Parameter matrices for UNIFAC and modified UNIFAC (Dortmund) group contribution property method. Availability of binary interaction parameters of used groups.

parameters exist, the interaction between these two groups is ignored. Figure 5.2 shows the parameter matrix for the groups needed to model all components in this process. For both UNIFAC and the modified version, most of the binary interaction parameters are available with an exception of the anhydride group in the Dortmund modified property method, which are only available to consortium members [166–168]. Therefore, the physical properties of the relevant component AHIBC are calculated using UNIFAC. The only missing binary interaction parameter affects the epoxide group. However, the interaction between anhydride and epoxide can be neglected, as the anhydride ring is opened within the reaction pathway before epoxide groups are introduced.

In the second process step **2** (Figure 5.1), an esterification takes place using allyl alcohol. Due to the condensation reaction, water accumulates in the solvent stream. Thus, a separation of the solvent-condensate mixture is required. Allyl alcohol and water form an azeotropic composition whose behavior can be described with the nonrandom two-liquid (NRTL) method. For an accurate prediction of the vapor-liquid equilibrium, the binary interaction parameters are regressed using literature data [169–171]. Three sets of data points under isobaric conditions are used. Figure 5.3 shows the literature data on the isobaric vapor liquid equilibrium for 0.3 bar, 0.6 bar, and 1.013 bar with lines indicating prediction by the adjusted NRTL model. The regressed binary interaction parameters are listed in Table 5.4 and are used exclusively in the distillation sections of allyl alcohol. The global property method of the flowsheet is UNIFAC.

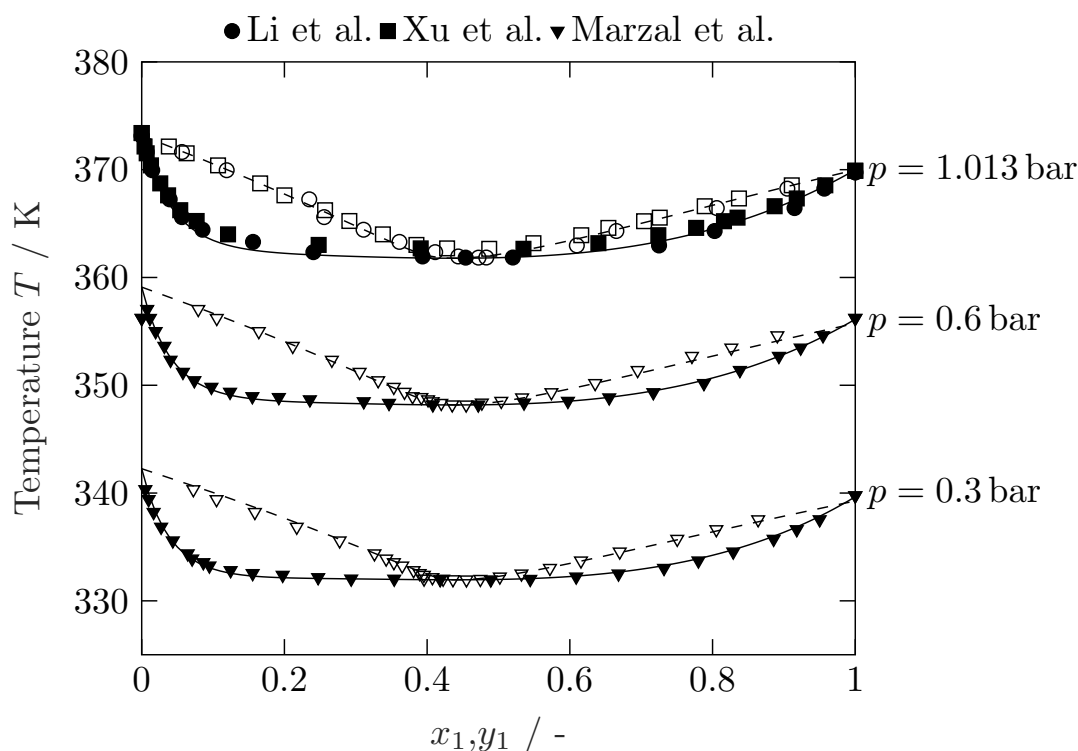


Figure 5.3: Vapor-liquid equilibrium for the mixture of (1) allyl alcohol and (2) water. Solid and dashed lines represent predicted liquid and vapor compositions by NRTL, respectively. Experiments are indicated by markers with open and closed symbols describing vapor and liquid, respectively [169–171].

Table 5.4: Regressed NRTL parameter for the system: allyl alcohol (AA) and water.

i,j	$a_{i,j}$	$b_{i,j}$
H ₂ O, AA	1.937 ± 0.824	192.114 ± 293.679
AA, H ₂ O	-2.022 ± 0.490	673.013 ± 174.181

5.2.3 Kinetic Models

To incorporate the different reactions into the process simulation, their respective kinetic models are required to achieve an accurate description of each step. As already stated, the three main steps (cf. Figure 5.1) are a [4 + 2]-cycloaddition **1**, an esterification **2**, and an epoxidation reaction **3**. In our previous study, reaction models were established for each reaction and regressed with data acquired in laboratory measurements [69]. The following sections briefly depict the reaction models with their particular kinetic parameters. For further details, refer to our previous work [69].

5.2.3.1 Diels-Alder

The Diels-Alder reaction between allyl sorbate and maleic anhydride (Figure 5.1, reaction **1**) is modeled as an irreversible reaction second order. Therefore, the reaction rate can be written as:

$$r = k_{\text{DA}} c_{\text{AS}} c_{\text{MA}} \quad (5.2)$$

with the reaction rate constant k_{DA} and the molar concentration c_i of component i . Pre-exponential factor and activation energy are $k_{0,\text{DA}} = 8.075 \cdot 10^4 \text{ L}/(\text{mol s})$ and $E_{\text{A,DA}} = 60.32 \text{ kJ/mol}$, respectively [69].

5.2.3.2 Esterification

Reaction **2** in Figure 5.1 can be described by the reaction scheme displayed in Figure 5.4. The first reaction step opens the anhydride of structure I and leads to a diester in an acid catalyzed irreversible reaction. Two intermediates are possible due to the unsymmetrical structure of the educt I (AHIBC). Subsequently, allyl alcohol reacts with the intermediates IIa or IIb to form product III (TACHC) and water. All reactions are second order and acid catalysed with $k_i = k_i^* \cdot c_{\text{H}_2\text{SO}_4}$ using 0.5 vol% sulfuric acid. In our previous study it was shown that the reversible reactions towards TACHC exhibit equal reactivity and thus can be treated with the same kinetic constants [69].

Therefore, the resulting model can be described by four reactions and kinetic constants, as for the equilibrium reactions forward and backward reactions are explicitly defined. Hence, the formation rate of each species can be set up, which are shown in Equation 5.3a to Equation 5.3d.

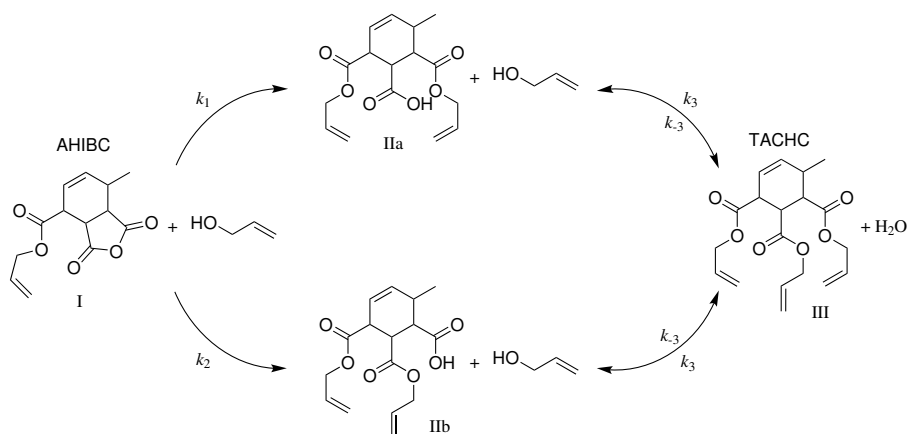


Figure 5.4: Acid catalyzed reaction path of the esterification reaction starting from the Diels-Alder product AHIBC (I) to TACHC (III) via the two intermediates IIa and IIb.

$$\frac{dc_I}{dt} = -(k_1 + k_2)c_I c_{AA} \quad (5.3a)$$

$$\frac{dc_{IIa}}{dt} = +k_1 c_I c_{AA} - k_3 c_{IIa} c_{AA} + k_{-3} c_{III} c_{H_2O} \quad (5.3b)$$

$$\frac{dc_{IIb}}{dt} = +k_2 c_I c_{AA} - k_3 c_{IIb} c_{AA} + k_{-3} c_{III} c_{H_2O} \quad (5.3c)$$

$$\frac{dc_{III}}{dt} = +k_3 (c_{IIa} c_{AA} + c_{IIb} c_{AA}) - 2k_{-3} c_{III} c_{H_2O} \quad (5.3d)$$

The results from regression of pre-exponential factors and activation energies are listed in Table 5.5.

Table 5.5: Pre-exponential factor and activation energy of the reaction rate constants k_1 , k_2 , k_3 and k_{-3} of the allylation reaction [69].

	$k_{0,i}$ in L/(mol s)	$E_{A,i}$ in kJ/mol
k_1	$1.14 \cdot 10^7$	62.76
k_2	$1.66 \cdot 10^6$	68.03
k_3	$1.14 \cdot 10^9$	83.96
k_{-3}	$3.07 \cdot 10^3$	47.72

5.2.3.3 Epoxidation

In the last reaction step, the oxirane functionalities are established. It has been shown that the double bonds in the product of the esterification step can be categorized into two groups [69]. The distinct sites for epoxidation are a double bond in the hexene ring and three terminal double bonds, respectively. Thus, the possible intermediates until complete conversion of all double bonds are indicated with the type of double bond reacted, e.g., for RTT, the ring bound and two terminal double bonds are epoxidized. The modeled reactions are irreversible and of second order in the respective reactant and *m*CPBA. It is assumed that the terminal bonds are chemically and kinetically not distinguishable. The reaction scheme that stems from a gradual epoxidation of each double bond is depicted in Figure 5.5. For better visibility, the scheme is simplified, showing only the components' alias.

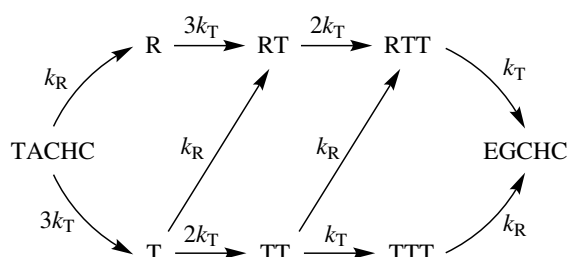


Figure 5.5: Reaction scheme of the epoxidation reaction of TACHC with *m*CPBA.

Due to equal reactivity of the terminal bonds the reaction system can be described by two rate constants k_R and k_T , respectively. As several terminal double bonds are available, the rate constants are multiplied with a factor resembling the possibility of the reaction. The pre-exponential factors and activation energies are listed in Table 5.6.

Table 5.6: Pre-exponential factor and activation energy of the epoxidation rate constants for ring and terminal bound double bonds, k_R and k_T [69].

	$k_{0,i}$ in L/(mol s)	$E_{A,i}$ in kJ/mol
k_R	$2.15 \cdot 10^7$	59.82
k_T	$1.81 \cdot 10^7$	65.57

To evaluate the progress of epoxidation and get a characteristic property of the epoxy, the oxirane oxygen content *OOC* is calculated. The parameter describes the molar content of oxygen atoms bound in epoxy functional groups in ratio to the total molar mass. Additionally, a relative oxirane oxygen content η can be defined, which is scaled to 1 and can be used to track the progress of epoxidation. Details on calculation of *OOC* and η are given in the Supplementary Information.

5.2.4 Process Model

5.2.4.1 Process Design

The process is designed closely to the laboratory procedures. Some process units are replaced with more industrially feasible operations. Since production capacities in the experimental setups are on a gram or milligram scale, no up scaling in size or operation mode has been implemented yet. The described process should demonstrate one possible and viable route to produce the epoxy EGCHC on an industrial scale. The gained insights of the system and the results of the implemented process simulation should pave the way towards decisions on a scale-up. The production process of EGCHC is separated into three sections which consist of the three main reaction steps **1–3** illustrated in Figure 5.1. The complete simulation is based on a constant allyl sorbate mass flow of 100 kg/h. Based on this feed rate, all other input streams are sized with respective design specifications derived from laboratory experience. The postulated process is drawn schematically in Figure 5.6. Process modeling is performed with Aspen Plus® V12 (38.0.0.380).

Results and optimizations are based on the typical chemical reaction data, conversion X_i , yield Y_i , and selectivity S_i which are calculated based on the continuous process flow scheme. Therefore, mole flows \dot{n}_i are taken directly from the stream results to get conversion, yield, and sensitivity data, as shown in Equation 5.4–Equation 5.6, respectively.

$$X_i = \frac{\dot{n}_{i,\text{in}} - \dot{n}_{i,\text{out}}}{\dot{n}_{i,\text{in}}} \quad (5.4)$$

$$Y_i = \frac{\dot{n}_{i,\text{out}} - \dot{n}_{i,\text{in}}}{\dot{n}_{j,\text{in}}} \left| \frac{V_j}{V_i} \right| \quad (5.5)$$

$$S_i = \frac{\dot{n}_{i,\text{out}} - \dot{n}_{i,\text{in}}}{\dot{n}_{j,\text{in}} - \dot{n}_{j,\text{out}}} \left| \frac{V_j}{V_i} \right| \quad (5.6)$$

In the first upstream section, allyl sorbate reacts with maleic anhydride to give the Diels-Alder product AHIBC. Toluene is used as the solvent. The feed rate of maleic anhydride is set to achieve a molar ratio of 1.02 mol/mol, in accordance with laboratory experience. Similarly, the molar fraction of allyl sorbate in the stream is set to 0.15 by varying the toluene make-up flow, accounting for the recycle streams. The reaction mixture is preheated and then fed to the reactor. A plug flow reactor is chosen for the liquid-liquid reaction. Industrial applications of Diels-Alder reactions with maleic anhydride as the dienophile comprise the synthesis of tetrahydrophthalic anhydride (THPA) or methyl tetrahydrophthalic anhydride (MTHPA). The diene is butadiene or isoprene, respectively

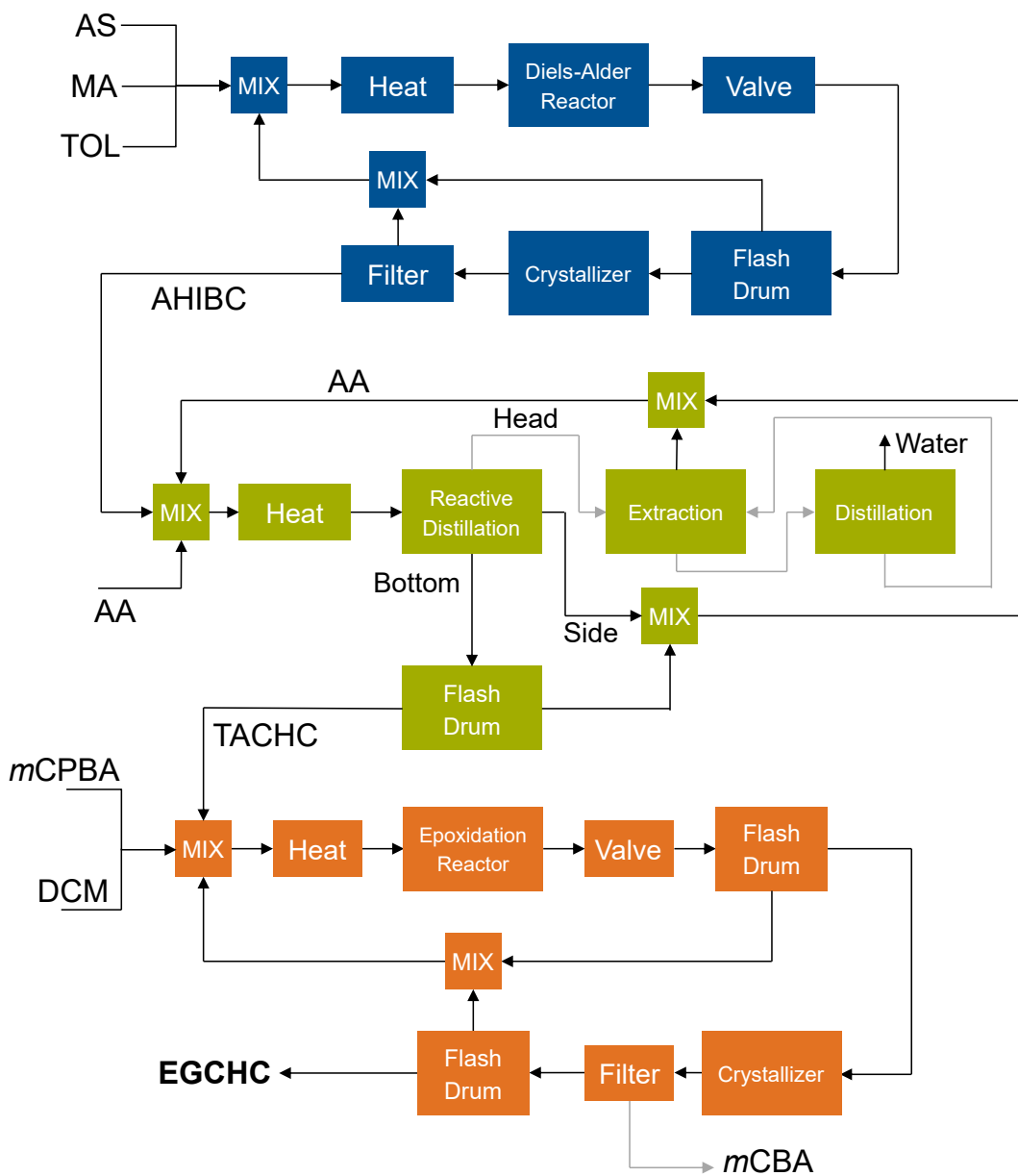


Figure 5.6: Proposed production of EGCHC using a three step cascade reaction starting from allyl sorbate. Section 1: Production of AHIBC, blue. Section 2: TACHC production, green. Section 3: EGCHC production, orange.

[172]. The cycloaddition of maleic anhydride and butadiene is continuously performed in a gas-liquid reactor, where butadiene is vaporized prior to injection [173]. The product THPA is separated by crystallization [174, 175]. MTHPA is synthesized in a liquid reactor in batch or continuously with product purification in a thin film evaporator to recover isoprene [176]. Similarly, after passing through the reactor, the mixture is decompressed, which enables partial vaporization of toluene. Thus, a fraction of the solvent is removed in an adiabatic flash to reduce the energy consumption of the crystallizer. The remaining liquid stream is transferred to a crystallizer, where solid AHIBC is separated from the residual solvent and educts. Both solvent rich streams are recycled and mixed with the feed stream. Afterwards, AHIBC enters the second process section, where it is first dissolved in recycle and make-up allyl alcohol to achieve a molar fraction of 0.1. The preheated liquid stream is fed to a reactive distillation unit, which enables a quick separation of the condensation product together with allyl alcohol at the head. The reactive distillation section implies a homogeneous catalyzed reaction with sulfuric acid. Industrially relevant are normally catalytic packings using ion-exchange materials which act as an acid catalyst due to the corrosive nature of sulfuric acid [177]. Though, there are some references demonstrating a successful application of the mineral acid in a reactive distillation unit [178–180]. As only small fractions of sulfuric acid are required, the component is neglected in the process section. Nevertheless, the kinetic constants already incorporate the acid catalyst and thus are applied as listed in Table 5.5. In preliminary studies, it has been shown that the mineral acid concentration remains fairly constant over the reactive section confirming the lumped kinetic approach. It is conceivable to represent the consecutive reaction from the intermediates IIa and IIb towards TACHC using chemical equilibrium rather than explicit rate expressions for the forward and backward reactions. However, the formation of the intermediates requires an irreversible reaction that still needs to be taken into account, resulting in a minimal computational benefit. Consequently, the kinetic model derived for the reaction network depicted in Figure 5.4 is applied as presented [69]. The allylation product TACHC exits at the bottom of the column and is further purified in a flash drum. A side stream is drawn from the reactive column, which consists of nearly pure allyl alcohol and is mixed together with the vapor phase of the flash drum. The distillate is made up of a mixture of allyl alcohol and water which forms a minimum azeotrope depicted in Figure 5.3. In general, to overcome the azeotropic point, special techniques are applied such as extractive distillation [181–183], azeotropic distillation [184–186] or pressure-swing distillation [187–189]. For the separation of an aqueous allyl alcohol solution extractive distillation [190], eutectic solvents [191] or phase splitting by salt addition [192] are possible methods. Extractive distillation is selected using *N*-methyl-2-pyrrolidone in a molar ratio of 5.9 as an entrainer as it shows promising results for that mixture [190]. The recovered allyl alcohol is then mixed with the recycle stream and added to the feed. In the last process section (reaction **3**), TACHC is epoxidized to the

final product EGCHC. Thus, TACHC is mixed with *m*CPBA and the solvent DCM and fed to a reactor after heating to reaction conditions. The epoxidation reaction is carried out according to experimental works using *m*CPBA with a 2% molar excess per double bond. In an industrial scale, the handling of the peracid is complicated due to safety reasons, i.e., fast decomposition at elevated temperatures in different solvents [193, 194]. A stable operation can be achieved in methylene chloride [193]. Nevertheless, even though the onset decomposition temperature of solid *m*CPBA is 89 °C [195], Zhang et al. recommend operation temperatures below 56 °C for *m*CPBA in DCM at a concentration of 1.1 g/mL [196]. As epoxidation reaction rates for alkenes are low, increased temperatures are favorable [197]. Thus, temperatures up to 90 °C are suggested by using radical inhibitors for stable operation [194]. Due to these concerns, *m*CPBA is often replaced by hydrogen peroxide as an oxidizing agents together with metallic catalysts [52–54], enzymes [57–59] or small chain carboxylic acids [55, 56]. The latter method is commercially applied in, e.g., the production of epoxidized soybean oil acting as a stabilizer in polyvinyl chloride [56, 198, 199]. Nonetheless, taking the safety recommendation into consideration, the epoxidation method with *m*CPBA is a viable option for this process. Furthermore, the route using *m*CPBA is advantageous due to the simple removal of the precipitating *m*CBA which is less soluble in DCM than the peracid [51]. Additionally, the reaction is backed by a reaction model, with kinetic data regressed specifically for the conversion of TACHC that is not available for other epoxidation methods. Moreover, different oxidizing agents have already been tested and were found to be unsuccessful in epoxidizing the terminal double bonds in TACHC [61]. Further downstream, a decompression vaporizes some of the DCM that reduces the amount of liquid processed in the second crystallizer. As residual *m*CPBA and especially *m*CBA solidify at low temperatures, an accurate separation of the oxidizing agents is achieved in a downstream solid filter. Lastly, the permeate is flashed again to effectively remove the remaining solvent fractions, and the epoxy EGCHC is received as the retentate.

5.2.4.2 Economic Evaluation

To evaluate the feasibility of the production of the postulated novel epoxy molecule, the total annual cost *TAC* which is based on the total operating cost *TOC* and the total capital investment *TCI* is calculated. The determination of the *TAC* should enable the rough comparison between commercially available standard epoxy (DGEBA) and special products with increased bio-based content. The *TAC* can be calculated from Equation 5.7, where t_p is the payback time.

$$TAC = \frac{TCI}{t_p} + TOC \quad (5.7)$$

Table 5.7: Raw material prices.

component	price	unit	ref.
allyl alcohol	2.20	\$/kg	[200]
allyl sorbate ^a	3.40	\$/kg	[200, 201]
DCM	0.60	\$/kg	[202]
maleic anhydride	1.80	\$/kg	[203]
<i>m</i> CPBA	36.00	\$/kg	[204]
N-methyl-2-pyrrolidone	4.30	\$/kg	[205]
toluene	0.77	\$/kg	[206]

^aprice computed from sorbic acid and allyl alcohol price.

The investment costs comprise mainly the equipment costs of the process units and their installation costs and are therefore a fixed number within a given process design. The total operating costs consist mainly of the utility and raw material usage, labor, and maintenance. For details and further reading on techno-economic analyses of chemical processes, more in-depth literature review is recommended [105, 108]. The costs for utility, labor and maintenance, and the total capital investment are estimated by Aspen Process Economic Analyzer® (APEA-V12) which is used for the techno-economic evaluation. Equipment costs are estimated from APEA applying a first quarter 2019 pricing basis (CEPCI 618.7). Raw material prices are taken from literature and market references and listed in Table 5.7. Waste water treatment is implemented with a stream price of 0.1 \$/kg. Prices for *m*CPBA in a large scale are harder to obtain and therefore taken from respective online pages [204]. Utilities used in the process are displayed, together with the corresponding prices, in Table 5.8. The costs and properties are directly taken from APEA. As data for *TAC* are unavailable for competitor epoxy production processes, a comparison of product prices is performed. Thus, with a given payback period and a desired rate of return, the target price for EGCHC is estimated and compared with available prices for commercial epoxy materials. The payback times is set to 5 years and the rate of return to 20 %. Setting a short payback time copes with unpredictable risks and costs not coverable here, e.g., piping and site preparation [107].

Table 5.8: Utility prices taken from APEA (2019).

utility	price	unit
electricity	0.0775	\$/kW h
cooling water	0.0317	\$/m ³
low pressure steam (6.90 bar)	17.91	\$/t
medium pressure steam (11.35 bar)	21.48	\$/t
high pressure steam (27.60 bar)	25.77	\$/t
refrigerant (freon 12)	0.17	\$/t

5.3 Results and Discussion

Process Model

As mentioned before, the results for the EGCHC production process are structured in the three main process sections: Diels-Alder reaction (reaction 1), allylation (reaction 2), and epoxidation (reaction 3). In addition to the whole process, each part is individually evaluated. The process flowchart is depicted in Figure 5.7. A complete overview of the equipment is given in the Supporting Information in Table 5.13. The stream results are listed for each section in Table 5.16, Table 5.17 and Table 5.18. Stream splitters are employed to enhance convergence by purging 5% of the recycle loops. This enables a higher stability and robustness of simulating the complex flowsheet with several recycle streams. The quantity of the respective purge streams S-116, S-213, S-218, and S-319 together with their composition can be retrieved from the stream results summary in Table 5.16–Table 5.18

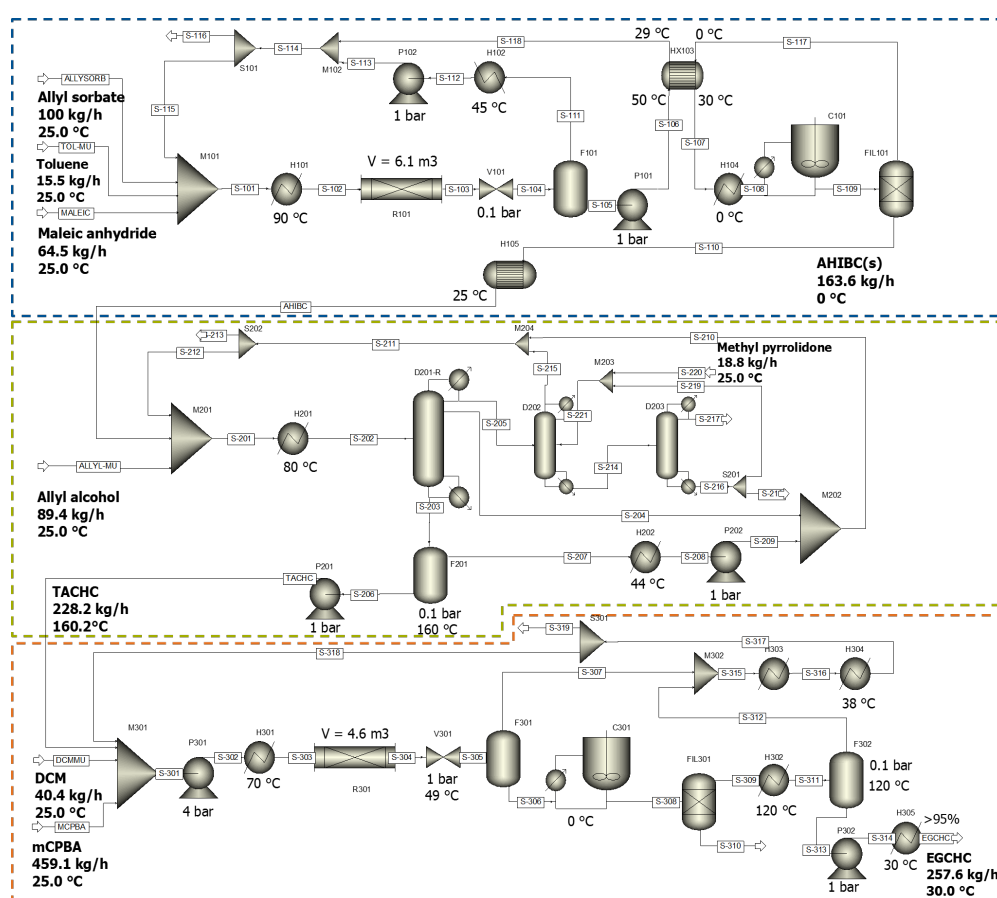
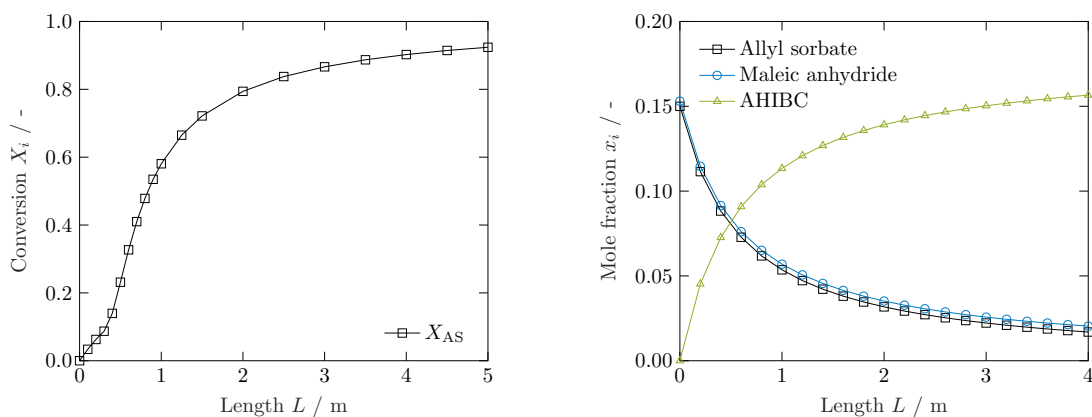


Figure 5.7: Flowsheet of the production of EGCHC with unit operations, streams and indication of process sections.

Diels-Alder

The feed stream consisting of allyl sorbate, maleic anhydride, and toluene and the recycle stream are preheated to a reaction temperature $T = 90^\circ\text{C}$ in a heater H101. The reaction is performed in a multitubular plug flow reactor due to the exothermic character of the Diels-Alder reaction which is operated isothermally ($\Delta_r H^0 = -185.5\text{ kJ/mol}$). Thus, a large heat-transfer area is required to effectively cool the reactor and avoid any hotspots. An industrial typical sizing is applied to the reactor, which consists of 3000 tubes with a standard diameter of 1 inch [207]. The reaction volume, i.e., length, is chosen by performing a sensitivity study of the geometry versus allyl sorbate conversion, which is illustrated in Figure 5.8a. The conversion is determined at the outlet of R101. For an acceptable conversion of $X > 90\%$, a reactor length of 4 m is chosen. The profiles of the molar fraction of the reactants and product are shown in Figure 5.8b. As the Diels-



(a) Conversion of allyl sorbate for varying lengths of multitubular reactor R101.

(b) Molar composition profile in R101. $T = 90^\circ\text{C}$, $L = 4\text{ m}$, $x_{AS,in} = 0.15$.

Figure 5.8: Sensitivity study of reactor tube length and resulting molar fraction profile for $L = 4\text{ m}$ in reactor R101.

Alder product AHIBC is collected in a solid form from the crystallization operation, the liquid stream needs to be cooled down. To reduce the required duty in C101, the reaction mixture is throttled down to 100 mbar so that a fraction of the solvent vaporizes, which can then be separated in the adiabatic flash drum F101. The still solvent-rich liquid phase exits the flash drum, is pressurized, and is then cooled down to 0°C before entering the crystallizer C101. The unit operation is sized by using solubility data of the Diels-Alder product estimated from laboratory experiments. The data are shown in the Supplementary Information section in Table 5.11. Here, only the Diels-Alder product solidifies out of the organic phase and can be removed from the liquid stream in the filter FIL101. Residual educts and solvent are recycled to M101 and used to pre-cool the liquid stream to the crystallizer. AHIBC is achieved with a product mass flow of 163.6 kg/h.

Allylation

The design parameter of the reactive distillation unit D201-R are summarized in Table 5.9. The column is split into two sections with packings as column internals. The bottom part up to feed stage 14 represents the reactive section. As no commercial catalytic packing is available in Aspen Plus, and in this case sulfuric acid is used, a ceramic packing type is applied. If sulfuric acid is explicitly added to the process, it would likely exit the column through the bottom, resulting in a slight dilution of the stream. To achieve the specified product purity, the reboiler duty would need to be increased, leading to a slightly higher bottom temperature than reported in Table 5.9. The residence time is kept short at 60 s. The section height and diameter are 1.2 m and 0.3 m, respectively. The theoretical stages up to the condenser act as the rectification part. Here, the solvent and the reactant allyl alcohol and the condensation product water are separated from the heavy boiling components AHIBC, TACHC, and the reaction intermediates. A side stream exits the column at stage 13 benefiting from nearly pure allyl alcohol which can be obtained here. Additionally, the condenser duty is effectively reduced due to the reflux being simulated by total condensation. Due to a decreased liquid flow rate in the upper part of the column, a smaller diameter is chosen to comply with the column hydraulics. The resulting section packed height and diameter are 2.4 m and 0.2 m, respectively.

Table 5.9: Design parameter of the reactive distillation column D201-R.

parameter	value	comment
R	2.0 mol/mol	molar reflux ratio
n_{stages}	20	number of stages
n_{feed}	14	feed stage number
n_{side}	13	side draw stage number
x_B	0.8	bottom specified TACHC molar purity
\dot{m}_{13}	150 kg/h	specified side mass flow
H	3.6 m	total column height
p_H	1.0 bar	head pressure
T_H^a	89.9 °C	condenser temperature
T_B^a	149.4 °C	boiler temperature

^acalculated values from set design specifications.

Different sensitivity studies are performed to adjust the reflux ratio and molar product purity as a function of the side mass flow. The results are summarized in Figure 5.9. Figure 5.9a illustrates the effect of side mass flow and reflux ratio on the condenser duty \dot{Q} . As expected, a higher back flow from the condenser increases the duty required to liquefy the vapor exiting the column head. Furthermore, the heat duty decreases linearly with the side mass flow. As more liquid is drawn from the middle section of the column, less vapor reaches the condenser. This effect coupled with a higher reflux leads to steeper

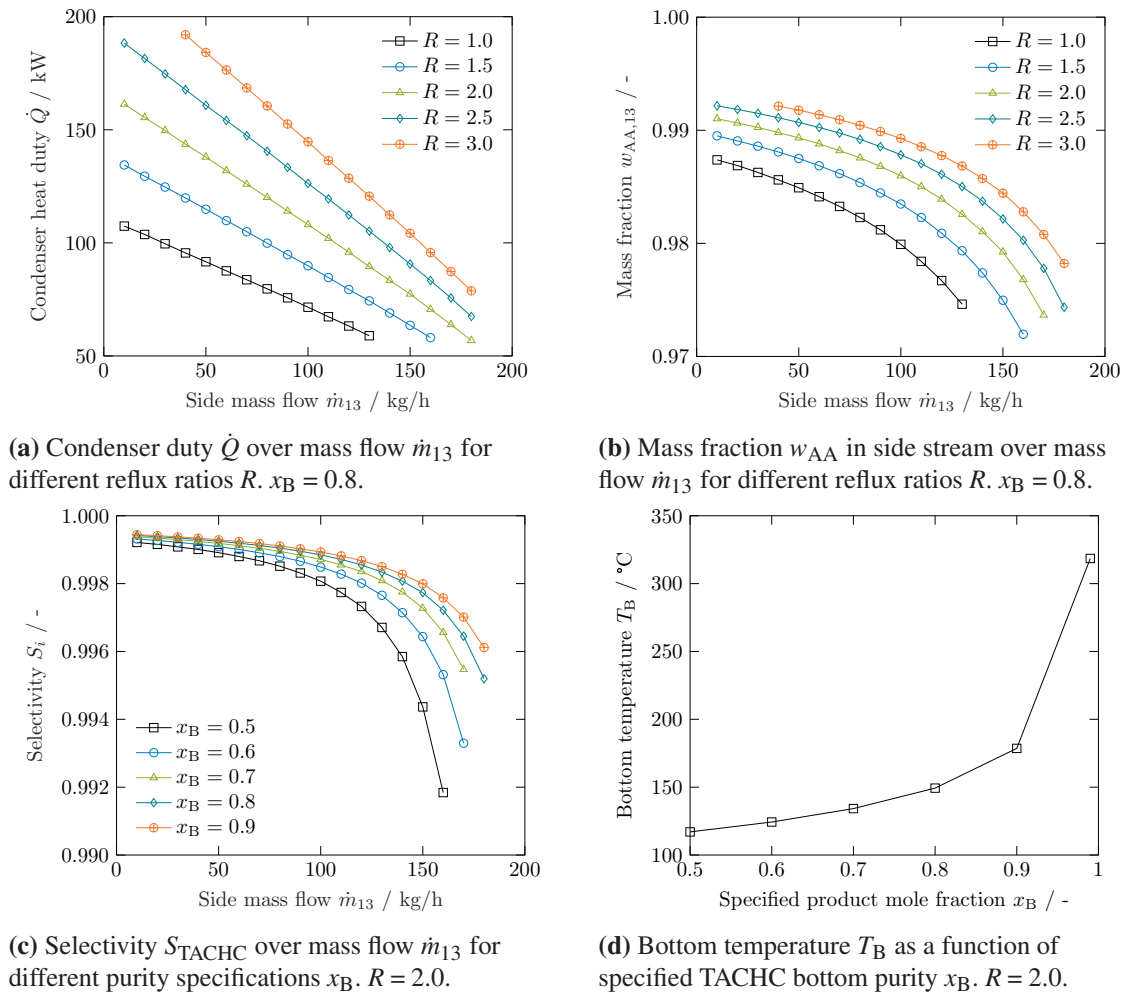


Figure 5.9: Sensitivity studies for reactive distillation column D201-R. Varying of reflux ratio R , side mass flow rate \dot{m}_{13} and bottom molar purity specification x_B .

slopes for the heat duty curves. Hence, e.g., increasing the side mass flow from 50 kg/h to 100 kg/h for $R = 3.0$ reduces the needed heat duty by 21 %. Taking only Figure 5.9a into consideration, the optimization result would lead to decreasing the reflux ratio as far as possible while maintaining a maximum side mass flow rate. It needs to be mentioned that missing data points in all charts stem from infeasible operation points in which too much liquid is extracted leading to a dry up of theoretical stages. Including the results from Figure 5.9b, it can be shown that an inverse trend for choosing an optimal reflux ratio is seen. The purity of allyl alcohol $w_{AA,13}$ in the side stream decreases with increasing side mass flow. Additionally, the purity benefits from higher values of R as more water exits the column through the condenser. Figure 5.9c indicates the development of selectivity of the allylation reaction towards the product TACHC. Here, the specified bottoms purity is altered while keeping the reflux ratio constant. The selectivity drops for large mass flows and lower set points of x_B . Both effects are negligible for low \dot{m}_{13} and only become relevant for high mass flows whereby in absolute terms the impact is less than 1 %. Different aspects are the cause of the selectivity development. As the specified molar

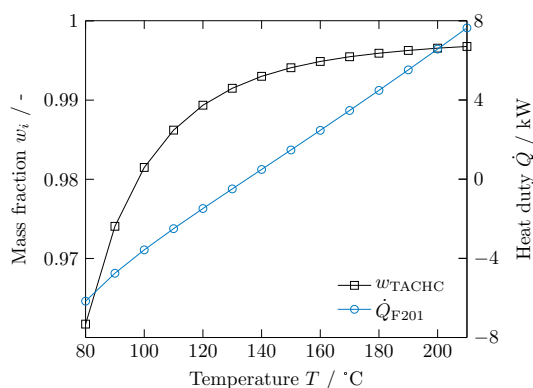


Figure 5.10: Sensitivity of flash drum F201. $p = 0.1$ bar.

fraction is increased, the temperature rises in the column which is also illustrated in Figure 5.9d. Hence, the reaction proceeds at an enhanced rate and less intermediates flow out of the bottom section of the column due to the constant residence time specification. Even though the molar fraction of TACHC is maintained by design specification, the mass fraction of TACHC decreases at high m . Due to the less extent of allyl alcohol, the reaction proceeds slower and produces more intermediates when large amounts are drawn out of stage 13. While a selectivity increase seems beneficial, Figure 5.9d illustrates that the required bottoms temperature of the column rises drastically for $x_B > 0.8$. Combining all results and taking the various influence variables into consideration, the varied parameters are set to the values stated in Table 5.9.

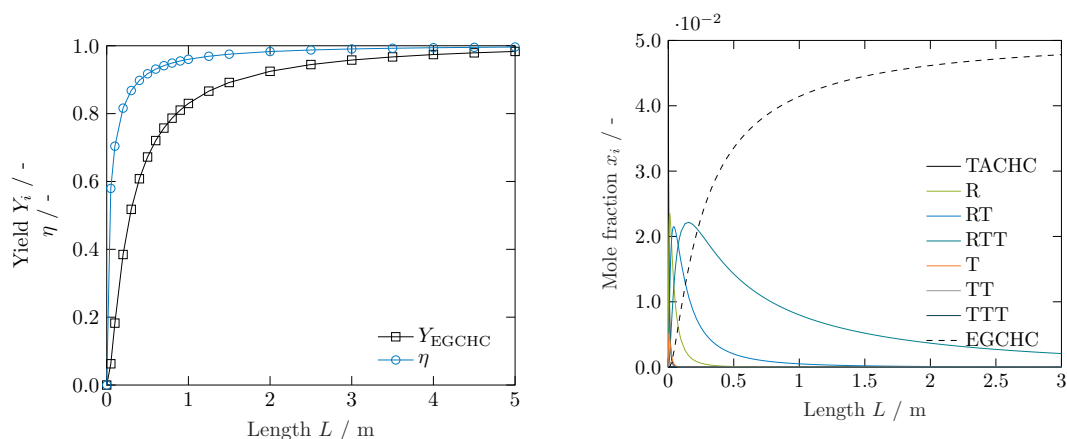
The allyl alcohol side stream is combined with the condensed vapor of flash F201 in the mixer M202. Water is separated from the distillate of column D201-R by using the entrainer NMP. In the first extraction column nearly pure allyl alcohol exits at the condenser, while water and the entrainer are fed to a second distillation column separating the mixture. Afterwards, NMP is recycled back to the extraction section. For better convergence, small stream fractions are purged. Losses are compensated by an entrainer make-up stream. Process parameters are adapted from the literature and summarized in Table 5.14 and Table 5.15 [190]. As water is formed as a condensation product, the amounts to be processed are in a limited range. Therefore, even though a high amount of entrainer of 5.9 mol/mol is proposed by the authors, the purification of allyl alcohol by extractive distillation shows good results due to the small water contents. The allyl alcohol distillate from D202 is mixed with the recycle stream and reused in the feed of the reactive distillation with a combined purity of $w_{AA} = 0.99$.

The crude TACHC stream enters the flash drum F201 where the remaining allyl alcohol is vaporized under a vacuum and at elevated temperature. Figure 5.10 illustrates the mass fraction of TACHC in the outlet liquid stream of flash drum F201 as a function of temperature. Additionally, the required heat duty is plotted on the secondary axis. The sensitivity study shows that a purity > 99 wt-% is achieved at 130 °C. As the bottom temperature for

the specified molar purity $x_B = 0.8$ is $149\text{ }^\circ\text{C}$, the curve illustrating the required heat duty of the flash drum crosses zero around that temperature. Thus, depending on the chosen operation temperature, cooling or heating is required. As the development of the purity flattens off for high temperatures, $160\text{ }^\circ\text{C}$ is selected yielding a TACHC mass fraction of $w_{\text{TACHC}} = 0.995$. The heat of the TACHC stream is used to partially pre-heat the epoxidation feed stream.

Epoxidation

The last reaction step **3** introduces four oxirane functionalities which enables the epoxy to build a cross-linked network. To increase the reaction rate and thus reduce the reactor volume the mixture of components is heated to $70\text{ }^\circ\text{C}$. As the atmospheric boiling point of DCM is below $40\text{ }^\circ\text{C}$ the pressure is increased to 4 bar. The mass flow of *m*CPBA is set by a stoichiometric excess of 1.02 per double bond leads to a mass concentration of 0.35 g/mL which is below 1.1 g/mL [196]. Hence, the chosen process parameters ensure both fast reaction and safe mode of operation regarding the handling of *m*CPBA. To further enhance safety, a multitubular reactor similar to R101 was chosen. The reactor geometry ensures high thermal controllability due to the increased heat transfer area. For a proper sizing of the plug flow reactor a sensitivity is performed. The results are displayed in Figure 5.11a and Figure 5.11b.



(a) Relative oxirane oxygen content η and EGCHC yield Y_{EGCHC} at reactor R301 outlet.

(b) Molar composition profiles in R301. $T = 70\text{ }^\circ\text{C}$, $L = 3\text{ m}$, $x_{\text{TACHC},\text{in}} = 0.05$.

Figure 5.11: Sensitivity study of tube length and resulting profile of molar fractions in reactor R301.

The important product properties are based on number of epoxy groups or oxirane oxygen content *OOC*. As the epoxidation of EGCHC comprises several intermediates a complete production towards the desired epoxy may not be feasible. To effectively form a network

the number of functional groups should extend two as commonly used hardeners provide a bi-functionality. The kinetic model employed allows a direct calculation of the composition at any reactor length and thus, a determination of the characteristic oxirane oxygen content. In Figure 5.11a the yield of product EGCHC and the relative oxirane oxygen content η are calculated for different tube lengths of reactor R301. A small increase in reaction volume leads to a steep curve of both values. Thus, a reactor length of 3 m is chosen, resulting in a yield of $Y = 95.8\%$ and relative oxirane number of $\eta = 99.1\%$. Figure 5.11b displays the profiles of the reactants (cf. Figure 5.5) for the given design specifications. The educt TACHC is rapidly converted. As expected by the reaction mechanism and the magnitude of the rate constants, the reaction proceeds mainly through the upper route drawn in Figure 5.5. The initial epoxidation of a terminal double bond is only slightly pronounced. The subsequent conversion of another terminal bond is negligible. After around 1 m the only remaining intermediate is RTT which slowly reacts due to the decreasing amount of *m*CPBA and low reactivity of the terminal double bond. The exiting reaction mixture consists of EGCHC and RTT with an average number of functional groups of 3.96. The crystallizer C301 operates at a temperature of 0 °C and is sized by the solid formation computed with the equilibrium constant derived from the physical property system using the Gibbs free energies. A large waste stream of $\dot{m} = 418\text{ kg/h}$ consisting of residual *m*-chloroperbenzoic acid and formed *m*-chlorobenzoic acid exits the solid filter FIL301. The consumed peroxy acid can be recycled and thus reused in the process. In general, 3-chlorobenzoic acid is transformed to 3-chlorobenzyl chloride using thionyl chloride [208, 209]. The latter is an industrial common intermediate in medicine for certain drugs or agriculture for herbicides [210, 211]. Also, *m*-chlorobenzyl chloride is the starting material for *m*CBPA production [212], which then closes the cycle. The required steps, chemicals and recycle loop are not implemented in the postulated process, which is out the scope of the present publication. Still, it is noted that with the effort and costs of reconditioning, a circular economy for *m*CBPA can be achieved. Thus, taking the yields of 91 % for *m*-chlorobenzyl chloride [209] and 90.6 % for *m*-chloroperbenzoic acid [212] production into consideration the feed stream of *m*CBPA shrinks to a make-up stream of $\dot{m} = 83.9\text{ kg/h}$.

The purification of the EGCHC product stream is done by vacuum evaporation realized in a flash drum. To determine the operating conditions of the flash drum Figure 5.12 shows the mass fraction of DCM in the product stream. A sensitivity study is performed to evaluate the influence of temperature and pressure on the purity and residual DCM content in the epoxy product stream. To achieve a DCM content of less than 0.1 wt-% the pressure needs to be smaller than 0.05 bar. To keep temperatures in a limited range a pressure of 10 mbar and a temperature of 120 °C is chosen, leading to a product mixture concentration of > 99.9 wt-%. Mixture contents are mainly EGCHC (95.9 wt-%) and epoxidation intermediate RTT (4.0 wt-%).

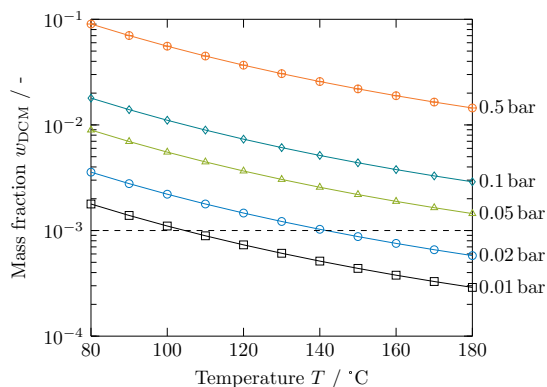


Figure 5.12: Parametric sensitivity of pressure and temperature in flash drum F302 on the purity of DCM in the liquid stream. Target purity of 0.1 wt-% indicated with dashed line.

The product purification realized here by a flash drum in Aspen Plus can industrially be implemented using thin film evaporators to effectively remove the solvent and protect the product EGCHC from degeneration. Thin film or wiped-film evaporators are often applied in industry if unstable and temperature sensitive compounds, e.g. for the purification of caprolactam [213–215] or cases where highly viscous components are processed [216, 217].

Economic Evaluation

To estimate the competitiveness of EGCHC, a techno-economic analysis is performed. As the study introduces a conceptual design study of the chemical process, the estimation of costs can only be made with reasonable accuracy. This is due to not only the early stage in planning but also the estimation of raw material costs, which are subject to most uncertainty. Nevertheless, the results should give a ballpark figure to compare EGCHC with available commercial epoxy resins. A summary of the economics of the process is given in Table 5.19 in the Supporting Information. While a comprehensive economic analysis is not the primary focus of this study, some preliminary insights into the economics of the proposed process are provided. The allylation section accounts for approximately 45 % of the total installed equipment costs for the majority of the capital costs. The reason is the set-up of three distillation units which include a complex reactive distillation column. Utility costs are split mainly between reaction steps 2 and 3 associated with the reactive distillation and crystallization, respectively. Raw material costs are largely driven by the *m*CPBA price. As mentioned in the Process Design section, a shift away from *m*CPBA could improve the process economics resulting in lower raw material costs and possibly cheaper purification techniques. However, alternative epoxidation agents have not achieved comparable yields in laboratory experiments, leading to their exclusion from

Table 5.10: Comparison of EGCHC price from TEA and commercial prices of epoxy resins. Selection of available bio-based epoxy resins together with their bio-based content and composition information from MSDS [218–220].

component	bio-based content	BPA-free	price	unit	ref.
EGCHC ^a	< 68 %	Yes	83.0	\$/kg	-
EGCHC ^b	< 68 %	Yes	21.5	\$/kg	-
DGEBA	0 %	No	2.2	\$/kg	[114]
phenol epoxy novolac	0 %	Yes/No ^c	4.8	\$/kg	[114]
phenoxy resins	0 %	No	11–17	\$/kg	[114]
Entropy Resins® One	< 29 %	No	36	\$/kg	[221]
Sicommin® Greenpoxy 56	< 56 %	No	35	\$/kg	[222]
Resoltech® ECO 1070	< 31 %	No	21	\$/kg	[223]

^ano recycle economy for oxidizing agent.

^bwith recycle economy for *m*CBPA.

^cnovolacs cover a class of epoxy which can depend on BPA.

the current process design. Therefore, the presented route is the basis for the reported economics. As it has been shown in the process results section, a waste stream containing *m*CBA leaves the plant which could be re-processed to close the cycle of the oxidizing agent and thus, reduce the make-up stream of *m*CPBA. To incorporate this in the techno-economic analysis, the raw material price is set to 7.2 \$/kg, representing 20 % of the original market price.

Table 5.10 indicates the resulting price for EGCHC from the TEA using the Aspen Economic Evaluation Analyzer together with market prices for different epoxy resins. Prices for commercial bio-based resins were taken from the manufacturers Web sites or direct quotations and should enable a basis for rough comparison. Additionally, the maximum bio-based content is listed together with the information, whether BPA is included in the composition of the resin. Values are taken from the respective material safety data sheets (MSDS) [218–220]. Clearly, bisphenol-A-diglycidylether (DGEBA) shows the lowest price as it stems from rather simple production processes and mostly relies on crude-oil prices. The resulting EGCHC price is not competitive compared to DGEBA but abstains from BPA usage. Furthermore, the high bio-based content of < 68 % puts it in a different market segment. Comparing EGCHC with other listed bio-based epoxy resins, which are commercially available, showcases that EGCHC with a closed *m*CPBA recycle would indeed be competitive in the high pricing segment of bio-based resins with a product price of 21.5 \$/kg. Also, eliminating the use of BPA allows EGCHC to have a unique selling point, further increasing its competitiveness. Therefore, the rough estimation of EGCHC prices should enable us to decide on proceeding investigations on the novel molecule.

5.4 Conclusion

In this study we could successfully show the implementation of the process for the production of a sustainable epoxy based on allyl sorbate and maleic anhydride. The process is divided into three main sections, resembling the conversion steps from allyl sorbate to EGCHC. The continuous process uses plug flow reactors for the Diels-Alder reaction and the epoxidation step. The allylation is performed in a reactive distillation. The reactors are simulated with available kinetic data. Separation steps are designed with applicable physical properties regressed or estimated for the specific use case. Each of the main process sections is coupled to build a complete plant scheme for the production of EGCHC. Thus, a holistic view emerges starting from the synthesis description in the laboratory [61] towards the kinetic modeling of the crucial reaction steps [69] leading to the process simulation presented here. Hence, in a short matter of time, an initial process flowsheet of the production of a novel compound could be employed. Additionally, a techno-economic analysis is performed that estimates the price for EGCHC from the process specifications. The results show the competitiveness of the novel epoxy in the rising market of bio-based epoxies and BPA-free materials and enable us to decide on further research.

Even though a complete process scheme could be drawn showing promising results for the production of EGCHC, the proposed flowsheet is open for further optimizations. A rigorous heat integration and sizing of heat exchangers are identified as one of the crucial next steps to further reduce energy consumption. Moreover, exchanging the epoxidation method could provide viable alternatives that increase the industrial relevance of the complete process. The energy intensive crystallizer and the reactant *m*CPBA could therefore be replaced. In that case, kinetic data for the epoxidation step must be gathered to facilitate accurate process simulation. Furthermore, experiments in laboratory and pilot scales are necessary to continue investigations and perform more accurate techno-economic analyses.

Supplementary Material

Component Structure Overview

This section provides an overview of the structures of the components present in the process simulation of EGCHC starting from the Diels-Alder product of allyl sorbate and maleic anhydride. Accordingly, educts, intermediates and products are shown and their respective description of UNIFAC groups is tabulated. The group numbering in

Table 5.11 is done in coherence with the documentation of the used software Aspen Plus and displayed in Table 5.12. Group numbers for each molecule are sorted in increasing order. Additionally, the chemical formula and structure are given together with their respective IUPAC names. The abbreviations listed are in accordance to the component names used in the process flowsheet.

It is to be noted that the displayed structures and names for the molecules RT, RTT, T and TT illustrate one possibility. For example, component T defined by the chemical formula $C_{19}H_{24}O_7$ and listed UNIFAC groups in Table 5.11 has an epoxy group which stems from a terminal double bond. Though, the group contribution method can not distinguish the location of the oxirane oxygen as three possibilities exist. Thus, the model treats these components equally. A more detailed analysis can not be derived from the present data, as only double bond conversions of type 'ring' and 'terminal' are reported by evaluation of the 1H -NMR.

Table 5.11: Components estimated with UNIFAC group contribution method. List of names, structures and their respective group description.

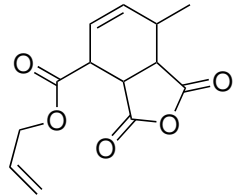
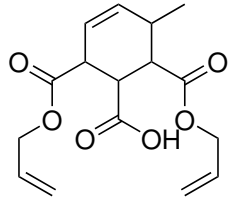
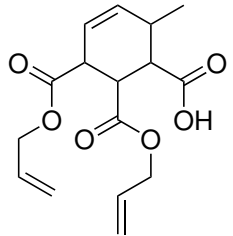
Abb.	Formula	Structure	Name	Group	Number
AHIBC	$C_{13}H_{14}O_5$		allyl 7-methyl-1,3-dioxo-1,3,3a,4,7,7a-hexahydroisobenzofuran-4-carboxylate	1005	4
				1010	4
				1015	1
				1065	1
				1070	1
				3300	1
				5000	1
IIa	$C_{16}H_{20}O_6$		2,6-diallyl-5-methylcyclohex-3-ene-1-carboxylic acid	1005	4
				1010	2
				1015	1
				1065	1
				1070	2
				1955	1
IIb	$C_{16}H_{20}O_6$		5,6-diallyl-2-methylcyclohex-3-ene-1-carboxylic acid	1005	4
				1010	2
				1015	1
				1065	1
				1070	2
				1955	1
				3300	2

Table 5.11: Components estimated with UNIFAC group contribution method. List of names, structures and their respective group description (continued).

Abb.	Formula	Structure	Name	Group	Number
TACHC	$C_{19}H_{24}O_6$		triallyl-6-methylcyclohex-4-ene-1,2,3-tricarboxylate	1005	4
				1010	3
				1015	1
				1065	1
				1070	3
				3300	3
R	$C_{19}H_{24}O_7$		1,2-epoxy-6-methyl-triallyl-3,4,5-cyclohexanetricarboxylate	1005	4
				1010	3
				1015	1
				1070	3
				3300	3
				3910	1
RT	$C_{19}H_{24}O_8$		1,2-epoxy-3-glycidyl-6-methyl-diallyl-3,4,5-cyclohexanetricarboxylate	1005	4
				1010	3
				1015	1
				1070	2
				3300	3
				3900	1
3910	1				

Table 5.11: Components estimated with UNIFAC group contribution method. List of names, structures and their respective group description (continued).

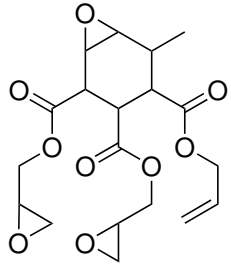
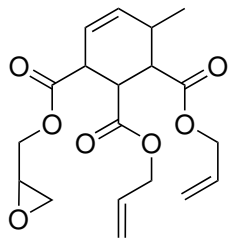
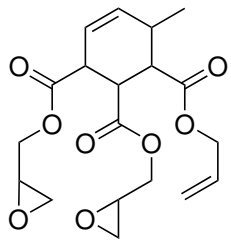
Abb.	Formula	Structure	Name	Group	Number
RTT	$C_{19}H_{24}O_9$		1,2-epoxy-3,4-diglycidyl-6-methyl-allyl-3,4,5-cyclohexanetricarboxylate	1005	4
				1010	3
				1015	1
				1070	1
				3300	3
				3900	2
				3910	1
T	$C_{19}H_{24}O_7$		1,2-diallyl 3-glycidyl-6-methylcyclohex-4-ene-1,2,3-tricarboxylate	1005	4
				1010	3
				1015	1
				1065	1
				1070	2
				3300	3
				3900	1
TT	$C_{19}H_{24}O_8$		1-allyl 2,3-diglycidyl-6-methylcyclohex-4-ene-1,2,3-tricarboxylate	1005	4
				1010	3
				1015	1
				1065	1
				1070	1
				3300	3
				3900	2

Table 5.11: Components estimated with UNIFAC group contribution method. List of names, structures and their respective group description (continued).

Abb.	Formula	Structure	Name	Group	Number
TTT	$C_{19}H_{24}O_9$		triglycidyl-6-methylcyclohex-4-ene-1,2,3-tricarboxylate	1005	4
				1010	3
				1015	1
				1065	1
				3300	3
				3900	3
EGCHC	$C_{19}H_{24}O_{10}$		1,2-epoxy-6-methyl-triglycidyl-3,4,5-cyclohexanetricarboxylate	1005	4
				1010	3
				1015	1
				3300	3
				3900	3
				3910	1

Table 5.12 lists all used UNIFAC groups with the respective group number and description. The individual groups are assigned to main groups which define the to be applied interaction parameters.

Table 5.12: UNIFAC group numbering and description.

Group	Main Group	Symbol	Description
1005		CH	
1010	1	CH ₂	alkane
1015		CH ₃	
1065	2	CH=CH	alpha-olefin group
1070		CH=CH ₂	
1955	20	COOH	acid
3300	41	COO	acrylate
3900	53	CH ₂ OCH	epoxide
3910		CHOCH	
5000	54	O=COC=O	anhydride

Oxirane Oxygen Content

The oxirane oxygen content OOC refers to the bound oxygen atoms in an epoxy functional group within a molecule. It is defined as the molecular mass all oxirane oxygens $n \cdot M_O$ divided by the molecular mass of the component M :

$$OOC = \frac{n \cdot M_O}{M} \quad (5.8)$$

If several oxirane functionalities can be formed within a synthesis process, often a relative oxirane oxygen content is calculated, as shown in Equation 5.9.

$$\eta = \frac{OOC}{OOC_{th}} \quad (5.9)$$

The content of epoxy groups is normalized with the theoretical maximum value. For the epoxy EGCHC, a maximum of four epoxy groups can be formed leading to $OOC_{th} = 0.155$. Thus, a dimensionless number η can be defined which depicts the progress of epoxidation.

Solubility of AHIBC

The solubility of the Diels-Alder product (AHIBC) in toluene was determined in the laboratory at three temperatures, each measured three times. 2 mL of toluene were put in a screwed cap vessel and agitated using a magnetic stirrer. AHIBC was added in small portions and left for several hours to assure complete solution of the solids. In Figure 5.13 the solubility of AHIBC in toluene at 25 °C, 35 °C and 50 °C is shown.

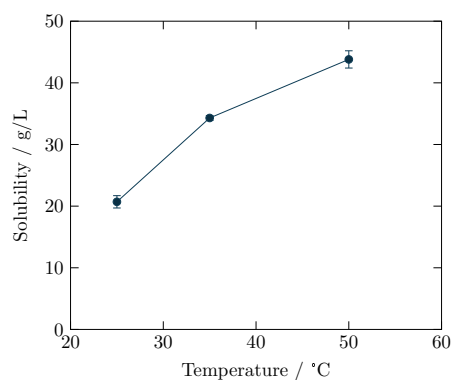


Figure 5.13: Solubility of AHIBC in toluene at different temperatures.

Equipment Overview

A complete list of unit operation models is given in Table 5.13.

Table 5.13: Equipment summary of the complete process scheme. Indicated temperatures and pressures are at the outlet.

Name	Equipment	$T / ^\circ\text{C}$	p / bar
C101	Crystallizer	0	1.0
C301	Crystallizer	0	1.0
D201-R	Reactive distillation column	149 ^a	1.0
D202	Distillation column	146 ^a	1.0
D203	Distillation column	204 ^a	1.0
F101	Flash drum	50	0.1
F201	Flash drum	160	0.1
F301	Flash drum	49	1.0
F302	Flash drum	120	0.1
FIL101	Flash drum	0	1.0
FIL301	Flash drum	0	1.0
H101	Heat exchanger	90	1.0
H102	Heat exchanger	45	0.1
HX103	Heat exchanger	30 ^b	1.0
H104	Heat exchanger	0	1.0
H105	Heat exchanger	25	1.0
H201	Heat exchanger	80	1.0
H202	Heat exchanger	44	0.1
H301	Heat exchanger	70	4.0
H302	Heat exchanger	100	1.0
H303	Heat exchanger	38	1.0
H304	Heat exchanger	38	1.0
H305	Heat exchanger	30	1.0
M101	Mixer	30	1.0
M102	Mixer	33	1.0
M201	Mixer	70	1.0
M202	Mixer	95	1.0
M203	Mixer	196	1.0
M204	Mixer	96	1.0
M301	Mixer	50	1.0
M302	Mixer	109	1.0

^a Bottom temperature.

^b Hot stream outlet temperature.

Table 5.13: Equipment summary of the complete process scheme. Indicated temperatures and pressures are at the outlet (continued).

Name	Equipment	$T / ^\circ\text{C}$	p / bar
P101	Pump	50	1.0
P102	Pump	45	1.0
P201	Pump	160	1.0
P202	Pump	44	1.0
P301	Pump	50	4.0
P302	Pump	120	1.0
R101	Multitubular reactor	90	1.0
R301	Multitubular reactor	70	4.0
S101	Splitter	33	1.0
S201	Splitter	204	1.0
S202	Splitter	96	1.0
S301	Splitter	38	1.0
V101	Valve	50	0.1
V301	Valve	49	1.0

The specifications of process units D202 and D203 are shortly discussed. The separation of allyl alcohol and water is known in literature [190–192]. Thus, a literature study was conducted to apply a published described separation technique. An extraction process using *N*-methyl-2-pyrrolidone (NMP) was chosen which uses two columns to extract water from the mixture achieving first pure allyl alcohol over head and then separating the remaining water/NMP mixture in a second distillation unit [190]. As the study lacked information about the process parameters of the columns and only showed results of observed stream purities, a reproduction was only partially possible. With the set property model used in the current simulation the first distillation column could not be sized successfully. As the scope of the presented study is not on the separation of the allyl alcohol/water mixture and due to the lack of data from the cited reference, the first distillation column was simplified by employing a separation block. To address this limitation, it was ensured that the temperatures in the condenser and reboiler of the simplified separation block accurately reflected the conditions reported in the reference. The design parameters are listed in Table 5.14.

Table 5.14: Design parameter of the distillation column D202.

parameter	value	comment
x_D	0.999	distillate specified AA molar purity
H	3.66 m	total column height
p_H	1 bar	pressure
T_H^a	96.6 °C	condenser temperature
T_B^a	146.2 °C	boiler temperature

^avalues calculated from flashing stream compositions.

For column D203, the separation of water and *N*-methyl-2-pyrrolidone with the specified purity of $x_B = 0.9999$ could be achieved. All design parameter and resulting temperatures are summarized in Table 5.15.

Table 5.15: Design parameter of the distillation column D203.

parameter	value	comment
R	1.5 mol/mol	molar reflux ratio
n_{stages}	15	number of stages
n_{feed}	7	feed stage number
x_B	0.9999	bottom specified NMP molar purity
H	15.2 m	total column height
p_H	1 bar	head pressure
T_H^a	99.1 °C	condenser temperature
T_B^a	203.6 °C	boiler temperature

^acalculated values from set design specifications.

Stream Results

Table 5.16, Table 5.17 and Table 5.18 list the stream results for the process separated in each process section. Stream names can be extracted from Figure 5.7. Components are only listed if they show a mass fraction $w_i > 1 \cdot 10^{-3}$.

Table 5.16: Stream results of the Diels-Alder section.

Name	$\dot{n}_i /$ kmol/h	$\dot{m}_i /$ kg/h	$T /$ °C	$p /$ bar	$w_i / -$			
					AS	MA	TOLUENE	AHIBC
ALLYSORB	0.66	100.00	25.00	1.00	1	0	0	0
MALEIC	0.66	64.50	25.00	1.00	0	1	0	0
TOL-MU	0.17	15.50	25.00	1.00	0	0	1	0
DCMMU	0.48	40.56	25.00	1.00	0	0	0	0
S-101	4.83	492.68	30.28	1.00	0.224	0.147	0.629	0.000
S-102	4.83	492.68	90.00	1.00	0.224	0.147	0.629	0.000
S-103	4.17	492.68	90.00	1.00	0.022	0.017	0.629	0.332
S-104	4.17	492.68	49.98	0.10	0.022	0.017	0.629	0.332
S-105	3.30	412.25	49.98	0.10	0.026	0.020	0.557	0.397
S-106	3.30	412.25	50.17	1.00	0.026	0.020	0.557	0.397
S-107	3.30	412.25	30.17	1.00	0.026	0.020	0.557	0.397
S-108	3.30	412.26	0.00	1.00	0.026	0.020	0.557	0.397
S-109	3.30	412.26	0.00	1.00	0.026	0.020	0.557	0.397
S-110	0.65	163.55	0.00	1.00	0	0	0	0
S-111	0.87	80.43	49.98	0.10	0.001	0.001	0.998	0.000
S-112	0.87	80.43	45.33	0.10	0.001	0.001	0.998	0.000
S-113	0.87	80.43	45.49	1.00	0.001	0.001	0.998	0.000
S-114	3.52	329.14	33.18	1.00	0.033	0.025	0.942	0.000
S-115	3.34	312.68	33.18	1.00	0.033	0.025	0.942	0.000
S-116	0.18	16.46	33.18	1.00	0.033	0.025	0.942	0.000
S-117	2.65	248.71	0.00	1.00	0.043	0.033	0.924	0
S-118	2.65	248.71	29.16	1.00	0.043	0.033	0.924	0

Table 5.17: Stream results of the Allylation section.

Name	$\dot{n}_i /$ kmol/h	$\dot{m}_i /$ kg/h	$T /$ °C	$p /$ bar	$w_i / -$						
					AA	H2O	AHIBC	IIA	IIB	TACHC	NMPYR
AHIBC	0.65	163.55	25.00	1.00	0	0	1	0	0	0	0
ALLYL-MU	1.54	89.37	25.00	1.00	1	0	0	0	0	0	0
S-201	6.53	498.35	69.76	1.00	0.666	0.006	0.328	0.000	0.000	0.000	0
S-202	6.53	498.35	80.00	1.00	0.666	0.006	0.328	0.000	0.000	0.000	0
S-203	0.82	237.01	149.41	1.00	0.039	0.000	0.000	0.001	0.001	0.959	0
S-204	2.70	150.00	94.29	1.00	0.979	0.021	0.000	0.000	0.000	0.000	0
S-205	2.36	111.34	89.85	1.00	0.896	0.104	0.000	0.000	0.000	0.000	0
S-206	0.67	228.35	160.00	0.10	0.003	0.000	0	0.001	0.001	0.995	0
S-207	0.15	8.65	160.00	0.10	0.998	0.001	0	0.000	0.000	0.001	0
S-208	0.15	8.65	43.91	0.10	0.998	0.001	0	0.000	0.000	0.001	0
S-209	0.15	8.65	44.02	1.00	0.998	0.001	0	0.000	0.000	0.001	0
S-210	2.85	158.65	94.79	1.00	0.980	0.020	0.000	0.000	0.000	0.000	0
S-211	4.57	258.34	95.51	1.00	0.988	0.012	0.000	0.000	0.000	0.000	0
S-212	4.34	245.42	95.51	1.00	0.988	0.012	0.000	0.000	0.000	0.000	0
S-213	0.23	12.92	95.51	1.00	0.988	0.012	0.000	0.000	0.000	0.000	0
S-214	4.44	388.36	146.23	1.00	0.000	0.030	0	0	0	0	0.970
S-215	1.72	99.69	96.60	1.00	1.000	0.000	0	0	0	0	0
S-216	3.80	376.71	203.64	1.00	0.000	0.000	0	0	0	0	1.000
S-217	0.64	11.65	99.08	1.00	0.005	0.995	0	0	0	0	0.000
S-218	0.19	18.84	203.64	1.00	0.000	0.000	0	0	0	0	1.000
S-219	3.61	357.87	203.64	1.00	0.000	0.000	0	0	0	0	1.000
S-220	0.19	18.83	25.00	1.00	0	0	0	0	0	0	1
S-221	3.80	376.71	196.06	1.00	0.000	0.000	0	0	0	0	1.000

Table 5.18: Stream results of the Epoxidation section.

Name	$\dot{n}_i /$ kmol/h	$\dot{m}_i /$ kg/h	$T /$ °C	$p /$ bar	$w_i / -$										
					AA	IIA	IIB	TACHC	EGCHC	MCPBA	MCBA	DCM	R	RT	RTT
TACHC	0.67	228.35	160.16	1.00	0.003	0.001	0.001	0.995	0	0	0	0	0	0	0
MCPBA	2.66	459.11	25.00	1.00	0	0	0	0	0	1	0	0	0	0	0
S-301	13.07	1508.50	49.60	1.00	0.009	0.000	0.000	0.151	0.000	0.304	0.000	0.535	0.000	0.000	0.000
S-302	13.07	1508.50	50.12	4.00	0.009	0.000	0.000	0.151	0.000	0.304	0.000	0.535	0.000	0.000	0.000
S-303	13.07	1508.50	70.00	4.00	0.009	0.000	0.000	0.151	0.000	0.304	0.000	0.535	0.000	0.000	0.000
S-304	13.07	1508.51	70.00	4.00	0.009	0.000	0.000	0	0.171	0.009	0.268	0.535	0.000	0.000	0.007
S-305	13.07	1508.51	48.81	1.00	0.009	0.000	0.000	0	0.171	0.009	0.268	0.535	0.000	0.000	0.007
S-306	11.37	1364.69	48.81	1.00	0.010	0.000	0.000	0	0.189	0.010	0.296	0.487	0.000	0.000	0.008
S-307	1.70	143.83	48.81	1.00	0.003	0.000	0.000	0	0.000	0.000	0.000	0.997	0.000	0.000	0.000
S-308	11.37	1364.69	0.00	1.00	0.010	0.000	0.000	0	0.189	0.010	0.296	0.487	0.000	0.000	0.008
S-309	8.71	946.41	0.00	1.00	0.015	0	0	0	0.272	0	0	0.702	0.000	0.000	0.011
S-310	2.66	418.28	0.00	1.00	0	0.001	0.001	0	0	0.033	0.966	0	0	0	0
S-311	8.71	946.41	120.00	1.00	0.015	0	0	0	0.272	0	0	0.702	0.000	0.000	0.011
S-312	8.06	677.73	120.00	0.01	0.020	0	0	0	0.000	0	0	0.980	0.000	0.000	0.000
S-313	0.65	268.68	120.00	0.01	0.000	0	0	0	0.959	0	0	0.001	0.000	0.001	0.040
S-314	0.65	268.68	120.13	1.00	0.000	0	0	0	0.959	0	0	0.001	0.000	0.001	0.040
S-315	9.75	821.56	109.69	1.00	0.017	0.000	0.000	0	0.000	0.000	0.000	0.983	0.000	0.000	0.000
S-316	9.75	821.56	37.94	1.00	0.017	0.000	0.000	0	0.000	0.000	0.000	0.983	0.000	0.000	0.000
S-317	9.75	821.56	38.18	1.00	0.017	0.000	0.000	0	0.000	0.000	0.000	0.983	0.000	0.000	0.000
S-318	9.26	780.48	38.18	1.00	0.017	0.000	0.000	0	0.000	0.000	0.000	0.983	0.000	0.000	0.000
S-319	0.49	41.08	38.18	1.00	0.017	0.000	0.000	0	0.000	0.000	0.000	0.983	0.000	0.000	0.000
EGCHC	0.65	268.68	30.00	1.00	0.000	0	0	0	0.959	0	0	0.001	0.000	0.001	0.040

Table 5.19 summarizes the economic metrics of the project which were calculated with the help of APEA.

Table 5.19: Executive summary of the investment costs from the APEA simulation results.

name	value	unit
Total capital investment	$7.268 \cdot 10^6$	USD
Total operating cost	$3.682 \cdot 10^7$	USD/year
Total raw material cost	$3.260 \cdot 10^7$	USD/year
Total utility cost	$1.192 \cdot 10^5$	USD/year
Total product sales	$4.640 \cdot 10^7$	USD/year
Rate of return	20	%/year
Payback period ^a	5	years

^adesign specification, calculated from adjusted product price.

6 Summary

6.1 Conclusions

This thesis presents a holistic picture of the development of a process simulation for the production of a novel epoxy molecule with four oxirane functionalities: 1,2-epoxy-6-methyl-triglycidyl-3,4,5-cyclohexanetricarboxylate (EGCHC). The study spans from laboratory synthesis using sustainable starting materials through kinetic modeling to a comprehensive process simulation encompassing all key reaction steps. The process starts with mainly bio-based components and fossil-based molecules, which have readily been proven to be derivable from natural feedstocks. The synthesis covers four steps to obtain EGCHC in high yields of 78 %. The reaction steps consist of an esterification, Diels-Alder reaction, allylation (addition twice of allyl alcohol), and an epoxidation reaction. The initial esterification step was excluded from further kinetic or process modeling since the product allyl sorbate is a commercially available substance. The thermo-mechanic properties of cured resins of EGCHC were evaluated using standard methods. In particular, composites containing EGCHC and the curing agent isophorone diamine showed promising glass transition temperatures, tensile moduli, and tensile strengths. The materials prepared with EGCHC exceeded the mechanical properties of its commercial competitor, DGEBA. Due to its lack of aromatic structure, the glass transition temperature of 130 °C of cured EGCHC cannot fully reach the high T_g of the DGEBA-based resin.

The bio-based content of EGCHC was assessed by applying the respective DIN EN and ASTM standards using a conservative approach. Due to the different calculation methods, a bio-based content of 53.2 % (DIN) and 68.4 % (ASTM) was derived. DGEBA was chosen as a commercial standard epoxy to evaluate potentials of the bio-based alternative. It was shown that EGCHC exceeded by 39.8 % the frequently used epoxy. Additionally, the bio-based content EGCHC and DGEBA cured with IPD was examined. Using 90 % bio-based IPD, a total bio-based content for cured resins of EGCHC and DGEBA of 74.7 % and 40.9 % was calculated, respectively.

Central to this work is the kinetic modeling of the individual reaction steps involved in the synthesis. The model development comprised model discrimination, parameter

estimation, and statistical analyses thereof. $^1\text{H-NMR}$ was used to gather the sets of experimental data necessary to regress the model parameters. Under controlled conditions, batch experiments were conducted with frequent sampling. Out of all probes, a total of 652 model responses were obtained. These consist of the concentrations or molar fractions of individual components in the three studied reactions. The sampling time defined the predictors. This measurement technique is capable of gathering observations in a fast, simple, and accurate way. The Diels-Alder reaction between allyl sorbate and maleic anhydride was confirmed to be second-order and irreversible, allowing for an analytical solution of the rate law. The derived model accurately describes allyl sorbate conversion, with random and independent errors, leading to reliable estimates for the pre-exponential factor and activation energy. The subsequent allylation was successfully modeled with two intermediates arising from the different ring-opening pathways. Information criteria and maximum likelihood were employed for model selection, revealing the empirically most supported model assuming equal reactivity of the intermediates towards EGCHC. It was shown that the carboxylate group's proximity influences the reactivity difference in ring-opening and subsequent intermediate concentrations. The final epoxidation step was modeled, tracking eight components, including starting materials and products. Despite the complexity, a model with two kinetic constants accurately depicted the reaction progress, reflecting the expected lower reactivity of terminal olefins compared to ring-bound double bonds. Overall, the proposed models precisely fit the experimental data, suggesting their effectiveness in describing the respective reactions. Statistical analyses confirmed random errors and no correlation in the gathered data, emphasizing the empirical support of each model.

A process design was conceptualized which was utilized to construct a process simulation leveraging the insights gained from the kinetic model. Following the reaction path, the process was divided into three sections covering the Diels-Alder reaction, allylation, and epoxidation reaction. A plug flow reactor was designed for the Diels-Alder reaction, allowing enhanced control of the reaction temperature necessary for the exothermic reaction. In the second step, process intensification was applied by coupling reaction and separation in a reactive distillation column. By utilizing sensitivity studies, optimal operation conditions could be derived for reflux ratio, reboiler duty, and the mass flow of a side stream of highly pure allyl alcohol. The addition of the side stream enabled a drastic reduction in energy consumption and unit sizing. The last reaction step introduces the functional groups necessary to build a cross-linked network. It was shown that the formation of the epoxy groups proceeded with different reactivities dependent on the location of the double bonds. The process was simulated with a plug flow reactor using the reaction model derived and regressed in the kinetic modeling section. Due to the traceability of only the type of double bond in the measurements, the process model allowed for a detailed understanding of the reaction progress. Thus, evaluating the oxirane

content enabled an optimal sizing of the reactor.

A techno-economic analysis was established to evaluate the economic feasibility of the proposed process, offering a ballpark figure for the final product price and enabling comparison to commercial bio-based products. A drastic reduction in the product price could be achieved by utilizing a recycling management of consumed epoxidation agent *m*CPBA. The estimated price is comparable to other readily available bio-based epoxy resins. However, EGCHC offers the benefit of abstaining from using BPA or ECH, which most of the commercial components still rely on.

6.2 Outlook

This thesis covers the preliminary development and feasibility study of the production of the novel epoxy resin EGCHC. It is shown that the resin is both technically and economically competitive, which should enable a starting point for further in-depth analyses to design the process. As the main focus of this work is based on the reactions involved, more research must be done to model the separation sections accurately. Here, studies on the physical properties of the generated molecules are inevitable. The intermediate components, starting from allyl sorbate towards EGCHC, do not exist in current physical properties databases. Therefore, group contribution methods are applied to predict these properties. Experimental works could showcase the accuracy and reliability of the predictions and lead to a more detailed and accurate simulation of the separation steps. Additionally, by optimizing energy consumption, this process can reduce costs and enhance its marketability as an environmentally friendly solution. Thus, heat integration can be employed within the process design.

Furthermore, laboratory work, both in scale and operation, needs to be followed to prove the concept of the process. Continuous operation must be evaluated for all reaction steps. This not only enables the validation of the production process but also allows for higher material output, which can be utilized to further assess other physical properties of the resin, which demand larger samples. If the postulated process design is verified, a scale-up of the units is necessary to assess the scalability of the reactions and separations. The precipitation of solids might introduce challenges that need to be tackled.

The applied methodology can broadly be deployed for other novel molecules synthesized in the laboratory. In the present study, $^1\text{H-NMR}$ was utilized as a fast measurement technique that can be used in many organic syntheses. Even if the detection of the individual components would not be accessible by $^1\text{H-NMR}$, modern analytical chemistry offers a wide range of *in situ* methods to track the reaction progress. On that basis, kinetic

modeling can be performed, which lays the foundation for further *a priori* process design. By leveraging the results of the process model, early predictions of technical and economic feasibility can be made. Therefore, the insights gained from this work are crucial for determining the following steps, i.e., whether to proceed with scale-up, dive deeper into research for process optimization, or explore alternative production methods altogether.

A UNIFAC Groups

A.1 UNIFAC

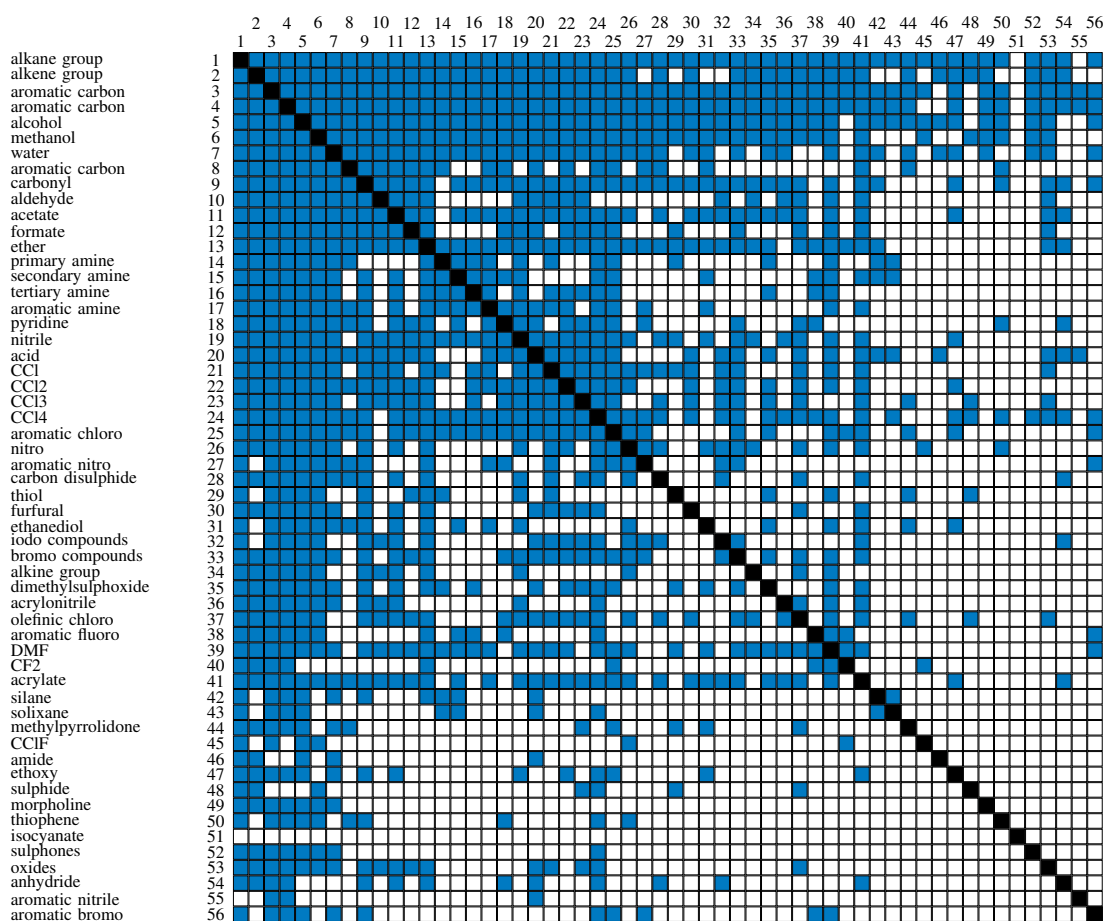


Figure A.1: Availability matrix of published binary interaction parameters $a_{m,k}$ for the UNIFAC model. Data from [166–168].

Table A.1: List of UNIFAC groups used in the model to determine physical properties of unknown structures.

main group	sub group symbol	description	main group	group symbol	description
1	C		20	COOH	
1	CH	alkane group	20	HCOOH	acid
1	CH ₂		21	CCl	
1	CH ₃		21	CHCl	CCl
2	C=C		21	CH ₂ Cl	
2	CH=C	alkene group	22	CCl ₂	
2	CH ₂ =C		22	CHCl ₂	CCl ₂
2	CH=CH		22	CH ₂ Cl ₂	
2	CH=CH ₂		23	CCl ₃	CCl ₃
3	ACH	aromatic carbon	23	CHCl ₃	
3	AC		24	CCl ₄	CCl ₄
4	ACCH	aromatic carbon	25	ACCl	aromatic chloro
4	ACCH ₂		26	CHNO ₂	
4	ACCH ₃		26	CH ₂ NO ₂	nitro
5	OH	alcohol	26	CH ₃ NO ₂	
6	CH ₃ OH	methanol	27	ACNO ₂	aromatic nitro
7	H ₂ O	water	28	CS ₂	carbon disulphide
8	ACOH	aromatic carbon	29	CH ₂ SH	
9	CH ₂ CO	carbonyl	29	CH ₃ SH	thiol
9	CH ₃ CO		30	furfural	furfural
10	HCO	aldehyde	31	DOH	ethane diol
11	CH ₂ COO	acetate	32	I	iodo compounds
11	CH ₃ COO		33	Br	bromo compounds
12	HCOO	formate	34	CC	
13	CHO	ether	34	CHC	alkene group
13	CH ₂ O		35	DMSO	dimethylsulphoxide
13	CH ₃ O		36	CH ₂ CHCN	acrylonitrile
13	THF		37	C=C-Cl	olefinic chloro
14	CHNH ₂	primary amine	38	ACF	aromatic fluoro
14	CH ₂ NH ₂		39	DMF	
14	CH ₃ NH ₂		39	HCON(CH ₂) ₂	DMF
15	CHNH	secondary amine	40	CF	
15	CH ₂ NH		40	CF ₂	CF ₂
15	CH ₃ NH		40	CF ₃	
16	CH ₂ N	tertiary amine	41	COO	acrylate
16	CH ₃ N		42	Si	
17	ACNH ₂	aromatic amine	42	SiH	silane
18	C ₅ H ₃ N	pyridine	42	SiH ₂	
18	C ₅ H ₄ N		42	SiH ₃	
18	C ₅ H ₅ N		43	SiO	siloxane
19	CH ₂ CN	nitrile	43	SiHO	
19	CH ₃ CN		43	SiH ₂ O	

Table A.1: List of UNIFAC groups used in the model to determine physical properties of unknown structures (continued).

main group	sub group symbol	description	main group	group symbol	description
44	NMP	methylpyrrolidone	49	morpholine	morpholine
45	CCl3F		50	C4H2S	
45	CCl2F		50	C4H3S	thiophene
45	HCCl2F		50	C4H4S	
45	HCClF		52	CH2SuCH	
45	CClF2	CClF	52	CH2SuCH2	sulphones
45	HCClF2		53	CH2OCH2	
45	CClF3		53	CH2OCH	
45	CCl2F2		53	CH2OC	oxides
46	CONH2		53	CHOCH	
46	CONCH3		53	CHOC	
46	CONCH2	amide	53	COC	
46	CON(CH3)2		54	O=COC=O	anhydride
46	CONCH3CH2		55	ACCN	aromatic nitrile
46	CON(CH2)2		56	ACBr	aromatic bromo
47	C2H4O2				
47	C2H5O2	ethoxy			
48	CH2				
48	CH2S	sulphide			
48	CH3S				

B Bibliography

- [1] H. Lee, K. Neville, *Handbook of Epoxy Resins*, McGraw-Hill, New York, **1982**.
- [2] C. A. May, *Epoxy Resins*, 2nd Edition, Routledge, New York, **1988**.
- [3] X. M. Chen, B. Ellis in *Chemistry and Technology of Epoxy Resins*, Springer, Dordrecht, **1993**, pp. 303–325.
- [4] F. A. M. M. Gonçalves, M. Santos, T. Cernadas, P. Ferreira, P. Alves, “Advances in the development of biobased epoxy resins: insight into more sustainable materials and future applications”, *Int. Mater. Rev.* **2022**, *67*, 119–149, DOI 10.1080/09506608.2021.1915936.
- [5] P. Skoczinski, M. Carus, G. Tweddle, P. Ruiz, N. Hark, A. Zhang, D. de Guzman, J. Ravenstijn, H. Käb, A. Raschka, *Bio-based Building Blocks and Polymers – Global Capacities, Production and Trends 2023–2028*, Hürth, Germany, **2024**, DOI 10.52548/vxth2416.
- [6] X. Wang, W. Guo, L. Song, Y. Hu, “Intrinsically flame retardant bio-based epoxy thermosets: A review”, *Compos. Part B-Eng.* **2019**, *179*, 107487, DOI 10.1016/j.compositesb.2019.107487.
- [7] B. M. Bell, J. R. Briggs, R. M. Campbell, S. M. Chambers, P. D. Gaarenstroom, J. G. Hippler, B. D. Hook, K. Kearns, J. M. Kenney, W. J. Kruper, D. J. Schreck, C. N. Theriault, C. P. Wolfe, “Glycerin as a Renewable Feedstock for Epichlorohydrin Production. The GTE Process”, *CLEAN-Soil Air Water* **2008**, *36*, 657–661, DOI 10.1002/c1en.200800067.
- [8] G. M. Lari, G. Pastore, C. Mondelli, J. Pérez-Ramírez, “Towards sustainable manufacture of epichlorohydrin from glycerol using hydrotalcite-derived basic oxides”, *Green Chem.* **2018**, *20*, 148–159, DOI 10.1039/C7GC02610B.
- [9] European Commission Joint Research Centre, BTG Biomass Technology Group B.V., *Insights into the European market for bio-based chemicals: factsheets for 10 biobased product categories*, Publications Office of the European Union, Luxembourg, **2019**.

- [10] M. Ricciardi, D. Cespi, M. Celentano, A. Genga, C. Malitesta, A. Proto, C. Capacchione, R. Cucciniello, “Bio-propylene glycol as value-added product from Epicerol® process”, *Sustain. Chem. Pharm.* **2017**, *6*, 10–13, DOI 10.1016/j.scp.2017.06.003.
- [11] W. H. Lawrence, M. Malik, J. E. Turner, J. Autian, “Toxicity profile of epichlorohydrin”, *J. Pharm. Sci.* **1972**, *61*, 1712–1716, DOI 10.1002/jps.2600611103.
- [12] A. Giri, “Genetic toxicology of epichlorohydrin: A review”, *Mutat. Res.-Rev. Mutat.* **1997**, *386*, 25–38, DOI 10.1016/s1383-5742(96)00042-7.
- [13] K.-A. Hwang, K.-C. Choi in *Advances in Molecular Toxicology*, Vol. 9, (Eds.: J. C. Fishbein, J. M. Heilman), Elsevier, Amsterdam, **2015**, pp. 1–33.
- [14] S. Almeida, A. Raposo, M. Almeida-González, C. Carrascosa, “Bisphenol A: Food Exposure and Impact on Human Health”, *Compr. Rev. Food Sci. F.* **2018**, *17*, 1503–1517, DOI 10.1111/1541-4337.12388.
- [15] X. Gao, H.-S. Wang, “Impact of Bisphenol A on the Cardiovascular System - Epidemiological and Experimental Evidence and Molecular Mechanisms”, *Int. J. Environ. Res. Pu.* **2014**, *11*, 8399–8413, DOI 10.3390/ijerph110808399.
- [16] J.-H. Kang, D. Asai, R. Toita, “Bisphenol A (BPA) and Cardiovascular or Cardiometabolic Diseases”, *J. Xenobiotics* **2023**, *13*, 775–810, DOI 10.3390/jox13040049.
- [17] EU, “Commission Regulation 2016/2235 of 12 December 2016 amending Annex XVII to Regulation (EC) No 1907/2006 of the European Parliament and of the Council concerning the Registration, Evaluation, Authorisation and Restriction of Chemicals (REACH) as regards bisphenol A”, *O.J. L 337* **2016**, *59*, 3–6.
- [18] EU, “Commission Regulation 2018/213 of 12 February 2018 on the use of bisphenol A in varnishes and coatings intended to come into contact with food and amending Regulation (EU) No 10/2011 as regards the use of that substance in plastic food contact materials”, *O.J. L 41* **2018**, *61*, 6–13.
- [19] European Food Safety Authority, “Scientific Opinion on the risks to public health related to the presence of bisphenol A (BPA) in foodstuffs”, *EFSA Journal* **2015**, *13*, 3978, DOI 10.2903/j.efsa.2015.3978.
- [20] C. Lambré, J. M. Barat Baviera, C. Bolognesi, A. Chesson, P. S. Cocconcelli, R. Crebelli, D. M. Gott, K. Grob, E. Lampi, M. Mengelers, A. Mortensen, G. Rivière, V. Silano Until December, I.-L. Steffensen, C. Tlustos, L. Vernis, H. Zorn, M. Batke, M. Bignami, E. Corsini, R. FitzGerald, U. Gundert-Remy, T. Halldorsson, A. Hart, E. Ntzani, E. Scanziani, H. Schroeder, B. Ulbrich, D. Waalkens-Berendsen, D. Woelfle, Z. Al Harraq, K. Baert, M. Carfi, A. F. Castoldi, C. Croera, H. van Loveren, “Re-evaluation of the risks to public health related to

- the presence of bisphenol A (BPA) in foodstuffs”, *EFSA Journal* **2023**, *21*, 1–392, DOI 10.2903/j.efsa.2023.6857.
- [21] European Environment Agency, *Human exposure to Bisphenol A in Europe*, Publications Office of the European Union, Luxembourg, **2023**.
- [22] E. Ougier, F. Zeman, J.-P. Antignac, C. Rousselle, R. Lange, M. Kolossa-Gehring, P. Apel, “Human biomonitoring initiative (HBM4EU): Human biomonitoring guidance values (HBM-GVs) derived for bisphenol A”, *Environment Int.* **2021**, *154*, 106563, DOI 10.1016/j.envint.2021.106563.
- [23] E. Govarts, L. Gilles, L. Rodriguez Martin, T. Santonen, P. Apel, P. Alvito, E. Anastasi, H. R. Andersen, A.-M. Andersson, L. Andryskova, J.-P. Antignac, B. Appenzeller, F. Barbone, Z. Barnett-Itzhaki, R. Barouki, T. Berman, W. Bil, T. Borges, J. Buekers, A. Cañas-Portilla, A. Covaci, Z. Csako, E. den Hond, D. Dvorakova, L. Fabelova, T. Fletcher, H. Frederiksen, C. Gabriel, C. Ganzleben, T. Göen, T. I. Halldorsson, L. S. Haug, M. Horvat, P. Huuskonen, M. Imboden, M. Jagodic Hudobivnik, B. Janasik, N. Janev Holcer, S. Karakitsios, A. Katsonouri, J. Klanova, V. Kokaraki, T. Kold Jensen, J. Koponen, M. Laeremans, F. Laguzzi, R. Lange, N. Lemke, S. Lignell, A. K. Lindroos, J. Lobo Vicente, M. Luijten, K. C. Makris, D. Mazej, L. Melymuk, M. Meslin, H. Mol, P. Montazeri, A. Murawski, S. Namorado, L. Niemann, S. Nübler, B. Nunes, K. Olafsdottir, L. Palkovicova Murinova, N. Papaioannou, S. Pedraza-Diaz, P. Piler, V. Plichta, M. Poteser, N. Probst-Hensch, L. Rambaud, E. Rauscher-Gabernig, K. Rausova, S. Remy, M. Riou, V. Rosolen, C. Rousselle, M. Rütther, D. Sarigiannis, M. J. Silva, Z. Šlejkovec, J. Snoj Tratnik, A. Stajniko, T. Szigeti, J. V. Tarazona, C. Thomsen, Ž. Tkalec, H. Tolonen, T. Trnovec, M. Uhl, van Nieuwenhuysen, E. Vasco, V. J. Verheyen, S. Viegas, A. M. Vinggaard, N. Vogel, K. Vorkamp, W. Wasowicz, T. Weber, S. Wimmerova, M. Woutersen, P. Zimmermann, M. Zvonar, H. Koch, M. Kolossa-Gehring, M. Esteban López, A. Castaño, L. Stewart, O. Sepai, G. Schoeters, “Harmonized human biomonitoring in European children, teenagers and adults: EU-wide exposure data of 11 chemical substance groups from the HBM4EU Aligned Studies (2014-2021)”, *Int. J. Hyg. Envir. Heal.* **2023**, *249*, 114119, DOI 10.1016/j.ijheh.2023.114119.
- [24] E. Stokstad, “Europe proposes drastic cut of endocrine disruptor in plastic”, *Science* **2022**, *375*, 708, DOI 10.1126/science.ada1361.
- [25] Digital Science, Dimensions [Software], accessed on 26.03.2024, under license agreement, **2024**, <https://app.dimensions.ai>.
- [26] M. Natarajan, S. C. Murugavel, “Thermal stability and thermal degradation kinetics of bio-based epoxy resins derived from cardanol by thermogravimetric

- analysis”, *Polym. Bull.* **2016**, *74*, 3319–3340, DOI 10.1007/s00289-016-1885-y.
- [27] X. Wang, H. Niu, W. Guo, L. Song, Y. Hu, “Cardanol as a versatile platform for fabrication of bio-based flame-retardant epoxy thermosets as DGEBA substitutes”, *Chem. Eng. J.* **2021**, *421*, 129738, DOI 10.1016/j.cej.2021.129738.
- [28] K. Makwana, A. B. Ichake, V. Valodkar, G. Padmanaban, M. V. Badiger, P. P. Wadgaonkar, “Cardol: Cashew nut shell liquid (CNSL) - derived starting material for the preparation of partially bio-based epoxy resins”, *Eur. Polym. J.* **2022**, *166*, 111029, DOI 10.1016/j.eurpolymj.2022.111029.
- [29] I. Faye, M. Decostanzi, Y. Ecochard, S. Caillol, “Eugenol bio-based epoxy thermosets: from cloves to applied materials”, *Green Chem.* **2017**, *19*, 5236–5242, DOI 10.1039/c7gc02322g.
- [30] D. Santiago, D. Guzmán, X. Ramis, F. Ferrando, À. Serra, “New Epoxy Thermosets Derived from Clove Oil Prepared by Epoxy-Amine Curing”, *Polymers* **2019**, *12*, 44, DOI 10.3390/polym12010044.
- [31] S. Caillol, B. Boutevin, R. Auvergne, “Eugenol, a developing asset in biobased epoxy resins”, *Polymer* **2021**, *223*, 123663, DOI 10.1016/j.polymer.2021.123663.
- [32] D. Matykiewicz, K. Skórczewska, “Characteristics and Application of Eugenol in the Production of Epoxy and Thermosetting Resin Composites: A Review”, *Materials* **2022**, *15*, 4824, DOI 10.3390/ma15144824.
- [33] S. Nikafshar, O. Zabihi, S. Hamidi, Y. Moradi, S. Barzegar, M. Ahmadi, M. Naebe, “A renewable bio-based epoxy resin with improved mechanical performance that can compete with DGEBA”, *RSC Adv.* **2017**, *7*, 8694–8701, DOI 10.1039/c6ra27283e.
- [34] A. S. Amarasekara, R. Garcia-Obergon, A. K. Thompson, “Vanillin-based polymers: IV. Hydrovanilloin epoxy resins”, *J. Appl. Polym. Sci.* **2018**, *136*, DOI 10.1002/app.47000.
- [35] X. Su, Z. Zhou, J. Liu, J. Luo, R. Liu, “A recyclable vanillin-based epoxy resin with high-performance that can compete with DGEBA”, *Eur. Polym. J.* **2020**, *140*, 110053, DOI 10.1016/j.eurpolymj.2020.110053.
- [36] Z. Wang, P. Gnanasekar, S. Sudhakaran Nair, R. Farnood, S. Yi, N. Yan, “Biobased Epoxy Synthesized from a Vanillin Derivative and Its Reinforcement Using Lignin-Containing Cellulose Nanofibrils”, *ACS Sustain. Chem. Eng.* **2020**, *8*, 11215–11223, DOI 10.1021/acssuschemeng.0c02559.

- [37] H. Nabipour, H. Niu, X. Wang, S. Batool, Y. Hu, “Fully bio-based epoxy resin derived from vanillin with flame retardancy and degradability”, *React. Funct. Polym.* **2021**, *168*, 105034, DOI 10.1016/j.reactfunctpolym.2021.105034.
- [38] J. Xin, M. Li, R. Li, M. P. Wolcott, J. Zhang, “Green Epoxy Resin System Based on Lignin and Tung Oil and Its Application in Epoxy Asphalt”, *ACS Sustain. Chem. Eng.* **2016**, *4*, 2754–2761, DOI 10.1021/acssuschemeng.6b00256.
- [39] C. Gioia, M. Colonna, A. Tagami, L. Medina, O. Sevastyanova, L. A. Berglund, M. Lawoko, “Lignin-Based Epoxy Resins: Unravelling the Relationship between Structure and Material Properties”, *Biomacromolecules* **2020**, *21*, 1920–1928, DOI 10.1021/acs.biomac.0c00057.
- [40] X. Zhen, H. Li, Z. Xu, Q. Wang, S. Zhu, Z. Wang, Z. Yuan, “Facile synthesis of lignin-based epoxy resins with excellent thermal-mechanical performance”, *Int. J. Biol. Macromol.* **2021**, *182*, 276–285, DOI 10.1016/j.ijbiomac.2021.03.203.
- [41] J. Xin, P. Zhang, K. Huang, J. Zhang, “Study of green epoxy resins derived from renewable cinnamic acid and dipentene: synthesis, curing and properties”, *RSC Adv.* **2014**, *4*, 8525, DOI 10.1039/C3RA47927G.
- [42] M. Chrysanthos, J. Galy, J.-P. Pascault, “Preparation and properties of bio-based epoxy networks derived from isosorbide diglycidyl ether”, *Polymer* **2011**, *52*, 3611–3620, DOI 10.1016/j.polymer.2011.06.001.
- [43] P. Niedermann, G. Szebenyi, A. Toldy, “Novel high glass temperature sugar-based epoxy resins: Characterization and comparison to mineral oil-based aliphatic and aromatic resins”, *Express Polym. Lett.* **2015**, *9*, 85–94, DOI 10.3144/expresspolymlett.2015.10.
- [44] J. Łukaszczyk, B. Janicki, M. Kaczmarek, “Synthesis and properties of isosorbide based epoxy resin”, *Eur. Polym. J.* **2011**, *47*, 1601–1606, DOI 10.1016/j.eurpolymj.2011.05.009.
- [45] Z. Rapi, B. Szolnoki, P. Bakó, P. Niedermann, A. Toldy, B. Bodzay, G. Keglevich, G. Marosi, “Synthesis and characterization of biobased epoxy monomers derived from D-glucose”, *Eur. Polym. J.* **2015**, *67*, 375–382, DOI 10.1016/j.eurpolymj.2014.09.025.
- [46] C. Negrell, A. Cornille, P. de Andrade Nascimento, J.-J. Robin, S. Caillol, “New bio-based epoxy materials and foams from microalgal oil”, *Eur. J. Lipid Sci. Tech.* **2016**, *119*, DOI 10.1002/ejlt.201600214.
- [47] S. Nameer, T. Deltin, P.-E. Sundell, M. Johansson, “Bio-based multifunctional fatty acid methyl esters as reactive diluents in coil coatings”, *Prog. Org. Coat.* **2019**, *136*, 105277, DOI 10.1016/j.porgcoat.2019.105277.

- [48] A. Todorovic, K. Resch–Fauster, A. R. Mahendran, G. Oreski, W. Kern, “Curing of epoxidized linseed oil: Investigation of the curing reaction with different hardener types”, *J. Appl. Polym. Sci.* **2021**, *138*, 50239, DOI 10.1002/app.50239.
- [49] H. Silau, A. G. Garcia, J. M. Woodley, K. Dam-Johansen, A. E. Daugaard, “Bio-Based Epoxy Binders from Lignin Derivatized with Epoxidized Rapeseed Fatty Acids in Bimodal Coating Systems”, *ACS Appl. Polym. Mat.* **2022**, *4*, 444–451, DOI 10.1021/acsapm.1c01351.
- [50] N. Reinhardt, J. M. Breitsameter, K. Drechsler, B. Rieger, “Fully Bio-Based Epoxy Thermoset Based on Epoxidized Linseed Oil and Tannic Acid”, *Macromol. Mater. Eng.* **2022**, *307*, 2200455, DOI 10.1002/mame.202200455.
- [51] R. McDonald, R. Steppel, J. Dorsey, “m-Chloroperbenzoic acid”, *Org. Synth.* **1970**, *50*, 15, DOI 10.15227/orgsyn.050.0015.
- [52] R. Fareghi-Alamdari, S. M. Hafshejani, H. Taghiyar, B. Yadollahi, M. R. Farsani, “Recyclable, green and efficient epoxidation of olefins in water with hydrogen peroxide catalyzed by polyoxometalate nanocapsule”, *Catal. Commun.* **2016**, *78*, 64–67, DOI 10.1016/j.catcom.2016.02.007.
- [53] N. Mizuno, K. Yamaguchi, “Polyoxometalate catalysts: toward the development of green H₂O₂-based epoxidation systems”, *Chem. Rec.* **2006**, *6*, 12–22, DOI 10.1002/tcr.20067.
- [54] M. Colladon, A. Scarso, P. Sgarbossa, R. A. Michelin, G. Strukul, “Regioselectivity and diastereoselectivity in Pt(II)-mediated green catalytic epoxidation of terminal alkenes with hydrogen peroxide: mechanistic insight into a peculiar substrate selectivity”, *J. Am. Chem. Soc.* **2007**, *129*, 7680–7689, DOI 10.1021/ja071142x.
- [55] D. Swern in *Organic peroxides, Vol. 2*, (Ed.: D. Swern), Wiley, New York, **1971**, pp. 355–533.
- [56] G. Siel, R. Rieth, K. T. Rowbottom in *Ullmann’s Encyclopedia of Industrial Chemistry, Vol. 13*, Wiley-VCH Verlag GmbH & Co. KGaA, Weinheim, **2000**, pp. 139–154.
- [57] F. P. Cuperus, S. T. Bouwer, G. F. H. Kramer, J. T. P. Derksen, “Lipases Used for the Production of Peroxycarboxylic Acids”, *Biocatalysis* **1994**, *9*, 89–96, DOI 10.3109/10242429408992110.
- [58] C. Aouf, E. Durand, J. Lecomte, M.-C. Figueroa-Espinoza, E. Dubreucq, H. Fulcrand, P. Villeneuve, “The use of lipases as biocatalysts for the epoxidation of fatty acids and phenolic compounds”, *Green Chem.* **2014**, *16*, 1740–1754, DOI 10.1039/C3GC42143K.

- [59] E. Abdulmalek, M. Arumugam, H. N. Mizan, M. B. Abdul Rahman, M. Basri, A. B. Salleh, “Chemoenzymatic Epoxidation of Alkenes and Reusability Study of the Phenylacetic Acid”, *Sci. World J.* **2014**, 756418, DOI 10.1155/2014/756418.
- [60] M. Feigel, O. Hinrichsen, “Modeling of Process Operation Principles for the Immobilized Enzyme *Candida Antarctica* under Activity Decay”, *Chem. Ing. Tech.* **2022**, *94*, 652–662, DOI 10.1002/cite.202100187.
- [61] J. M. Breitsameter, N. Reinhardt, M. Feigel, O. Hinrichsen, K. Drechsler, B. Rieger, “Synthesis of a Sustainable and Bisphenol A-Free Epoxy Resin based on Sorbic Acid and Characterization of the Cured Thermoset”, *Macromol. Mater. Eng.* **2023**, 2300068, DOI 10.1002/mame.202300068.
- [62] Verbundvorhaben GreenCarbon: Konversion von CO₂ in Polymere und Carbonfaserbasierte Leichtbaumaterialien für die Flug-, Automobil- und Bauindustrie durch Synergien von Chemie und Biotechnologie - Neue Wege zur Integration von Leichtbaumaterialien zur Realisierung einer klimazentrierten Energiewende, FKZ: 03SF0577A, **2019**.
- [63] A. W. Hofmann, “Neue flüchtige Säure der Vogelbeeren”, *Liebigs Ann. Chem.* **1859**, *110*, 129–140, DOI 10.1002/jlac.18591100202.
- [64] E. Letzig, W. Handschack, “Vergleichende Untersuchungen über einige Inhaltsstoffe bitterer und süßer Ebereschenfrüchte während des Reifens”, *Food / Nahrung* **1963**, *7*, 591–605, DOI 10.1002/food.19630070807.
- [65] V. Canale, L. Tonucci, M. Bressan, N. d’Alessandro, “Deoxydehydration of glycerol to allyl alcohol catalyzed by rhenium derivatives”, *Catal. Sci. Technol.* **2014**, *4*, 3697–3704, DOI 10.1039/C4CY00631C.
- [66] X. Li, Y. Zhang, “Highly Efficient Process for the Conversion of Glycerol to Acrylic Acid via Gas Phase Catalytic Oxidation of an Allyl Alcohol Intermediate”, *ACS Catal.* **2016**, *6*, 143–150, DOI 10.1021/acscatal.5b01843.
- [67] R. Wojcieszak, F. Santarelli, S. Paul, F. Dumeignil, F. Cavani, R. V. Gonçalves, “Recent developments in maleic acid synthesis from bio-based chemicals”, *Sustain. Chem. Process.* **2015**, *3*, 1–11, DOI 10.1186/s40508-015-0034-5.
- [68] N. Alonso-Fagúndez, M. L. Granados, R. Mariscal, M. Ojeda, “Selective Conversion of Furfural to Maleic Anhydride and Furan with VO_x/Al₂O₃ Catalysts”, *ChemSusChem* **2012**, *5*, 1984–1990, DOI 10.1002/cssc.201200167.
- [69] M. Feigel, J. M. Breitsameter, K. Lechner, B. Rieger, O. Hinrichsen, “Kinetic Modeling of the Synthesis Path for the Production of a Sustainable Epoxy Resin based on Allyl Sorbate”, *Ind. Eng. Chem. Res.* **2023**, *62*, 13389–13400, DOI 10.1021/acs.iecr.3c01317.

- [70] M. Feigel, J. M. Breitsameter, B. Rieger, O. Hinrichsen, “Bridging the Gap from Laboratory to Production: Kinetic Modeling-Guided Process Development for a Novel Epoxy Resin”, *Ind. Eng. Chem. Res.* **2024**, *63*, 1271–1285, DOI 10.1021/acs.iecr.3c03339.
- [71] C. G. Hill, *An Introduction to Chemical Engineering Kinetics & Reactor Design*, John Wiley & Sons, Ltd, New York, **1977**.
- [72] O. Levenspiel, *Chemical Reaction Engineering*, 3rd ed., John Wiley & Sons, Ltd, New York, **1999**.
- [73] M. Baerns, A. Behr, A. Brehm, J. Gmehling, H. Hofmann, U. Onken, A. Renken, K.-O. Hinrichsen, R. Palkovits, *Technische Chemie*, 2nd ed., Wiley-VCH Verlag, Weinheim, Germany, **2013**.
- [74] H. S. Fogler, *Elements of chemical reaction engineering*, 6th ed., Pearson Education, **2022**.
- [75] M. Schwaab, J. C. Pinto, “Optimum reference temperature for reparameterization of the Arrhenius equation. Part 1: Problems involving one kinetic constant”, *Chem. Eng. Sci.* **2007**, *62*, 2750–2764, DOI 10.1016/j.ces.2007.02.020.
- [76] M. Schwaab, J. C. Pinto, “Optimum reparameterization of power function models”, *Chem. Eng. Sci.* **2008**, *63*, 4631–4635, DOI 10.1016/j.ces.2008.07.005.
- [77] G. E. P. Box, “FITTING EMPIRICAL DATA*”, *Ann. NY. Acad. Sci.* **1960**, *86*, 792–816, DOI 10.1111/j.1749-6632.1960.tb42843.x.
- [78] D. Pritchard, D. Bacon, “Statistical assessment of chemical kinetic models”, *Chem. Eng. Sci.* **1975**, *30*, 567–574, DOI 10.1016/0009-2509(75)80028-5.
- [79] A. K. Agarwal, M. L. Brisk, “Sequential experimental design for precise parameter estimation. 1. Use of reparameterization”, *Ind. Eng. Chem. Proc. DD.* **1985**, *24*, 203–207, DOI 10.1021/i200028a034.
- [80] M. Schwaab, J. E. C. Biscaia, J. L. Monteiro, J. C. Pinto, “Nonlinear parameter estimation through particle swarm optimization”, *Chem. Eng. Sci.* **2008**, *63*, 1542–1552, DOI 10.1016/j.ces.2007.11.024.
- [81] M. Schwaab, L. P. Lemos, J. C. Pinto, “Optimum reference temperature for reparameterization of the Arrhenius equation. Part 2: Problems involving multiple reparameterizations”, *Chem. Eng. Sci.* **2008**, *63*, 2895–2906, DOI 10.1016/j.ces.2008.03.010.
- [82] H. Akaike in *2nd International Symposium on Information Theory*, (Eds.: B. Petrov, F. Csaki), Tsahkadsor, Armenia, **1973**, pp. 267–281.
- [83] S. Guiasu, *Information Theory with Applications*, 2nd ed., McGraw-Hill, New York, **1977**.

- [84] T. M. Cover, J. A. Thomas, *Elements of Information Theory*, 2nd ed., John Wiley & Sons, Ltd, Hoboken, **2005**.
- [85] K. P. Burnham, D. R. Anderson, *Model selection and multimodel inference: A practical information-theoretic approach*, 2nd ed., Springer, New York, **2010**.
- [86] A. Robinson, “Did Einstein really say that?”, *Nature* **2018**, 30, DOI 10.1038/d41586-018-05004-4.
- [87] J. Wei, “Least Square Fitting of an Elephant”, *Chemtech* **1975**, 5, 128–129.
- [88] S. Kullback, R. A. Leibler, “On Information and Sufficiency”, *Ann. Math. Stat.* **1951**, 22, 79–86.
- [89] H. Akaike, “A new look at the statistical model identification”, *IEEE T. Automat. Contr.* **1974**, 19, 716–723, DOI 10.1109/TAC.1974.1100705.
- [90] H. Akaike, “Factor analysis and AIC”, *Psychometrika* **1987**, 52, 317–332, DOI 10.1007/BF02294359.
- [91] H. Akaike in *A Celebration of Statistics*, (Eds.: A. C. Atkinson, S. E. Fienberg), Springer New York, New York, **1985**, pp. 1–24.
- [92] D.-Y. Peng, D. B. Robinson, “A New Two-Constant Equation of State”, *Ind. Eng. Chem. Fund.* **1976**, 15, 59–64, DOI 10.1021/i160057a011.
- [93] G. Soave, “Equilibrium constants from a modified Redlich-Kwong equation of state”, *Chem. Eng. Sci.* **1972**, 27, 1197–1203, DOI 10.1016/0009-2509(72)80096-4.
- [94] O. Redlich, J. N. S. Kwong, “On the Thermodynamics of Solutions. V. An Equation of State. Fugacities of Gaseous Solutions.”, *Chem. Rev.* **1949**, 44, 233–244, DOI 10.1021/cr60137a013.
- [95] M. Benedict, G. B. Webb, L. C. Rubin, “An Empirical Equation for Thermodynamic Properties of Light Hydrocarbons and Their Mixtures I. Methane, Ethane, Propane and *n*-Butane”, *J. Chem. Phys.* **1940**, 8, 334–345, DOI 10.1063/1.1750658.
- [96] J. G. Hayden, J. P. O’Connell, “A Generalized Method for Predicting Second Virial Coefficients”, *Ind. Eng. Chem. Proc. DD.* **1975**, 14, 209–216, DOI 10.1021/i260055a003.
- [97] G. M. Wilson, “Vapor-Liquid Equilibrium. XI. A New Expression for the Excess Free Energy of Mixing”, *J. Am. Chem. Soc.* **1964**, 86, 127–130, DOI 10.1021/ja01056a002.
- [98] H. Renon, J. M. Prausnitz, “Local compositions in thermodynamic excess functions for liquid mixtures”, *AIChE J.* **1968**, 14, 135–144, DOI 10.1002/aic.690140124.

- [99] D. S. Abrams, J. M. Prausnitz, “Statistical thermodynamics of liquid mixtures: A new expression for the excess Gibbs energy of partly or completely miscible systems”, *AIChE J.* **1975**, *21*, 116–128, DOI 10.1002/aic.690210115.
- [100] A. Fredenslund, R. L. Jones, J. M. Prausnitz, “Group-contribution estimation of activity coefficients in nonideal liquid mixtures”, *AIChE J.* **1975**, *21*, 1086–1099, DOI 10.1002/aic.690210607.
- [101] A. Fredenslund, J. Gmehling, P. Rasmussen, *Vapor-Liquid Equilibria Using UNI-FAC: A Group-Contribution Method*, Elsevier, Amsterdam, **1977**.
- [102] T. Holderbaum, J. Gmehling, “PSRK: A Group Contribution Equation of State Based on UNIFAC”, *Fluid Phase Equilib.* **1991**, *70*, 251–265, DOI 10.1016/0378-3812(91)85038-v.
- [103] A. Klamt, G. J. P. Krooshof, R. Taylor, “COSMOSPACE: Alternative to conventional activity-coefficient models”, *AIChE J.* **2002**, *48*, 2332–2349, DOI 10.1002/aic.690481023.
- [104] U. Weidlich, J. Gmehling, “A modified UNIFAC model. 1. Prediction of VLE, h^E , and γ^∞ ”, *Ind. Eng. Chem. Res.* **1987**, *26*, 1372–1381, DOI 10.1021/ie00067a018.
- [105] J. M. Douglas, *Conceptual design of chemical processes*, 4th print, McGraw-Hill, New York, N.Y., **2000**.
- [106] J. D. Seader, E. J. Henley, D. K. Roper, *Separation process principles with applications using process simulators*, 3rd ed., John Wiley & Sons, Ltd, Chichester, England, **2010**.
- [107] W. L. Luyben, *Principles and case studies of simultaneous design*, Wiley, Hoboken, N.J., **2011**.
- [108] R. Turton, R. C. Bailie, W. B. Whiting, J. A. Shaeiwitz, D. Bhattacharyya, *Analysis, synthesis, and design of chemical processes*, Fourth edition, Prentice Hall, Upper Saddle River, N.J. and Munich, **2012**.
- [109] J. Haydary, *Chemical process design and simulation: Aspen Plus and Aspen HYSYS applications*, American Institute of Chemical Engineers and John Wiley & Sons, Ltd, Hoboken, NJ, **2019**.
- [110] K. Al-Malah in *Aspen Plus®: Chemical Engineering Applications*, John Wiley & Sons, Ltd, Hoboken, NJ, **2016**, Chapter 17, pp. 523–564.
- [111] M. S. Peters, K. D. Timmerhaus, *Plant design and economics for chemical engineers*, McGraw-Hill, New York, **1991**.
- [112] G. Towler, R. K. Sinnott, *Chemical engineering design*, Butterworth-Heinemann, Oxford, England, **2007**.

- [113] S. Kumar, S. K. Samal, S. Mohanty, S. K. Nayak, “Synthesis and characterization of itaconic-based epoxy resins”, *Polym. Advan. Technol.* **2018**, *29*, 160–170, DOI 10.1002/pat.4098.
- [114] H. Q. Pham, M. J. Marks in *Ullmann’s Encyclopedia of Industrial Chemistry*, (Eds.: M. Bohnet, F. Ullmann), Wiley-VCH Verlag GmbH & Co. KGaA, Weinheim, **2003**, pp. 155–244.
- [115] R. L. Hall, B. L. Oser, “Recent Progress in the Consideration of Flavoring Ingredients Under the Food Additives Amendment: III. GRAS Substances”, *Food Technol.* **1965**, *19*, 151–197.
- [116] M. L. A. Fluchaire, G. Collardeau (Rhône-Poulenc S.A.), *US Patent*, 2573001, **1951**.
- [117] R. S. Igoe in *Dictionary of Food Ingredients*, (Ed.: R. S. Igoe), Springer US, Boston, **2011**, pp. 3–160.
- [118] A. I. Tkachuk, A. G. Zagora, I. V. Terekhov, R. R. Mukhametov, “Isophorone Diamine - A Curing Agent for Epoxy Resins: Production, Application, Prospects. A Review”, *Polym. Sci. Ser. D+* **2022**, *15*, 171–176, DOI 10.1134/s1995421222020289.
- [119] J. Wan, C. Li, Z.-Y. Bu, C.-J. Xu, B.-G. Li, H. Fan, “A comparative study of epoxy resin cured with a linear diamine and a branched polyamine”, *Chem. Eng. J.* **2012**, *188*, 160–172, DOI 10.1016/j.cej.2012.01.134.
- [120] Kunststoffe – Bestimmung der Zugeigenschaften – Teil 2: Prüfbedingungen für Form- und Extrusionsmassen (ISO 527-2:2012); Deutsche Fassung EN ISO 527-2:2012, Berlin, DOI 10.31030/1860304.
- [121] D20 Committee, Standard Test Methods for Determining the Biobased Content of Solid, Liquid, and Gaseous Samples Using Radiocarbon Analysis, West Conshohocken, PA, DOI 10.1520/D6866-22.
- [122] E. Lück, M. Jager, N. Raczek in *Ullmann’s Encyclopedia of Industrial Chemistry*, Vol. 24, Wiley-VCH Verlag GmbH & Co. KGaA, Weinheim, **2000**, pp. 507–513.
- [123] Godavari Biorefineries Ltd., Crotonaldehyde - 99%, retrieved 25.11.2022, **2022**, <https://godavaribiorefineries.com/products/chemicals/crotonaldehyde-99-5>.
- [124] E. d. J. Avantium, H. Stichnothe, G. Bell, H. Jorgensen, Bio-Based Chemicals: A 2020 Update, (Ed.: IEA Bioenergy), retrieved 24.03.2023, **2020**, <https://www.ieabioenergy.com/blog/publications/new-publication-bio-based-chemicals-a-2020-update>.

- [125] J. C. Burnett, R. A. Keppel, W. D. Robinson, “Commercial production of maleic anhydride by catalytic processes using fixed bed reactors”, *Catal. Today* **1987**, *1*, 537–586, DOI 10.1016/0920-5861(87)85005-8.
- [126] K. Lohbeck, H. Haferkorn, W. Fuhrmann, N. Fedtke in *Ullmann’s Encyclopedia of Industrial Chemistry*, John Wiley & Sons, Ltd, **2000**.
- [127] *Handbook of Maleic Anhydride Based Materials: Syntheses, Properties and Applications*, (Ed.: O. M. Musa), Springer International Publishing, Cham, **2016**.
- [128] M. Novelli, M. Leonardo, C. Cortelli in *Handbook of Advanced Methods and Processes in Oxidation Catalysis: From Laboratory to Industry. Edited by Daniel Duprez and Fabrizio Cavani*, Imperial College Press, **2015**, Chapter Chapter 14, pp. 334–352.
- [129] Z. Du, J. Ma, F. Wang, J. Liu, J. Xu, “Oxidation of 5-hydroxymethylfurfural to maleic anhydride with molecular oxygen”, *Green Chem.* **2011**, *13*, 554, DOI 10.1039/C0GC00837K.
- [130] W. Jia, Z. Si, Y. Feng, X. Zhang, X. Zhao, Y. Sun, X. Tang, X. Zeng, L. Lin, “Oxidation of 5-[(Formyloxy)methyl]furfural to Maleic Anhydride with Atmospheric Oxygen Using α -MnO₂/Cu(NO₃)₂ as Catalysts”, *ACS Sustain. Chem. Eng.* **2020**, *8*, 7901–7908, DOI 10.1021/acssuschemeng.0c01144.
- [131] J. Lan, J. Lin, Z. Chen, G. Yin, “Transformation of 5-Hydroxymethylfurfural (HMF) to Maleic Anhydride by Aerobic Oxidation with Heteropolyacid Catalysts”, *ACS Catal.* **2015**, *5*, 2035–2041, DOI 10.1021/cs501776n.
- [132] R. Cucciniello, D. Cespi, M. Riccardi, E. Neri, F. Passarini, F. M. Pulselli, “Maleic anhydride from bio-based 1-butanol and furfural: a life cycle assessment at the pilot scale”, *Green Chem.* **2023**, *25*, 5922–5935, DOI 10.1039/D2GC03707F.
- [133] DIN EN 16785-2:2018-05, Biobasierte Produkte - Biobasierter Gehalt - Teil 2: Bestimmung des biobasierten Gehalts unter Verwendung der Materialbilanzmethode; Deutsche Fassung EN 16785-2:2018, Berlin, DOI 10.31030/2731585.
- [134] “News”, *Chem. Ind.* **2022**, *86*, 5–13, DOI 10.1002/cind.864_3.x.
- [135] EVONIK, The eCO Portfolio: Performance meets Sustainability, retrieved on 25.11.2022, **2022**, <https://crosslinkers.evonik.com/en/products/eco-grades>.
- [136] E. A. Baroncini, S. Kumar Yadav, G. R. Palmese, J. F. Stanzione, “Recent advances in bio-based epoxy resins and bio-based epoxy curing agents”, *J. Appl. Polym. Sci.* **2016**, *133*, DOI 10.1002/app.44103.
- [137] J. S. Terry, A. C. Taylor, “The properties and suitability of commercial bio-based epoxies for use in fiber-reinforced composites”, *J. Appl. Polym. Sci.* **2021**, *138*, 50417, DOI 10.1002/app.50417.

- [138] S. Bérard, C. Vallée, D. Delcroix, “Sorbic Acid as a Renewable Resource for Atom-Economic and Selective Production of *p*-Toluic Acid and Alkyl-*p*-Toluates: Intermediates to Bioterephthalic Acid and Esters”, *Ind. Eng. Chem. Res.* **2015**, *54*, 7164–7168, DOI 10.1021/acs.iecr.5b01972.
- [139] O. Diels, K. Alder, “Synthesen in der hydroaromatischen Reihe. III. Mitteilung: Synthese von Terpenen, Camphern, hydroaromatischen und heterocyclischen Systemen. Mitbearbeitet von den Herren Wolfgang Lübbert, Erich Naujoks, Franz Querberitz, Karl Röhl, Harro Segeberg”, *Liebigs Ann. Chem.* **1929**, *470*, 62–103, DOI 10.1002/jlac.19294700106.
- [140] Z. W. Wicks, O. W. Daly, H. Lack, “THE DIENE ADDITION OF MALEIC ANHYDRIDE TO SORBIC ACID”, *J. Org. Chem.* **1947**, *12*, 713–717, DOI 10.1021/jo01169a004.
- [141] L. J. Andrews, R. M. Keefer, “A Kinetic Study of the Diels-Alder Reaction of Various Anthracene and Maleic Anhydride Derivatives”, *J. Am. Chem. Soc.* **1955**, *77*, 6284–6289, DOI 10.1021/ja01628a066.
- [142] H.-J. Bart, J. Reidetschläger, K. Schatka, A. Lehmann, “Kinetics of esterification of succinic anhydride with methanol by homogeneous catalysis”, *Int. J. Chem. Kinet.* **1994**, *26*, 1013–1021, DOI 10.1002/KIN.550261006.
- [143] J. Böeseken, J. S. P. Blumberger, “Observations sur la Vitesse D’oxydation de Quelques Dérivés Aromatiques de L’éthylène par le Réactif de Prileshajew”, *Recl. Trav. Chim. Pay.-B.* **1925**, *44*, 90–95, DOI 10.1002/recl.19250440108.
- [144] J. Böeseken, J. Stuurman, “The oxidation velocities of some alkenes with peracetic acid”, *Recl. Trav. Chim. Pay.-B.* **1937**, *56*, 1034–1038, DOI 10.1002/recl.19370561105.
- [145] D. I. Metelitsa, “Reaction Mechanisms of the Direct Epoxidation of Alkenes in the Liquid Phase”, *Russ. Chem. Rev.* **1972**, *41*, 807–821, DOI 10.1070/RC1972v041n10ABEH002095.
- [146] R. D. Bach, C. Canepa, J. E. Winter, P. E. Blanchette, “Mechanism of Acid-Catalyzed Epoxidation of Alkenes with Peroxy Acids”, *J. Org. Chem.* **1997**, *62*, 5191–5197, DOI 10.1021/jo950930e.
- [147] L. F. Shampine, M. W. Reichelt, “The MATLAB ODE Suite”, *SIAM J. Sci. Comput.* **1997**, *18*, 1–22, DOI 10.1137/S1064827594276424.
- [148] K. Levenberg, “A method for the solution of certain non-linear problems in least squares”, *Q. Appl. Math.* **1944**, *2*, 164–168, DOI 10.1090/qam/10666.
- [149] D. W. Marquardt, “An Algorithm for Least-Squares Estimation of Nonlinear Parameters”, *J. Soc. Ind. Appl. Math.* **1963**, *11*, 431–441, DOI 10.1137/0111030.

- [150] J. J. Moré in *Numerical Analysis*, (Ed.: G. A. Watson), Lecture Notes in Mathematics, Springer, Heidelberg, **1978**, pp. 105–116.
- [151] G. Schwarz, “Estimating the Dimension of a Model”, *Ann. Stat.* **1978**, *6*, DOI 10.1214/aos/1176344136.
- [152] W. Hoffmann, Y. Kang, J. C. Mitchell, M. J. Snowden, “Kinetic Data by Non-isothermal Reaction Calorimetry: A Model-Assisted Calorimetric Evaluation”, *Org. Process Res. Dev.* **2007**, *11*, 25–29, DOI 10.1021/op060144j.
- [153] J. P. McMullen, K. F. Jensen, “Rapid Determination of Reaction Kinetics with an Automated Microfluidic System”, *Org. Process Res. Dev.* **2011**, *15*, 398–407, DOI 10.1021/op100300p.
- [154] S. T. Oyama in *Mechanisms in homogeneous and heterogeneous epoxidation catalysis*, Elsevier, Amsterdam, **2008**, pp. 3–99.
- [155] *Name reactions for functional group transformations*, (Eds.: J. J. Li, E. J. Corey), Wiley-Interscience, Hoboken, N.J., **2007**.
- [156] D. M. Bates, D. G. Watts, *Nonlinear regression analysis and its applications*, Wiley, New York, **1988**.
- [157] H. Hong, B. G. Harvey, G. R. Palmese, J. F. Stanzione, H. W. Ng, S. Sakkiah, W. Tong, J. M. Sadler, “Experimental Data Extraction and in Silico Prediction of the Estrogenic Activity of Renewable Replacements for Bisphenol A”, *Int. J. Env. Res. Pub. He.* **2016**, *13*, 705, DOI 10.3390/ijerph13070705.
- [158] C. Pappa, E. Feghali, K. Vanbroekhoven, K. S. Triantafyllidis, “Recent advances in epoxy resins and composites derived from lignin and related bio-oils”, *Curr. Opin. Green and Sustain. Chem.* **2022**, *38*, 100687, DOI 10.1016/j.cogsc.2022.100687.
- [159] J. D. Piper, P. W. Piper, “Benzoate and Sorbate Salts: A Systematic Review of the Potential Hazards of These Invaluable Preservatives and the Expanding Spectrum of Clinical Uses for Sodium Benzoate”, *Compr. Rev. Food Sci. F.* **2017**, *16*, 868–880, DOI 10.1111/1541-4337.12284.
- [160] Y. Kikuchi, K. Mayumi, M. Hirao in *20th European Symposium on Computer Aided Process Engineering*, Computer Aided Chemical Engineering, Elsevier, **2010**, pp. 1051–1056.
- [161] D. Kralisch, I. Streckmann, D. Ott, U. Krtschil, E. Santacesaria, M. Di Serio, V. Russo, L. de Carlo, W. Linhart, E. Christian, B. Cortese, M. H. J. M. de Croon, V. Hessel, “Transfer of the Epoxidation of Soybean Oil from Batch to Flow Chemistry Guided by Cost and Environmental Issues”, *ChemSusChem* **2012**, *5*, 300–311, DOI 10.1002/cssc.201100445.

- [162] H. Hu, Y. Wang, “Application of Computer Simulation Technology in Chemical Synthesis of Resin Material ADH”, *Chem. Engineer. Trans.* **2017**, *59*, 595–600, DOI 10.3303/CET1759100.
- [163] L. M. Ramírez, J. G. Cadavid, A. Orjuela, M. F. Gutiérrez, W. F. Bohórquez, “Epoxidation of used cooking oils: Kinetic modeling and reaction optimization”, *Chem. Eng. Process.: Process Intensif.* **2022**, *176*, 108963, DOI 10.1016/j.cep.2022.108963.
- [164] H. Rahman, R. Yunus, A. S. Intan, Z. Z. Abidin, D. Kuang, “Preliminary Design of Semi-Batch Reactor for Synthesis 1,3-Dichloro-2-Propanol Using Aspen Plus”, *Int. J. Chem.* **2011**, *3*, 196–201, DOI 10.5539/ijc.v3n1p196.
- [165] J. Lohmann, R. Joh, J. Gmehling, “From UNIFAC to Modified UNIFAC (Dortmund)”, *Ind. Eng. Chem. Res.* **2001**, *40*, 957–964, DOI 10.1021/ie0005710.
- [166] K. Balslev, J. Abildskov, “UNIFAC Parameters for Four New Groups”, *Ind. Eng. Chem. Res.* **2002**, *41*, 2047–2057, DOI 10.1021/ie010786p.
- [167] H. K. Hansen, P. Rasmussen, A. Fredenslund, M. Schiller, J. Gmehling, “Vapor-liquid equilibria by UNIFAC group contribution. 5. Revision and extension”, *Ind. Eng. Chem. Res.* **1991**, *30*, 2352–2355, DOI 10.1021/ie00058a017.
- [168] R. Wittig, J. Lohmann, J. Gmehling, “Vapor-Liquid Equilibria by UNIFAC Group Contribution. 6. Revision and Extension”, *Ind. Eng. Chem. Res.* **2003**, *42*, 183–188, DOI 10.1021/ie0205061.
- [169] P. Marzal, J. B. Montón, M. A. Rodrigo, “Isobaric Vapor–Liquid Equilibria of the Water + 2-Propanol System at 30, 60, and 100 kPa”, *J. Chem. Eng. Data* **1996**, *41*, 608–611, DOI 10.1021/je9503113.
- [170] J. Li, C. Hua, S. Xiong, F. Bai, P. Lu, J. Ye, “Vapor–Liquid Equilibrium for Binary Systems of Allyl Alcohol + Water and Allyl Alcohol + Benzene at 101.3 kPa”, *J. Chem. Eng. Data* **2017**, *62*, 3004–3008, DOI 10.1021/acs.jced.6b00893.
- [171] L. Xu, D. Xu, P. Shi, K. Zhang, X. Ma, J. Gao, Y. Wang, “Salts effect on isobaric vapor–liquid equilibrium for separation of the azeotropic mixture allyl alcohol + water”, *Fluid Phase Equilibr.* **2018**, *457*, 11–17, DOI 10.1016/j.fluid.2017.10.025.
- [172] H. Keskinen, *136. Cyclic acid anhydrides*, Arbetslivsinstitutet, Stockholm, **2004**.
- [173] X. Wang, Y. Zheng (Puyang Huicheng Electronic Material Co Ltd.), *CN Patent*, 211847757, **2020**.
- [174] G. Weng, J. Shen, J. Zhang (Zhejiang Alpharm Chemical Technology Co Ltd.), *CN Patent*, 203820667, **2014**.
- [175] S. Tani, K. Nishio (New Japan Chem Co Ltd.), *EU Patent*, 0432797, **1991**.

- [176] L. Yang, J. Shen, H. Fan, Y. Qiu, M. S. Shi, R. Wu (Zhejiang Zhengda New Material Technology Co Ltd.), *CN Patent*, 112661735, **2021**.
- [177] R. S. Hiwale, N. V. Bhate, Y. S. Mahajan, S. M. Mahajani, “Industrial Applications of Reactive Distillation: Recent Trends”, *Int. J. Chem. React. Eng.* **2004**, *2*, 1–52, DOI 10.2202/1542-6580.1109.
- [178] J. L. Solis-Sanchez, H. Alcocer-Garcia, E. Sanchez-Ramirez, J. G. Segovia-Hernandez, “Innovative reactive distillation process for levulinic acid production and purification”, *Chem. Eng. Res. Des.* **2022**, *183*, 28–40, DOI 10.1016/j.cherd.2022.04.041.
- [179] Y. T. Tang, H.-P. Huang, I.-L. Chien in *Process Systems Engineering 2003, 8th International Symposium on Process Systems Engineering*, Computer Aided Chemical Engineering, Elsevier, **2003**, pp. 1044–1049.
- [180] V. Agreda (Eastman Kodak Company), *EU Patent*, 0105885, **1983**.
- [181] V. Gerbaud, I. Rodriguez-Donis, L. Hegely, P. Lang, F. Denes, X. You, “Review of extractive distillation. Process design, operation, optimization and control”, *Chem. Eng. Res. Des.* **2019**, *141*, 229–271, DOI 10.1016/j.cherd.2018.09.020.
- [182] O. A. Deorukhkar, B. S. Deogharkar, Y. S. Mahajan, “Purification of tetrahydrofuran from its aqueous azeotrope by extractive distillation: Pilot plant studies”, *Chem. Eng. Process: Process Intensif.* **2016**, *105*, 79–91, DOI 10.1016/j.cep.2016.04.006.
- [183] Z.-g. Zhang, D.-h. Huang, M. Lv, P. Jia, D.-z. Sun, W.-x. Li, “Entrainer selection for separating tetrahydrofuran/water azeotropic mixture by extractive distillation”, *Sep. Purif. Technol.* **2014**, *122*, 73–77, DOI 10.1016/j.seppur.2013.10.051.
- [184] R. H. Ewell, J. M. Harrison, L. Berg, “Azeotropic Distillation”, *Ind. Eng. Chem.* **1944**, *36*, 871–875, DOI 10.1021/ie50418a002.
- [185] V. Gomis, R. Pedraza, O. Francés, A. Font, J. C. Asensi, “Dehydration of Ethanol Using Azeotropic Distillation with Isooctane”, *Ind. Eng. Chem. Res.* **2007**, *46*, 4572–4576, DOI 10.1021/ie0616343.
- [186] L. Silva, S. Mattedi, R. Gonzalez-Olmos, M. Iglesias, “Azeotropic behaviour of (benzene+cyclohexane+chlorobenzene) ternary mixture using chlorobenzene as entrainer at 101.3 kPa”, *J. Chem. Thermodyn.* **2006**, *38*, 1725–1736, DOI 10.1016/j.jct.2005.12.003.

- [187] R. Li, Q. Ye, X. Suo, X. Dai, H. Yu, “Heat-Integrated Pressure-Swing Distillation Process for Separation of a Maximum-Boiling Azeotrope Ethylenediamine/Water”, *Chem. Eng. Res. Des.* **2016**, *105*, 1–15, DOI 10.1016/j.cherd.2015.10.038.
- [188] Y. Wang, Z. Zhang, H. Zhang, Q. Zhang, “Control of Heat Integrated Pressure-Swing-Distillation Process for Separating Azeotropic Mixture of Tetrahydrofuran and Methanol”, *Ind. Eng. Chem. Res.* **2015**, *54*, 1646–1655, DOI 10.1021/ie505024q.
- [189] W. L. Luyben, “Methanol/Trimethoxysilane Azeotrope Separation Using Pressure-Swing Distillation”, *Ind. Eng. Chem. Res.* **2014**, *53*, 5590–5597, DOI 10.1021/ie500043c.
- [190] J. Wu, D. Xu, P. Shi, J. Gao, L. Zhang, Y. Ma, Y. Wang, “Separation of azeotrope (allyl alcohol + water): Isobaric vapour-liquid phase equilibrium measurements and extractive distillation”, *J. Chem. Thermodyn.* **2018**, *118*, 139–146, DOI 10.1016/j.jct.2017.11.009.
- [191] H. Jiang, B. Diao, D. Xu, L. Zhang, Y. Ma, J. Gao, Y. Wang, “Deep eutectic solvents effect on vapor-liquid phase equilibrium for separation of allyl alcohol from its aqueous solution”, *J. Mol. Liq.* **2019**, *279*, 524–529, DOI 10.1016/j.molliq.2019.01.163.
- [192] S. Matsuhira (Shōwa Denkō KK), *EU Patent*, 0249648, **1987**.
- [193] A. Kubota, H. Takeuchi, “An Unexpected Incident with *m*-CPBA”, *Org. Process Res. Dev.* **2004**, *8*, 1076–1078, DOI 10.1021/op049825+.
- [194] Y. Kishi, M. Aratani, H. Tanino, T. Fukuyama, T. Goto, S. Inoue, S. Sugiyama, H. Kakoi, “New epoxidation with *m*-chloroperbenzoic acid at elevated temperatures”, *J. Chem. Soc. Chem. Comm.* **1972**, *2*, 64–65, DOI 10.1039/C39720000064.
- [195] J. Yang, J. Jiang, J. Jiang, X. Pan, Y. Pan, L. Ni, “Thermal instability and kinetic analysis on *m*-chloroperbenzoic acid”, *J. Therm. Anal. Calorim.* **2019**, *135*, 2309–2316, DOI 10.1007/s10973-018-7470-x.
- [196] X. Zhang, A. Hu, C. Pan, Q. Zhao, X. Wang, J. Lu, “Safer Preparation of *m*-CPBA/DMF Solution in Pilot Plant”, *Org. Process Res. Dev.* **2013**, *17*, 1591–1596, DOI 10.1021/op400208b.
- [197] A. S. Rao, H. R. Mohan, A. Charette in *Encyclopedia of Reagents for Organic Synthesis*, John Wiley & Sons, Ltd, Chichester, **2001**.
- [198] A. F. Chadwick, D. O. Barlow, A. A. D’Addieco, J. G. Wallace, “Theory and practice of resin-catalyzed epoxidation”, *J. Am. Oil Chem. Soc.* **1958**, *35*, 355–358, DOI 10.1007/bf02640551.

- [199] G. Dieckelmann, K. Eckwert, L. Jeromin, E. Peukert, U. Steinberner (Henkel AG & Co KGaA), *DE Patent*, 3320219, **1984**.
- [200] A. Kostyniuk, D. Bajec, P. Djinović, B. Likozar, “Allyl alcohol production by gas phase conversion reactions of glycerol over bifunctional hierarchical zeolite-supported bi- and tri-metallic catalysts”, *Chem. Eng. J.* **2020**, 397, 125430, DOI 10.1016/j.cej.2020.125430.
- [201] M. B. Viswanathan, D. R. Raman, K. A. Rosentrater, B. H. Shanks, “A Technoeconomic Platform for Early-Stage Process Design and Cost Estimation of Joint Fermentative–Catalytic Bioprocessing”, *Processes* **2020**, 8, 229, DOI 10.3390/pr8020229.
- [202] N. A. Sayar, S. Durmaz Şam, O. Pinar, D. Serper, B. Sarıyar Akbulut, D. Kazan, A. A. Sayar, “Techno-economic analysis of caffeine and catechins production from black tea waste”, *Food Bioprod. Process.* **2019**, 118, 1–12, DOI 10.1016/j.fbp.2019.08.014.
- [203] I. Agirre, I. Gandarias, M. L. Granados, P. L. Arias, “Process design and techno-economic analysis of gas and aqueous phase maleic anhydride production from biomass-derived furfural”, *Biomass Convers. Biorefin.* **2020**, 10, 1021–1033, DOI 10.1007/s13399-019-00462-w.
- [204] Indiamart, m-Chloroperbenzoic acid price, retrieved 19.08.2023, **2023**, <https://dir.indiamart.com/impcat/m-chloroperbenzoic-acid.html>.
- [205] P. V. Tozzi, C. M. Wisniewski, N. J. Zalewski, M. J. Savelski, C. S. Slater, F. A. Richetti, “Life cycle assessment of solvent extraction as a low-energy alternative to distillation for recovery of N-methyl-2-pyrrolidone from process waste”, *Green Process. Synth.* **2018**, 7, 277–286, DOI 10.1515/gps-2017-0030.
- [206] A. M. Niziolek, O. Onel, C. A. Floudas, “Production of benzene, toluene, and xylenes from natural gas via methanol: Process synthesis and global optimization”, *AIChE J.* **2016**, 62, 1531–1556, DOI 10.1002/aic.15144.
- [207] MAN Energy Solutions, Special reactors, retrieved 24.03.2023, **2023**, <https://www.man-es.com/process-industry/products/chemical-reactors/special-reactors>.
- [208] W. H. Miller, A. M. Dessert, G. W. Anderson, “The Synthesis of Some 6-Substituted-2-thiouracils”, *J. Am. Chem. Soc.* **1948**, 70, 500–502, DOI 10.1021/ja01182a020.
- [209] M. Y. Kang, T. Y. Park, S. Cho, J. W. Mun, M. W. Jung, J. H. Lee (LG Chem Ltd.), *US Patent*, 2020039971, **2020**.
- [210] Y. Li, S. Zuo (Yixing branch of Shadong Shen), *CN Patent*, 101774908, **2010**.

- [211] A. T. Jurewicz (Mobil Oil Corp.), *US Patent*, 3996274, **1976**.
- [212] J. H. Blumbergs (FMC Corp.), *US Patent*, 3231605, **1966**.
- [213] J. Ritz, H. Fuchs, H. Kieczka, W. C. Moran in *Ullmann's Encyclopedia of Industrial Chemistry*, Wiley-VCH Verlag GmbH & Co. KGaA, Weinheim, **2000**.
- [214] H. Fuchs, O. A. Grosskinsky, E. Froemmer, K. Kartte (BASF AG), *US Patent*, 4301073, **1981**.
- [215] W. Laufer, H. Kasper, S. Schattner, K. Allgoewer, B. Kray, M. Wuehr (Rhein Chemie Rheinau GmbH), *US Patent*, 2012071648, **2012**.
- [216] T. F. McKenna, "Design model of a wiped film evaporator. Applications to the devolatilisation of polymer melts", *Chem. Eng. Sci.* **1995**, *50*, 453–467, DOI 10.1016/0009-2509(94)00257-R.
- [217] A. de San Luis, C. C. Santini, Y. Chalamet, V. Dufaud, "Removal of Volatile Organic Compounds from Bulk and Emulsion Polymers: A Comprehensive Survey of the Existing Techniques", *Ind. Eng. Chem. Res.* **2019**, *58*, 11601–11623, DOI 10.1021/acs.iecr.9b00968.
- [218] EntropyResins, High Bio-based Laminating Epoxy Resin Safety Data Sheet, **2023**.
- [219] Sicomin, SR Greenpoxy 56 Safety Sata Sheet, **2016**.
- [220] Resoltech, 1070 ECO Safety Data Sheet, **2020**.
- [221] EntropyResins, retrieved 26.08.2023, **2023**, <https://eu.entropyresins.com>.
- [222] Sicomin, Epoxy Resin, retrieved 26.08.2023, **2023**, <https://www.boutique-resine-epoxy.fr/>.
- [223] Resoltech, Quotation, retrieved 29.08.2023, **2023**.

Nomenclature

Latin Symbols

<i>a</i>	interaction parameter	-
<i>a</i>	correction factor, attractive forces	-
<i>AIC</i>	Akaike information criterion	-
<i>b</i>	interaction parameter	-
<i>b</i>	correction factor, volume	-
<i>BIC</i>	Bayesian information criterion	-
<i>c</i>	concentration	mol/L
<i>c</i>	interaction parameter	-
<i>C</i>	constant	-
<i>C</i>	cost	a.u.
<i>CI</i>	cost index	-
<i>CI</i>	confidence interval	a.u.
COV	coefficient variance	a.u.
<i>dof</i>	degree of freedom	-
<i>E</i>	statistical expectation	-
<i>E</i>	stage equilibrium condition	-
<i>E_A</i>	activation energy	kJ/mol
<i>f</i>	function, custom term	-
<i>f</i>	fugacity	Pa
<i>F</i>	area	a.u.
<i>g</i>	function	-
<i>H</i>	height	m
<i>H</i>	enthalpy	kJ/mol
<i>i</i>	number	-
<i>I</i>	Kullback-Leibler distance	-
<i>j</i>	number	-
J	Jacobian	a.u.
<i>k</i>	kinetic constant	L/(mol s)
<i>K</i>	equilibrium constant	-

L	length	m
\mathcal{L}	log-likelihood function	-
m	number	-
m	mass	kg
\dot{m}	mass flow	kg/h
M	molar mass	g/mol
M	stage mass balance	-
n	number	-
\dot{n}	molar flow rate	mol/s
N	number	-
\mathcal{N}	normal distribution function	-
OOO	oxirane oxygen content	-
p	pressure	bar
q	sum of group areas	-
Q	normalized group surface area parameter	-
\dot{Q}	heat duty	kW
r	reaction rate	mol/(L s)
r	sum of group volumes	-
R	reflux ratio	mol/mol
R	normalized group volume parameter	-
R	gas constant	J/(mol K)
\dot{R}	net formation rate	mol/(L s)
R^2	coefficient of determination	-
S	selectivity	-
S	stage component summation	-
SSE	sum of squares errors	a.u.
SST	sum of squares total	a.u.
t	time	s
t^{-1}	reverse Student's t -distribution	-
T	temperature	K
T_g	glass transition temperature	K
TAC	total annular costs	\$/a
TCI	total capital investment	\$
TOC	total operating costs	\$/a
u	space velocity	m/s
V	volume / capacity	L
w	mass fraction	-
x	liquid mole fraction	-
X	conversion	-

X	predictor vector	a.u.
X	group mole fraction	a.u.
y	vapor mole fraction	-
Y	yield	-
Y	response vector	a.u.
Y	response matrix	a.u.
\hat{Y}	measurements	a.u.
z	coordination number	-

Greek Symbols

α	concentration difference	mol/L
α	reaction order	-
γ	activity coefficient	-
Γ	activity coefficient at mixture condition	-
δ	shift	ppm
Δ_{AIC}	Akaike criterion difference	-
ε	error term	a.u.
η	relative oxirane oxygen content	-
θ	molecular surface fraction	-
Θ	reparameterized parameter	-
Θ	area fraction of a functional group	-
μ	mean	a.u.
ν	stoichiometric coefficient	-
ν	group occurrences	-
σ^2	variance of the distribution	-
ϕ	fugacity coefficient	-
Φ	parameter vector	a.u.
Φ	molecular volume fraction	-
Ψ	binary interaction parameter	-
ω	ratio of educt and oxygen molar mass	-

Sub- and Superscript

a	component a
assum	assumption
b	component b

b	boiling
B	bottom
c	corrected
c	critical
comp	component
data	data set
e	educt
end	end
exp	experiment
f	feed
H	head
l	liquid
m	molar
p	product
P	payback
par	parameter
r/R	ring
R	reactor
ref	reference
res	residual
resp	response
t/T	terminal
tot	total
v	vapor

Abbreviations

AA	allyl alcohol
AHIBC	allyl 7-methyl-1,3-dioxo-1,3,3a,4,7,7a-hexahydroisobenzofuran-4-carboxylate
APEA	Aspen Process Economic Analyzer®
AS	allyl sorbate
BADGE	bisphenol-A-diglycidylether
BPA	bisphenol A
CAGR	component annual growth rate
CEPCI	chemical engineering plant cost index
CSTR	continuously stirred tank reactor
DA	Diels-Alder
DCM	dichloromethane

DGEBA	diglycidyl ether of bisphenol A
DMA	dynamic mechanical analysis
ECH	epichlorohydrin
EFSA	European food safety authority
EGCHC	1,2-epoxy-6-methyl-triglycidyl-3,4,5-cyclohexanetricarboxylate
EOS	equation of state
GCM	group contribution method
I	Diels-Alder product AHIBC
Ia	allylation intermediate a: 2,6-diallyl-5-methylcyclohex-3-ene-1-carboxylic acid
Ib	allylation intermediate b: 5,6-diallyl-2-methylcyclohex-3-ene-1-carboxylic acid
III	allylation product TACHC
IPD	isophorone diamine
K-L	Kullback-Leibler
<i>m</i> CBA	3-chlorobenzoic acid
<i>m</i> CPBA	3-chloroperbenzoic acid
HMB-GV	human biomonitoring guidance value
MA	maleic anhydride
MESH	material-equilibrium-summation-heat
MLE	maximum likelihood estimation
MSDS	material safety data sheet
MTHPA	methyl tetrahydrophthalic anhydride
NMP	<i>N</i> -methyl-2-pyrrolidone
NMR	nuclear magnetic resonance
NRTL	non-random two-liquid
O	oxygen
ODE	ordinary differential equation
OO	oxirane oxygen
R	1,2-epoxy-6-methyl-triallyl-3,4,5-cyclohexanetricarboxylate
RT	1,2-epoxy-3-glycidyl-6-methyl-diallyl-3,4,5-cyclohexanetricarboxylate
RTT	1,2-epoxy-3,4-diglycidyl-6-methyl-allyl-3,4,5-cyclohexanetricarboxylate
SA	sorbic acid
T	1,2-diallyl 3-glycidyl-6-methylcyclohex-4-ene-1,2,3-tricarboxylate
TACHC	triallyl-6-methylcyclohex-4-ene-1,2,3-tricarboxylate
TDI	tolerable daily intake
TEA	techno-economic analysis
THPA	tetrahydrophthalic anhydride

TOL	toluene
TT	1-allyl 2,3-diglycidyl-6-methylcyclohex-4-ene-1,2,3-tricarboxylate
TTT	triglycidyl-6-methylcyclohex-4-ene-1,2,3-tricarboxylate
UNIFAC	universal quasichemical functional group activity coefficients
UNIFAC-DMD	modified universal quasichemical functional group activity coefficients (Dortmund)
UNIQUAC	universal quasichemical
VLE	vapor-liquid-equilibrium

List of Figures

1.1	Development of the worldwide polymer production capacities for fossil and bio-based plastics from 1950 to 2022 and forecast until 2028. Modified after [5].	1
1.2	Development of the total number of journal articles published from 1950 to 2023 in comparison to the normalized fraction of number of articles published with the keywords "epoxy" and "bio-based" in the title or abstract. Data from [25].	3
2.1	Schematic illustration of the principle of parsimony. Bias and variance as function of the number of parameters n_{par} . Modified after [85].	12
2.2	Schematic representation of the mass balance on a theoretical stage.	22
3.1	Reaction steps for the synthesis of the epoxy EGCHC starting from sorbic acid. Modified from [61].	28
3.2	Tensile testing after DIN EN ISO 527-2 of cured EGCHC and DGEBA samples [120].	31
3.3	Comparison of bio-based carbon content between epoxy EGCHC (left) and industrial standard DGEBA (right) using ASTM D6866 [121].	32
3.4	Contribution of different components to the total bio-based content of EGCHC calculated using ASTM D6866 [121] (left) and DIN EN 16785-2 [133] (right). SA: sorbic acid, AA: allyl alcohol, MA: maleic anhydride, Epox: epoxidation with <i>m</i> CPBA.	33
3.5	Comparison of bio-based carbon content of cured resins EGCHC and IPD eCO (left) and DGEBA and IPD eCO (right) using ASTM D6866 [121].	33
4.1	Diels-Alder reaction of allyl sorbate and maleic anhydride to AHIBC.	39
4.2	Acid catalyzed reaction path of the esterification reaction starting from the Diels-Alder product (I) to TACHC (III) via the two intermediates IIa and IIb.	40
4.3	Simplified epoxidation reaction of TACHC with <i>m</i> CPBA forming EGCHC.	42

4.4	Possible reaction paths of the step-wise epoxidation of TACHC with indication of the respective rate constants for terminal k_t or ring-bound double bonds k_r	43
4.5	Linear parity plot of the allyl sorbate conversion for all measurements. Dashed lines mark the $\pm 10\%$ region.	47
4.6	Distribution with normal distribution curve approximation ($\mu = -0.0082$, $\sigma^2 = 0.0013$) and lag plot of the residuals of fitting the Diels-Alder reaction at different temperatures.	48
4.7	Linear parity plots of the esterification reaction of the Diels-Alder reaction (I) to TACHC (III) for each component. Experiments with only three responses are indicated by closed symbols. Dashed lines mark the $\pm 10\%$ region.	50
4.8	Residual distribution with normal distribution curve approximation ($\mu = -0.0002$, $\sigma^2 = 0.0007$) and lag plot of the residuals of fitting the esterification reaction at different temperatures. Residuals are normalized by $c_{I,0}$	51
4.9	Linear parity plot of the epoxidation of TACHC. Double bond in ring is represented by closed symbols, terminal double bonds by open symbols. Dashed lines mark the $\pm 10\%$ region.	52
4.10	Residual distribution with normal distribution curve approximation ($\mu = 0.0024$, $\sigma^2 = 0.0008$) and lag plot of the residuals of fitting the epoxidation reaction at different temperatures.	53
4.11	Comparison of ring and terminal double bond epoxidation and reaction progress of the modeled epoxidation scheme.	54
4.12	Simulated versus experimental determined relative oxirane oxygen content η over time for all measured temperatures.	55
4.13	Section of the $^1\text{H-NMR}$ spectrum of the Diels-Alder reaction between maleic anhydride and allyl sorbate at a conversion of 49.9% after a reaction time of 15 min at 103 °C. Displayed values denote the area of the peaks for conversion determination.	60
4.14	Progress of the Diels-Alder reaction at 103 °C in $^1\text{H-NMR}$	60
4.15	Exemplary $^1\text{H-NMR}$ after 8 min reaction time of the allylation reaction at 78.5 °C.	61
4.16	Progress of the allylation reaction at 78.5 °C in $^1\text{H-NMR}$	61
4.17	Section of the $^1\text{H-NMR}$ spectrum of the epoxidation reaction of TACHC after a reaction time of 48 min at 26.2 °C.	62
4.18	Progress of the epoxidation reaction at 26.2 °C in $^1\text{H-NMR}$	62

4.19	Fit of the experimental allyl sorbate conversion data at various temperatures. Experimental points as markers, model fits as lines. Total coefficient of determination $R_{\text{tot}}^2 = 0.9861$	63
4.20	Measured concentration values with model fits denoted as lines for the allylation of the Diels-Alder product (I) over the two intermediates IIa and IIb towards TACHC (III). Experimental points as markers, model fits as lines (Model 4). Dashed lines show individual model results from fitting the sum of IIa+III. Total coefficient of determination $R_{\text{tot}}^2 = 0.9942$	64
4.21	Double bond conversion of ring-bound double bond X_R and terminal bond X_T for different temperatures. Experimental points as markers, model fits as lines. Total coefficient of determination $R_{\text{tot}}^2 = 0.9952$	66
4.22	Residuals of ring-bound double bond conversion versus time. Abscissa scaled logarithmically.	66
5.1	Reaction steps for the production of EGCHC starting from sorbic acid and allyl alcohol.	69
5.2	Parameter matrices for UNIFAC and modified UNIFAC (Dortmund) group contribution property method. Availability of binary interaction parameters of used groups.	72
5.3	Vapor-liquid equilibrium for the mixture of (1) allyl alcohol and (2) water. Solid and dashed lines represent predicted liquid and vapor compositions by NRTL, respectively. Experiments are indicated by markers with open and closed symbols describing vapor and liquid, respectively [169–171].	73
5.4	Acid catalyzed reaction path of the esterification reaction starting from the Diels-Alder product AHIBC (I) to TACHC (III) via the two intermediates IIa and IIb.	75
5.5	Reaction scheme of the epoxidation reaction of TACHC with <i>m</i> CPBA.	76
5.6	Proposed production of EGCHC using a three step cascade reaction starting from allyl sorbate. Section 1: Production of AHIBC, blue. Section 2: TACHC production, green. Section 3: EGCHC production, orange.	78
5.7	Flowsheet of the production of EGCHC with unit operations, streams and indication of process sections.	82
5.8	Sensitivity study of reactor tube length and resulting molar fraction profile for $L = 4$ m in reactor R101.	83
5.9	Sensitivity studies for reactive distillation column D201-R. Varying of reflux ratio R , side mass flow rate \dot{m}_{13} and bottom molar purity specification x_B	85
5.10	Sensitivity of flash drum F201. $p = 0.1$ bar.	86
5.11	Sensitivity study of tube length and resulting profile of molar fractions in reactor R301.	87

5.12	Parametric sensitivity of pressure and temperature in flash drum F302 on the purity of DCM in the liquid stream. Target purity of 0.1 wt-% indicated with dashed line.	89
5.13	Solubility of AHIBC in toluene at different temperatures.	98
A.1	Availability matrix of published binary interaction parameters $a_{m,k}$ for the UNIFAC model. Data from [166–168].	111

List of Tables

2.1	Sampling protocol with the number of samples taken at temperatures T_i (example).	9
3.1	Synthesis summary with concentrations and mass yields of each reaction step [61].	30
3.2	Summary of curing procedure conditions for EGCHC and DGEBA samples [61].	30
3.3	Glass transition temperature, tensile modulus and tensile strength for the four cured samples [61].	31
4.1	Selection of different tested models for the esterification reaction of the Diels-Alder product with allyl alcohol.	42
4.2	Total coefficient of determination, Akaike and Bayesian information criteria for the different tested models for the esterification reaction of the Diels-Alder product with allyl alcohol.	49
4.3	Estimated parameters Φ_i with 95 % confidence intervals and re-parameterized variables $k_{0,i}$ and $E_{A,i}$ for a reference temperature of $T_{\text{ref}} = 348.16 \text{ K}$ for candidate model 4.	49
4.4	Estimated parameters Φ_i with 95 % confidence intervals and re-parameterized variables pre-exponential factor $k_{0,i}$ and activation energy $E_{A,i}$ for a reference temperature of $T_{\text{ref}} = 294.92 \text{ K}$	53
4.5	Estimated parameters Φ_i with 95 % confidence intervals and re-parameterized variables $k_{0,i}$ and $E_{A,i}$ for a reference temperature of $T_{\text{ref}} = 348.16 \text{ K}$ for models 2, 3, 5 and 6. Akaike and Bayesian information criteria for model comparison.	65
5.1	Components with names and formula included in the model. Source of their respective physical properties indicated.	70
5.2	List of UNIFAC groups used in the model to determine physical properties of unknown structures. Breakdown of groups required to build the structures of AHIBC, Ila, I Ib, TACHC and EGCHC.	71

5.3	Volume parameter R_k and surface parameter Q_k of the anhydride group O=COC=O [166].	71
5.4	Regressed NRTL parameter for the system: allyl alcohol (AA) and water.	73
5.5	Pre-exponential factor and activation energy of the reaction rate constants k_1, k_2, k_3 and k_3 of the allylation reaction [69].	75
5.6	Pre-exponential factor and activation energy of the epoxidation rate constants for ring and terminal bound double bonds, k_R and k_T [69].	76
5.7	Raw material prices.	81
5.8	Utility prices taken from APEA (2019).	81
5.9	Design parameter of the reactive distillation column D201-R.	84
5.10	Comparison of EGCHC price from TEA and commercial prices of epoxy resins. Selection of available bio-based epoxy resins together with their bio-based content and composition information from MSDS [218–220].	90
5.11	Components estimated with UNIFAC group contribution method. List of names, structures and their respective group description.	93
5.12	UNIFAC group numbering and description.	97
5.13	Equipment summary of the complete process scheme. Indicated temperatures and pressures are at the outlet.	99
5.14	Design parameter of the distillation column D202.	101
5.15	Design parameter of the distillation column D203.	101
5.16	Stream results of the Diels-Alder section.	102
5.17	Stream results of the Allylation section.	103
5.18	Stream results of the Epoxidation section.	104
5.19	Executive summary of the investment costs from the APEA simulation results.	105
A.1	List of UNIFAC groups used in the model to determine physical properties of unknown structures.	112

List of Publications

Journal Publications

- M. Feigel, O. Hinrichsen, “Modeling of Process Operation Principles for the Immobilized Enzyme *Candida Antarctica* under Activity Decay”, *Chem. Ing. Tech.* **2022**, *94*, 652–662, DOI 10.1002/cite.202100187
- J. M. Breitsameter, N. Reinhardt, M. Feigel, O. Hinrichsen, K. Drechsler, B. Rieger, “Synthesis of a Sustainable and Bisphenol A-Free Epoxy Resin based on Sorbic Acid and Characterization of the Cured Thermoset”, *Macromol. Mater. Eng.* **2023**, 2300068, DOI 10.1002/mame.202300068
- M. Feigel, J. M. Breitsameter, K. Lechner, B. Rieger, O. Hinrichsen, “Kinetic Modeling of the Synthesis Path for the Production of a Sustainable Epoxy Resin based on Allyl Sorbate”, *Ind. Eng. Chem. Res.* **2023**, *62*, 13389–13400, DOI 10.1021/acs.iecr.3c01317
The authors contributed equally to this work.
- M. Feigel, J. M. Breitsameter, B. Rieger, O. Hinrichsen, “Bridging the Gap from Laboratory to Production: Kinetic Modeling-Guided Process Development for a Novel Epoxy Resin”, *Ind. Eng. Chem. Res.* **2024**, *63*, 1271–1285, DOI 10.1021/acs.iecr.3c03339

Oral Presentations

- M. Feigel, J. M. Breitsameter, B. Rieger, O. Hinrichsen, "Conjunction of kinetic and process modelling - Paving the way to a green epoxy resin", *The 27th International Symposium on Chemical Reaction Engineering* **2023**, Quebec City, Canada.

Poster Presentations

- M. Feigel, O. Hinrichsen, "Process Development and Design of the Chemo-Enzymatic Production of a Bio-Based Thermoplastic Using an Algae Feedstock", *Jahrestreffen Reaktionstechnik 2021*, Würzburg, Germany. (online event)
- M. Feigel, O. Hinrichsen, "Integration of Immobilized Enzyme Reactors under Activity Decay in Commercial Process Simulation Tools", *The 27th North American Catalysis Society Meeting 2022*, New York, USA.
- M. Feigel, J. M. Breitsameter, B. Rieger, O. Hinrichsen, "Algae Biomass as a Raw Material – Production and Process Simulation of a Bio-Based Polymer", *Jahrestreffen Reaktionstechnik 2022*, Würzburg, Germany.
- M. Feigel, J. M. Breitsameter, B. Rieger, O. Hinrichsen, "Synergy of Kinetic and Process Modelling - A Case Study", *Jahrestreffen Reaktionstechnik 2023*, Frankfurt, Germany.